

---

# Advancing Single-Molecule Fluorescence Spectroscopy and Super-Resolution Microscopy with Organic Fluorophores

Jan Vogelsang

---



Munich, September 2009



---

**Advancing Single-Molecule Fluorescence Spectroscopy and  
Super-Resolution Microscopy with Organic Fluorophores**

---

Dissertation

Submitted by  
Jan Vogelsang  
from Herford

at

Faculty of Physics  
Ludwig-Maximilians-University  
Munich

Munich, September 2009

Erstgutachter: Prof. Dr. Philip Tinnefeld

Zweitgutachter: Prof. Dr. Wolfgang Zinth

Tag der mündlichen Prüfung: 26.10.2009

In vielen der aktuellen Anwendungen in der Mikroskopie, Biophysik, Nanotechnologie oder der hochauflösenden Mikroskopie werden zahlreiche unterschiedliche Anforderungen an (einzelne) organische Farbstoffmoleküle gestellt. Ein hoher Absorptionskoeffizient, hohe Fluoreszenzquantenausbeute und Wasserlöslichkeit werden mittlerweile als Standardeigenschaften von organischen Farbstoffen angesehen. Allerdings erfordern Anwendungen, welche die Vorteile von Einzelmolekülmessungen ausnutzen, sowie die jüngst eingeführten supraauflösenden Mikroskopietechniken (bezeichnet mit Abkürzungen wie STORM, PALM, STED, SSIM,...) eine zusätzliche Langlebigkeit der einzelnen Farbstoffe und spezifisches Emissionsverhalten, wie kontinuierliche oder fluktuierende Fluoreszenz.

Das Ziel dieser Arbeit ist es, den Einfluss der spezifischen Umgebung, welche für die jeweilige (biophysikalische) Anwendung benötigt wird, auf die fluoreszierenden Eigenschaften der Farbstoffe zu verstehen, und diese Erkenntnisse auszunutzen, um eine ausgezeichnete Kontrolle über die Fluoreszenz zu erhalten. Ein neuer Ansatz für die Manipulation organischer Farbstoffe wird präsentiert, welcher ladungsseparierte Zustände durch photoinduzierten Elektronentransfer in organischen Farbstoffen ausnutzt. Dabei spielt ein neu eingeführtes Puffersystem, das sowohl Reduktions- als auch Oxidationsmittel enthält (ROXS), eine entscheidende Rolle. Auf der Basis thermodynamischer Betrachtungen und der zugrunde liegenden Redoxreaktionen wird eine umfangreiche und vereinheitlichende Theorie über blinkende und bleichende organische Farbstoffe erhalten.

Es wird gezeigt, dass durch ROXS die Photostabilität von organischen Farbstoffen verschiedener Farbstoffklassen um bis zu drei Größenordnungen erhöht wird. Gleichzeitig wird das Blinken drastisch reduziert, wodurch fluoreszenzspektroskopische und bildgebende Anwendungen bei hoher Fluoreszenzintensität und einer langen Beobachtungsdauer ermöglicht werden.

Im zweiten Schritt wird demonstriert, wie durch eine sorgfältige Auswahl der Farbstoffeigenschaften (Redoxeigenschaften) und der Umgebungsbedingungen (Pufferzusätze) gewöhnliche Farbstoffe als effiziente Einzelmolekülschalter verwendet werden können: Durch Hinzufügen bzw. Entfernen reduzierender oder oxidierender Substanzen wird die Fluoreszenz von mehreren Oxazin-Farbstoffen zwischen stabiler Fluoreszenz und nicht fluoreszierenden Dunkelzuständen geschaltet. Bei geringer Sauerstoffkonzentration ist der Auszustand, der dem Radikalzustand zuschreiben ist, thermisch stabil mit einer Lebensdauer im Minutenbereich. Der molekulare Schalter zeigt eine bemerkenswerte Zuverlässigkeit mit bis zu 3000 Schaltzyklen auf Einzelmolekülebene. In Anwesenheit von reduzierenden und oxidierenden Substanzen wird ein kontinuierliches Schalten (Blinken) erzeugt mit unabhängig einstellbaren An- und Auszeiten, in sowohl sauerstoffarmer als auch in sauerstoffhaltiger Umgebung.

Erstmalig können damit konventionelle Farbstoffe zur Superauflösungsmikroskopie unter biologisch relevanten Bedingungen benutzt werden, wie Abbildungen von Aktinfilamenten und Bündeln von Aktinfilamenten in fixierten Zellen mit einer Auflösung unterhalb des Beugungslimits zeigen. Desweiteren kann das „Blinken“ als eine Observable betrachtet werden, welche detaillierte Auskunft über die Redoxumgebung des Farbstoffes gibt. Dies wird benutzt um den stabilisierenden Mechanismus von Trolox (Vitamin E) auf die Fluoreszenz organischer Farbstoffe aufzuklären.

Schließlich wird ein neuartiges Konzept fluoreszenter Proben realisiert, welche eine intrinsische Auflösungserhöhung in konfokalen Mikroskopen erzeugen. Bei diesen so genannten „Energietransfer blockierenden Proben“ bewirkt die Sättigung eines oder mehrerer Farbstoffe ein superlinear fluoreszierendes Ansprechen eines anderen Farbstoffes. Eine theoretische Behandlung der Fluoreszenzeigenschaften dieser ETBPs zeigt die faszinierende Möglichkeit einer Auflösung < 100 nm in einem gewöhnlichen, konfokalen Mikroskop nur durch Modifikation der Fluoreszenzsonden.



The manifold exciting applications of fluorescence in biophysics, nano-technology or super-resolution microscopy, pose extraordinary and multiple demands on the (single) organic dye molecules employed. A high extinction coefficient together with a high fluorescence quantum yield and water-solubility are nowadays considered as standard properties of suitable organic dyes. However, single-molecule fluorescence resonance energy transfer (single-molecule FRET) and recently introduced super-resolution techniques (termed STORM, PALM, STED, SSIM,...) additionally require a strong resistance against photobleaching and specific functionalities, e.g., stable & non-fluctuating vs. blinking fluorescence intensity, even on the level of single molecules.

It is the aim of this work to understand the influence of the specific fluorophore environment, i.e., the composition of the aqueous buffer system needed for the respective (biophysical) application, on the emission properties of organic fluorophores and to utilize this knowledge for the exquisite control of their fluorescence properties. Inducing and quenching radical ion states by photo-induced electron transfer is used to depopulate reactive intermediates such as triplet states to minimize photobleaching. Therefore a buffer system, which contains reducing as well as oxidizing agents (ROXS), is introduced. Its working principle is explained on the basis of thermodynamic considerations of the underlying redox reactions, yielding a comprehensive and unifying picture of blinking and photobleaching of organic fluorophores.

In detail, it is demonstrated that ROXS substantially increases the photostability of organic fluorophores from different dye-classes. Simultaneously, blinking is dramatically reduced, enabling fluorescence spectroscopy and imaging applications at higher fluorescence count rates over extended periods of time.

In a second step it is demonstrated that a careful selection of fluorophore properties (redox-properties) and environmental conditions (buffer additives) allows the use of ordinary fluorescent dyes as efficient single-molecule switches: Addition or removal of reducing or oxidizing agents switches the fluorescence of several oxazine dyes between stable fluorescent and non-fluorescent dark states. At low oxygen concentrations, the OFF-state – ascribed to a radical anion – is thermally stable with a lifetime in the minute range. The molecular switches show a remarkable reliability with intriguing fatigue resistance even on the single-molecule level with up to 3000 switching cycles.

For the first time conventional organic fluorophores were used for super-resolution microscopy using subsequent localization of single blinking molecules (“Blink Microscopy”) under biological relevant conditions, as shown by super-resolution imaging of actin filaments and actin filament bundles in fixed cells with sub-diffraction resolution. Further, “blinking” was used as an observable which sensitively reports on the local redox environment of the fluorophore. Sensing of redox environments is exploited to reveal that the anti-fading mechanism of the commonly used vitamin E analogue Trolox is due to an oxidized Trolox-quinone and thus is in accordance with the ROXS-concept.

Finally, by merging all the acquired knowledge, a realization of fluorescent probes, which show an intrinsic resolution improvement in a confocal microscope, is demonstrated. In these so-called “Energy Transfer Blockade Probes” the saturation of one or more fluorophores is converted into a super-linear fluorescence response of another fluorophore, yielding intrinsic sub-diffraction resolution in any confocal microscope. A theoretical description highlights the fascinating vision of sub-diffraction resolution below 100 nm in a standard confocal microscope just by modification of the fluorescent probes.





---

1.	Introduction .....	1
1.1.	Single-Molecule Fluorescence Spectroscopy .....	1
1.2.	Super-Resolution Microscopy .....	3
1.3.	Organic Fluorophores as Emitters .....	5
2.	Theory .....	7
2.1.	Photophysics of Organic Fluorophores.....	7
2.2.	Photoinduced Electron-Transfer Reactions .....	9
2.3.	The Reducing and Oxidizing System (ROXS).....	10
3.	Materials and Methods.....	12
3.1.	Confocal Microscopy.....	12
3.2.	Total Internal Reflection Fluorescence Microscopy.....	13
3.3.	Super-Resolution Microscopy .....	14
3.4.	Single-Molecule Immobilization .....	16
3.5.	Auto-Correlation Analysis.....	16
4.	Results .....	19
4.1.	Stable Fluorescent Fluorophores (P1).....	19
4.1.1.	Depopulation of the Excited States .....	19
4.1.2.	Minimizing Photobleaching and Blinking.....	20
4.1.3.	Applicability in Biological Systems.....	23
4.2.	Controlling the Fluorescence (P2) .....	23
4.2.1.	Single-Molecule Switching .....	24
4.2.2.	Super-Resolution Microscopy.....	28
4.3.	Single-molecule Redox Sensor (SMRS) (P3).....	29
4.3.1.	Influence of Accessibility on Redox-Blinking .....	29
4.3.2.	Influence of the DNA Sequence on Redox-Blinking .....	30

4.3.3.	pH-Dependency .....	31
4.3.4.	Ratiometric SMRS .....	33
4.4.	Trolox as Antiblinking and Antibleaching Reagent (P4) .....	34
4.4.1.	SMRS and Trolox .....	35
4.4.2.	(Photo-) Oxidation of Trolox .....	36
4.5.	Resolution Enhancing Probes (P5) .....	37
4.5.1.	Resolution Enhancement in Confocal Microscopy .....	38
4.5.2.	Energy Transfer Blockade Probe .....	39
4.5.3.	Theoretical Description of the ETBP .....	43
4.5.4.	Demonstration of Intrinsic Sub-Diffraction Resolution .....	46
5.	Conclusion and Outlook .....	49
6.	References .....	51
7.	Acknowledgements .....	58
8.	Appendix: .....	59
8.1.	Associated Publications .....	59
	P1 .....	61
	P2 .....	63
	P3 .....	65
	P4 .....	67
	P5 .....	69
8.2.	Further Publications .....	71
9.	Curriculum Vitae .....	79

## 1. Introduction

“Don’t kill the messenger” is a well known expression, first stated by Sophocles in the year 442 B.C. However, in fluorescence spectroscopy and microscopy this has long appeared to be a necessary evil. The emitters can be seen as messengers, who report sensitively on their local environment while the photons are the messages. Each message can contain a wealth of different information about the emitter and the specific environment, e.g. color (energy), polarization (orientation), rate at which they are being emitted (lifetime) and finally the position of the emitter. Therefore it becomes important to collect as many photons as possible from the emitter, which ultimately leads to the destruction of the emitter, because this allows obtaining the most detailed information about the emitter and its environment. Hence, the ability of an emitter to emit photons, i.e., its photophysical properties (photobleaching time, absorption coefficient, quantum yield) evolve to key figures for the success of modern fluorescence-based experiments. Due to exciting developments of fluorescence microscopy and different single-molecule techniques – all based on fluorophore emission – extreme and sometimes contradicting properties are demanded from the emitters: Extreme stable and bright emission, or continuous switching between bright and dark states are required from a single molecule (emitter) over expanded time periods.

It is the goal of this work to contribute to the development of ultra-stable and controllable emitters for fluorescence microscopy. This work hence introduces a generic and easy method that allows controlling the photophysical properties of organic fluorophores – for use in current state-of-the-art methods. The most important milestones in single molecule fluorescence spectroscopy (SMFS) and super-resolution microscopy are introduced in this chapter. This overview is intended to demonstrate the demand and the importance of ultra-stable and controllable emitters in fluorescence microscopy.

### 1.1. Single-Molecule Fluorescence Spectroscopy

Within the last decade SMFS has become a versatile and auspicious tool to study conformational states or conformational dynamics, and the activity of single (biological) molecules. Single-molecule experiments can be conducted without the need for synchronization of all molecules in the experiment whereas ensemble experiments only yield an average value of a specific observable is obtained (a fact that hampers the observation of sub-ensembles).

The position, the velocity (including speed and direction) and conformational dynamics of a single (bio)molecule are important parameters obtained in SMFS experiments. A first approach utilizes the fact that single (fluorescently labeled) molecules can be localized with nanometer precision, depending on the actual number of emitted photons.<sup>[1]</sup> This was already used to follow the motion of individual motor proteins,<sup>[2, 3]</sup> direct imaging of receptors inside synapses,<sup>[4]</sup> the diffusional trajectories of labeled lipid molecules in membranes, and the diffusion of molecules in gels, in solutions, and at the liquid-solid interface.<sup>[5, 6]</sup> The quality of the acquired data is thereby always directly linked to the number of detected photons. In addition, the more photons are detected during a certain time interval, the higher the time resolution is, due to the trade-off between signal to noise and acquisition time, i.e., sufficient spatial resolution in a certain time interval.

High spatial resolution can also be acquired by utilizing fluorescence resonance energy transfer (FRET). In particular, FRET is perfectly suited to study conformational dynamics and activity inside (bio)molecules. The technique relies on the distance dependent energy transfer between a donor fluorophore and acceptor fluorophore that are both attached to distinct parts of the structure

of interest. FRET has a dynamic range of 3-10 nm. Since the first FRET experiments between a single donor and a single acceptor,<sup>[7]</sup> the technique has been successfully used to study ligand-receptor interactions,<sup>[8]</sup> dynamics of motor proteins and dynamic DNA nano-structures.<sup>[9, 10]</sup>

To demonstrate the capabilities of single-molecule FRET, the two conformational states of a fluctuating DNA nano-structure, a so-called ‘‘Holliday junction’’, are shown in Figure 1.1. The Holliday junction consists of four DNA strands that hybridize to a four-way junction. In the presence of metal ions such as magnesium the junction forms an x-shaped structure with pair wise anti-parallel coaxial stacking of the neighboring helices.<sup>[10]</sup> Dynamic flipping of the helices on the ms-timescale leads to the existence of two conformers, one where helix X stacks on helix R and helix H stacks on helix B (HJA), and one where stacking of helix X on helix B and of helix H on helix R is favored (HJB) (see Figure 1.1).

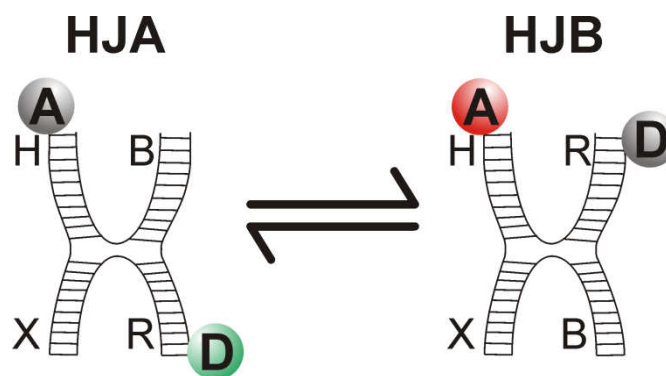


**Figure 1.1.** Scheme of the labeled Holliday junction and its conformational change is shown. On the left hand side the conformation ‘‘HJA’’ is shown, with no FRET occurring between the donor fluorophore (green spot D) and the acceptor fluorophore (grey spot A). On the right hand side the conformation ‘‘HJB’’ is shown, with FRET occurring between the donor fluorophore (grey spot D) and the acceptor fluorophore (red spot A).

The dynamics in the Holliday junction are now visualized by attaching donor and acceptor fluorophores to distinct parts of the Holliday junction (e.g. see Figure 1.1) and recording the fluorescence of both detection channels. The fluctuations in fluorescence intensity in both signals correspond to changing distances between the donor and acceptor fluorophore, and therefore changing FRET (Figure 1.2a); the two FRET values each correspond to one of the conformers of the Holliday junction. Whereas in ensemble experiments only an average FRET is obtained and no distinct conclusion can be drawn about the origin of the FRET value, i.e., the specimen can consist of two or more different populations with different FRET values or one population with a changing FRET value, SMFS experiments reveal two interconverting states on a single molecule level.

Although single-molecule FRET can provide detailed insights into the dynamics and conformational changes of (bio)molecules its applicability is drastically influenced and limited by the photophysics of the reporter fluorophores. Photophysical artifacts, such as blinking (i.e., frequent occurrence of non-fluorescent dark-states that can manifest as ‘‘low-FRET’’ periods) or bleaching, limit the observation of dynamic processes or lead to erroneous results and have to be separated from biophysics (see e.g. ref.<sup>[11]</sup> and <sup>[12]</sup>). In Figure 1.2b a similar ‘‘fluctuating’’ FRET-signal is presented corresponding to a FRET pair at a fixed distance. Here, the fluctuations are caused by photophysical processes, generated by the acceptor fluorophore. The acceptor fluorophore enters a radical anion state, where it cannot function as an acceptor, resulting in an increased fluorescence of the donor fluorophore.<sup>[13-15]</sup> This striking similarity between FRET-

changes caused by biophysics (Figure 1.2a) and photophysics (Figure 1.2b) demonstrates the necessity to obtain control of the fluorescent properties of the reporter fluorophore.

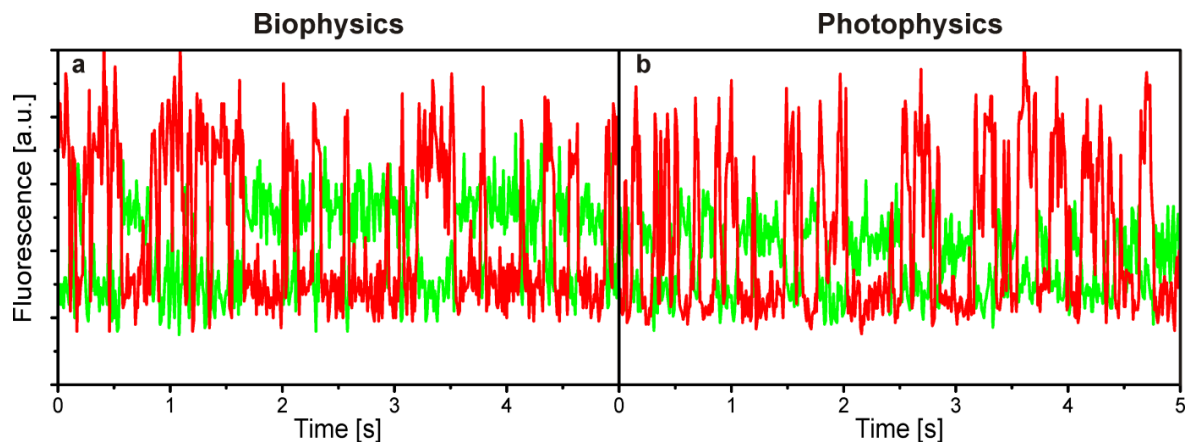


**Figure 1.2.** Comparison of a single molecule signal generated through biophysics and generated through photophysics. (a) Typical fluorescent transient of a single Holliday junction labeled with Cy3 as a donor and Cy5 as an acceptor fluorophore. (a, b) the green and red curves correspond to the donor and acceptor signal, respectively. (a) Fluctuations in the signal are assigned to different FRET-efficiencies, due to conformational changes of the Holliday junction. (b) Typical fluorescent transient of a single dsDNA strand labeled with ATTO647N as a donor and ATTO680 as an acceptor fluorophore. Fluctuations are assigned to frequent transitions of the acceptor fluorophore ATTO680 into a non-fluorescent dark-state. The acceptor fluorophore cannot function as an FRET-acceptor residing in the radical anion state, resulting in an increased fluorescence of the donor fluorophore.

## 1.2. Super-Resolution Microscopy

Approximately a decade ago the field of fluorescence microscopy started to emerge in the exciting field of super-resolution fluorescence microscopy based on far-field excitation, which tries to circumvent the resolution barrier, given by the diffraction limit of light. Light of a wavelength  $\lambda$ , which is focused by a lens with a given numerical aperture  $NA = n \cdot \sin(\alpha)$  ( $n$  = diffraction index of the medium,  $\alpha$  = half angle of the maximal cone of light that can enter or exit the lens), cannot be used to discern objects closer together than the distance  $d = \lambda / (2 \cdot NA)$ .<sup>[16-18]</sup> An example is given in Figure 1.3a, where two emitters (red dots) are closer together than the distance  $d$  (here calculated for a wavelength  $\lambda = 640$  nm and an objective with a numerical aperture  $NA = 1.2$ ). The key in circumventing the diffraction barrier lies in the principle of having only one active object at a time within a diffraction limited area and therefore two objects can be separated in time (see Figure 1.3b-d). Essentially all super-resolution techniques are based on this principle. However, the super-resolution techniques can be divided into two major categories, which require two complementary fluorescent behaviors of the probes used.

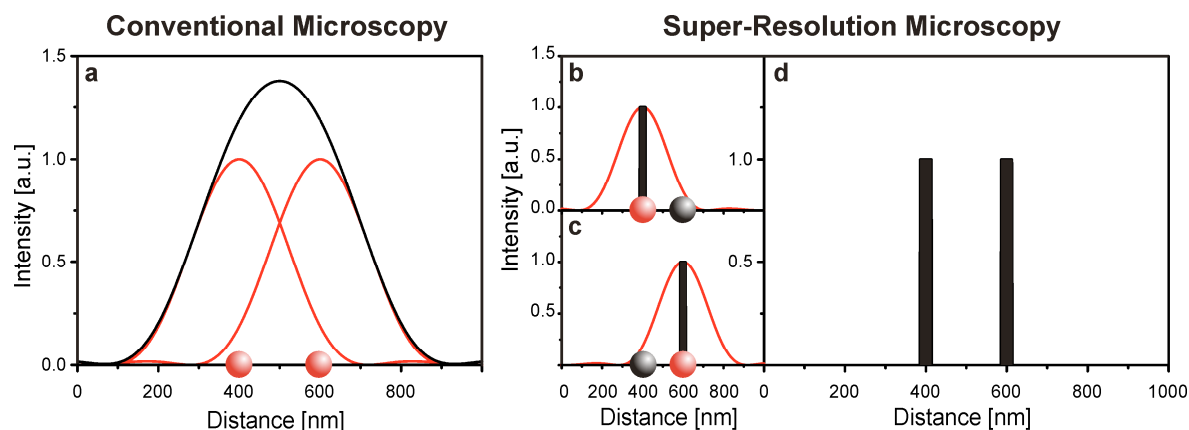


**Figure 1.3.** Comparison of conventional microscopy and super-resolution microscopy. (a) Two emitters are fluorescent at the same time (red dots) in conventional microscopy and the exact positions cannot be discerned, due to the overlap (black curve) of the photon distributions generated from a point-like emitter (red curves). (b) In super-resolution microscopy the left emitter is fluorescent (red dot) and the right emitter is switched off (black dot). The fluorescent emitter can be localized with high precision (black bar), given by the full width at half maximum (FWHM) of the photon distribution and the number of detected photons  $n$  ( $\text{FWHM}/(n)^{1/2}$ ).<sup>[1]</sup> (c) This is followed by switching of the left emitter and switching on the right emitter to localize the exact position of the right emitter. (d) The positions of both emitters are given and summed for reconstruction.

In the first category, the single emitters are switched within a defined region between a fluorescent and a non-fluorescent state. Within the first category there are the following techniques: stimulated emission depletion (STED) microscopy,<sup>[19, 20]</sup> ground state depletion (GSD) microscopy,<sup>[21, 22]</sup> saturated pattern excitation microscopy (SPEM) or saturated structured illumination microscopy (SSIM).<sup>[23, 24]</sup> STED and GSD microscopy are based on a scanning confocal microscope. In principle an additional light intensity pattern in the shape of a doughnut, which switches the majority of molecules in a diffraction limited area off, is used around the diffraction limited excitation focus. Only the molecules in the center of the doughnut, which are excited below a certain threshold, are still able to fluoresce. The off-switching can be achieved by driving the molecules via stimulated emission into the ground state (STED)<sup>[19]</sup> or common photophysical phenomena can be exploited, like driving the molecules in the triplet-state (GSD), where they are switched off for a certain time-period.<sup>[21]</sup>

On first sight, SPEM and SSIM appear conceptually different compared to STED and GSD as they are based on widefield microscopy, but essentially they can be referred to as “highly parallelized scanning microscopy”. A standing wave interference pattern excites the molecules strongly to the fluorescent state, resulting in a depletion of the ground state outside the line-shaped zeros. To generate a complete image, the pattern is shifted by phase-shifting the maxima of the interference pattern and reading out the fluorescence imaged with a camera for each step. To cover all directions the line pattern has to be tilted several times because resolution is only improved perpendicular to the line-shaped zeros.<sup>[23-26]</sup> Mathematical analysis, i.e., Fourier analysis of the data, renders super-resolved images.

The key for a successful implementation of these techniques is a high number of switching cycles between the fluorescent state and any non-fluorescent state of the emitters. For example, if a super-resolution image has to be acquired using STED or GSD microscopy with a resolution of about 10 nm, all molecules within a diffraction limited area of about 50 000 nm<sup>2</sup> ( $\pi \cdot (d/2)^2$  with  $d \approx 250$  nm minus  $10 \cdot 10$  nm<sup>2</sup>) will have to be switched off. Further, this area has to be scanned at least with a resolution of about 5 nm according to the Nyquist criterion,<sup>[27]</sup> resulting in approximately 2000

scanning steps for the diffraction limited area. This means that the emitters have to show at least 2000 switching cycles between a fluorescent state and a non-fluorescent state. This is in principle also true for SPEM or SSIM. The number of switching cycles limits the number of phase-shifts of the pattern, which consequently limits the achievable resolution.

In summary, the resolution for these kinds of super-resolution techniques is mainly determined by the number of switching cycles the emitters can undergo. On the other hand only one photon detected from a molecule is sufficient to localize it (at infinite S/N ratio, i.e. no background).

In the second category of super-resolution techniques, the single emitters are switched stochastically between a fluorescent and a non-fluorescent state. These techniques are based on widefield fluorescence microscopy with imaging by a sensitive camera and the common principle is given by subsequent single-molecule localizations. Several variants of this approach are termed: stochastic optical reconstruction microscopy (STORM),<sup>[28-31]</sup> photoactivation localization microscopy (PALM),<sup>[32, 33]</sup> ground state depletion followed by individual molecule return (GSDIM),<sup>[34]</sup> Blink-Microscopy<sup>[35]</sup> and point accumulation for imaging in nanoscale topography (PAINT).<sup>[36]</sup> The main difference to the first category is that instead of switching off a defined region of emitters, a stochastically distributed region of emitters is switched off. The remaining fluorescent emitters have to be distributed such that only one emitter is active within a diffraction limited area. These emitters are then localized with high precision. The localization precision is dependent on the number of emitted photons. In contrast to the first category, the emitters don't have to undergo many switching cycles – actually one switching cycle is enough – but a rather high photon count is required for the localization and noise can easily blur the reconstructed image.

### 1.3. Organic Fluorophores as Emitters

The fluorescence of single emitters is the sole information in experiments performed in any field of fluorescence microscopy and spectroscopy. The single fluorescent emitters can be nanocrystals,<sup>[37]</sup> nanodiamonds,<sup>[38]</sup> conjugated polymers,<sup>[39]</sup> fluorescent proteins<sup>[40]</sup> or all sorts of organic fluorophores.<sup>[41-43]</sup> Easy processing and wide applicability of organic fluorophores makes them invaluable tools for fluorescence microscopy and spectroscopy. Furthermore, organic fluorophores are available over a broad range of the electro-magnetic spectrum, ranging from the near-ultraviolet into the near-infrared region. Most importantly, in contrast to other fluorescent emitters such as fluorescent proteins or quantum dots, organic fluorophores are less invasive, due to their small size of 1 nm or less.

However, fluorophores are confronted with extreme demands in SMFS and superresolution microscopy. These different properties range from stable and long-lasting fluorescence over switching between a fluorescent and a dark state with high cycling numbers to switching between a very bright fluorescent state and dark state with low cycling numbers. With the development of detectors approaching 100% quantum efficiencies and sophisticated collection optics, the bottleneck of current fluorescence microscopy are hence the fluorophores used, which pose severe limitations owing to photobleaching and blinking. The advancement of classical organic dyes such as rhodamine or cyanine derivatives has been incremental despite some progress with regard to labeling chemistry, solubility in water, and the availability of bright and photostable near-IR dyes. Approaches to improve them comprise increased brightness by multichromophore systems, intramolecular triplet quenching, and decreasing the sensibility for reactions with singlet oxygen.<sup>[44, 45]</sup> For different reasons, none of these approaches have been implemented with great success in fluorescence microscopy. Further, only empirical searches were carried out for new fluorophores and environmental conditions suitable for SMFS or super-resolution microscopy.

In order to advance SMFS and super-resolution microscopy, the objective of this thesis is to investigate and to understand the influence of the nanoenvironment on organic fluorophores. Further, an exquisite control has to be achieved over the fluorescent properties of organic fluorophores. Therefore, a new approach will be investigated, which comprises generic charge separated states using photo-induced electron transfer reactions. In a first step, the feasibility of using these charge separated states to stabilize or to switch organic fluorophores with independently controllable on- and off-times will be investigated. On the one hand the stability of fluorescent fluorophores will be explored under the influence of photo-induced electron transfer reactions with high rate constants. These reactions will be exploited for a fast depopulation of the reactive excited triplet states – which are considered as the main bleaching pathway – to a radical state, followed by a fast recovery to the ground state. On the other hand switching between a fluorescent state and non-fluorescent dark-state of ordinary dye molecules will be investigated. Therefore generic radical ion states will be used as controllable OFF-states.

In the second step, the switching will be exploited for super-resolution microscopy based on STORM<sup>[28]</sup> and sensing capabilities, regarding the redox-environment of the fluorophore. Finally, a new way will be highlighted for the development of fluorescent probes which show intrinsic resolution enhancement in any confocal microscope. Therefore an approach will be presented, which uses the radical anion states for a reversible saturation at low excitation intensities. This is followed by a conversion of the saturation to a super-linear dependency of another fluorophore by FRET, which exhibits a direct resolution improvement in confocal microscopes.



## 2. Theory

In the past electron transfer reactions were mainly neglected in the discussion and interpretation of photophysical processes in organic fluorophores. Instead, the attention focuses on the singlet and triplet states of the fluorophores and their respective properties. This chapter gives a more complete overview of fluorophore photophysics by including the influence of photoinduced electron transfer reactions, theoretically based on the electron transfer theory of Marcus. Finally, the theoretical concept will be introduced, which allows to stabilize and control the fluorescence of organic fluorophores using a so-called reducing and oxidizing system (“ROXS”).

### 2.1. Photophysics of Organic Fluorophores

Organic fluorophores are molecules consisting of covalently coupled atoms – in most cases carbon, oxygen and nitrogen – that bear a planar, and therefore strongly delocalized,  $\pi$ -electron system. Their lowest energy transition, i.e., an electronic excitation of the molecule, is commonly found in the UV/vis spectral range, depending on the actual number of involved delocalized electrons and attached substituents. The high number of atoms in a single dye molecule also causes the existence of additional degrees of freedom resulting in vibrational and rotational quantization of a single electronic state.<sup>[46]</sup> The so-called Jablonski-diagram gives a comprehensive overview of the processes that can occur in dye molecules after light excitation (Figure 2.1). The energetic states of the molecule consists of different electronic states, which are the singlet ground-state  $S_0$ , excited singlet-states  $S_N$  (with  $N = 1,2,3\dots$ ) and excited triplet-states  $T_N$  (black bars, Figure 2.1, with  $N = 1,2,3\dots$ ). For clearness of the Scheme only vibrational levels have been integrated (grey bars, Figure 2.1). At room temperature, where all of the presented experiments were conducted, the molecules populate the zero vibrational level of the electronic ground state. The rotational degree of freedom is neglected due the fact that several rotational states are already populated at room temperature, i.e.  $k_b T \approx 200 \text{ cm}^{-1}$ ; with  $k_b$  being Boltzmann’s constant and  $T$  being the absolute temperature.

If a photon with a sufficient amount of energy – represented by the wavelength – is absorbed, the electronic molecule is transferred into a higher excited state, e.g. the  $S_N$ -state. The energy of a photon is given by Planck’s relation:

$$E = h \cdot \frac{c}{\lambda} \quad (2.1)$$

This energy must correspond to the energetic difference between the  $S_N$ - and the  $S_0$ -state which is typically in the range of 1-10 eV. The rate of excitation  $k_{\text{Exc}}$  of a single-molecule is given by the product of the absorption cross-section and the applied excitation intensity. The value is in the range of  $10^7 \text{ s}^{-1}$  for typical organic fluorophores  $k_{\text{Exc}}$  under moderate excitation intensities (1  $\text{kW}/\text{cm}^2$ ). After excitation, according the Franck-Condon principle,<sup>[47]</sup> the molecule relaxes back into the first excited state  $S_1$  with an internal conversion rate  $k_{\text{Ic}}$  of  $< 10^{12} \text{ s}^{-1}$  (green arrows, Figure 2.1), which is followed by vibrational relaxation into the vibrational ground state of the  $S_1$ -state with rate constant  $k_{\text{vib}}$  of  $< 10^{11} \text{ s}^{-1}$  (blue arrows, Figure 2.1). Residing in this state, the molecule can return to the electronic ground-state  $S_0$  via different pathways: (i) The molecule can undergo a non-radiative process with the rate constant  $k_{\text{Nr}}$ , that is typically in the order of  $10^6 - 10^9 \text{ s}^{-1}$  for organic fluorophores (please note that rate constant for this process is strongly dependent on the structure of the molecule and can be up to  $10^{12} \text{ s}^{-1}$ ). (ii) The molecule can undergo a forbidden spin reversion, also called intersystem crossing into the triplet-state  $T_1$  with a rate constant  $k_{\text{isc}}$  in the

range of  $10^5 - 10^{11} \text{ s}^{-1}$ . This will be followed by reverse intersystem crossing, which can be either radiative (Phosphorescence) or non-radiative and is expressed by the rate constant  $k_T$ , which is in the order of  $10^6 - 10^4 \text{ s}^{-1}$ . (iii) The molecule emits a photon, during the relaxation process into the ground state with the radiative rate constant  $k_{FI}$  which is in the order of  $10^6 - 10^9 \text{ s}^{-1}$ .<sup>[48]</sup> In average the emitted photons are shifted to longer wavelengths compared to the absorbed photons (Stokes-shift), which is explained by the Franck-Condon principle. The energy difference of the absorbed photon and the emitted photon is equivalent to the vibrational relaxation of the molecule.<sup>[47]</sup> The molecule has returned to the ground state  $S_0$ , after one of these three processes completing one excitation and relaxation cycle. A single molecule is only capable of emitting one photon at maximum during one cycle, which can be used to identify single molecules via antibunching. The method exploits the fact that a molecule can only emit one photon per laser pulse when the lifetime of its excited state is long compared to the laser pulse duration.<sup>[49-51]</sup>

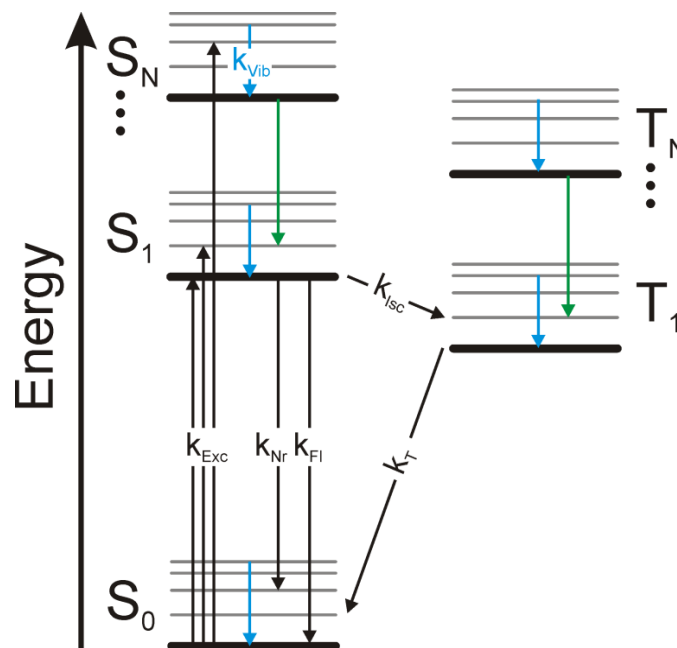


**Figure 2.1.** Schematic drawing of the Jablonski diagram including all important transitions in a molecule.

The difference between a simple molecule and a fluorophore is expressed by a high absorption cross-section and a high fluorescence quantum yield  $\Phi_{FI}$  for the fluorophore, which is given by:

$$\Phi_{FI} = \frac{k_{FI}}{k_{FI} + k_{Nr} + k_{ISC}} \quad (2.2)$$

A fluorophore can emit a distinct number of photons when frequently cycled between the ground and fluorescent excited state. This value is directly linked to the number of cycles a fluorophore can undergo before an irreversible reaction occurs, also referred to as bleaching. Due to the fact that the excited states have a higher reactivity, the fluorophores will bleach faster, if the excited states are more often populated over a certain time period. The excited singlet state  $S_1$  has a lifetime of about several nanoseconds, whereas the excited triplet state  $T_1$  can have lifetimes up to several milliseconds, as can be seen by the orders of magnitude for the rate constants (see above). As a consequence, this leads to infrequent blinking of the fluorophore and the excited triplet state  $T_1$  can be significantly populated over a given time period, which can lead to side reactions, e.g. with oxygen, due to the triplet ground state of oxygen.<sup>[52]</sup>

## 2.2. Photoinduced Electron-Transfer Reactions

Electronic excitation can deposit a high amount of excess energy in the molecular system which facilitates photoinduced electron transfer (PET) reactions that will be discussed in this chapter. PET reactions play an important role in the photosynthesis of plants and for conjugated polymers as low cost, easily processed materials for a diverse set of applications including biomedical sensors, inexpensive solar cells, polymer LEDs, and printable electronics.<sup>[53, 54]</sup> As a central part of this work it is shown that these reactions can also be used to manipulate the photophysics of fluorophores.<sup>[55, 56]</sup> An excited fluorophore  $F^*$  has strongly differing energetically properties compared to its ground state and can undergo electron transfer reactions as depicted in Figure 2.2.

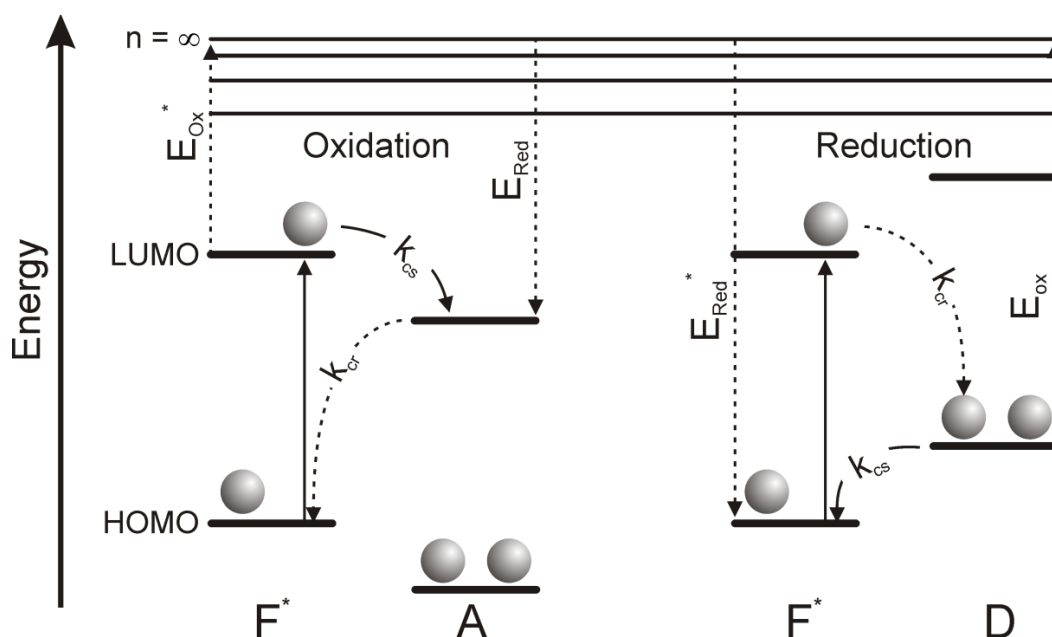


**Figure 2.2.** Energy level scheme for the photoinduced electron transfer between a molecule in the excited state (denoted  $F^*$ ) and an acceptor or donor (denoted A and D), respectively ( $k_{cs}$  rate of charge separation;  $k_{cr}$  rate of charge recombination).

After absorption of a photon, an electron is transferred from the highest occupied molecular orbit (HOMO) into the lowest unoccupied molecular orbit (LUMO). This results in a lower ionization energy and therefore a lower oxidation potential  $E_{Ox}^*$  and a higher reducing potential  $E_{Red}^*$  of the excited fluorophore. Provided that a suitable acceptor or donor molecule (denoted A and D, Figure 2.2) is present in the surroundings of the excited fluorophore  $F^*$  it can transfer or accept an electron to the acceptor or from the donor, respectively. In the case of an oxidation of the fluorophore, the electron will be transferred from the LUMO of the excited fluorophore to the LUMO of the acceptor. This process generates a radical cation, i.e., the fluorophore in the state  $F^{\bullet+}$  and a radical anion of the acceptor  $A^{\bullet-}$ . In the event of reduction an electron from the HOMO of a donor molecule will be transferred to the HOMO of the excited fluorophore, resulting in the formation of a radical anion of the fluorophore  $F^{\bullet-}$  and a radical cation of the donor  $D^{\bullet+}$ .<sup>[57]</sup> The kinetics of these electron transfer reactions are expressed through the rate of charge separation  $k_{cs}$  and the rate of charge recombination  $k_{cr}$ . The rate of charge recombination can be neglected in water, because of the fast dissociation processes of ion pairs, due to the high polarity of water.<sup>[58]</sup> The rate of charge separation  $k_{cs}$  can be estimated using the Marcus Theory.<sup>[59]</sup>

$$k_{cs} = Z \cdot \exp\left(-\frac{(\lambda + \Delta G^0)^2}{4\lambda k_b T}\right) \quad (2.3)$$

Where  $Z$  is the collision number of the reactants,  $\lambda$  the reorganization energy,  $k_b$  equals the Boltzmann constant,  $T$  the temperature and  $\Delta G^0$  the free energy change of charge separation. The free energy change  $\Delta G^0$  can be calculated using the classical Rehm-Weller equation:<sup>[60]</sup>

$$\Delta G^0 = e \cdot (E_{Ox} - E_{Red}) - E_{0,0} + \Delta G_{Coul}^0 \quad (2.4)$$

With  $e$  as the unit electrical charge,  $E_{Ox}$  the first one-electron oxidation potential of the donor,  $E_{Red}$  the first one-electron reduction potential of the acceptor,  $E_{0,0}$  the transition energy between the  $S_1$ - and  $S_0$ -state at the vibrational ground state and  $\Delta G_{Coul}^0$  the coulomb term, which accounts for the electrostatic interaction between the reactants. The transition energy  $E_{0,0}$  can be estimated from the mean energy of the maximum absorption and emission, while  $E_{Ox}$  and  $E_{Red}$  can be measured using cyclic voltammetry.<sup>[61, 62]</sup> Since the free energy change  $\Delta G^0$  is also found in the exponential term of equation (2.3) it determines the order of magnitude of the charge separation constant  $k_{cs}$ , whereas the collision number  $Z$  is directly proportional to  $k_{cs}$ . Hence, with  $\Delta G^0$  and equation (2.4) a first estimation on the efficiency of a photoinduced electron transfer reaction is possible.

### 2.3. The Reducing and Oxidizing System (ROXS)

To gain control over the fluorescence properties of fluorophores, e.g. the blinking and bleaching, the rate constants of a fluorophore must be accessible. For example to reduce blinking and bleaching, the rate constant  $k_{Isc}$  into the triplet state  $T_1$  has to be as low as possible, whereas the rate constant  $k_T$  from the triplet state  $T_1$  into the ground state  $S_0$  has to be as high as possible. Further, the lifetimes of the excited states have to be small, meaning that all rates depopulating the excited states have to be very high. These rate constants are intrinsic properties of the fluorophores and are difficult to alter. However, additional (non-reactive or short-lived) states besides  $S_0$ ,  $S_1$  and  $T_1$  can be assumed, which can change the probability for a molecule to reside in an excited state or undergo intersystem crossing into the triplet state.

Considering a photoinduced reaction from an excited state to a non-absorbing intermediate state and then back to the ground state would yield an additional rate constant  $k_{In}$  from the excited states into the intermediate state and a rate constant  $k_{Back}$  back from the intermediate state to the ground state. Assuming these rate constants  $k_{In}$  and  $k_{Back}$  are controllable, will result in the following: First, the rate constant  $k_{In}$  will control the number of cycles a fluorophore can undergo between the ground state  $S_0$  and the excited states  $S_1$  and  $T_1$ , before it enters the intermediate state. Therefore the number of emitted photons can be controlled. Further, the lifetime of the excited states will be controlled and can be reduced, due to the additional rate constant  $k_{In}$ . Second,  $k_{Back}$  controls the time the molecule will spend in the intermediate state. These considerations can be experimentally realized by introducing a reducing and oxidizing system (ROXS) utilizing the concept of photoinduced electron transfer reactions: thereby radical conformations of the fluorophore are considered as intermediate states (see Figure 2.3 and P1) and are hence integrated into the energetic diagram of a fluorophore.

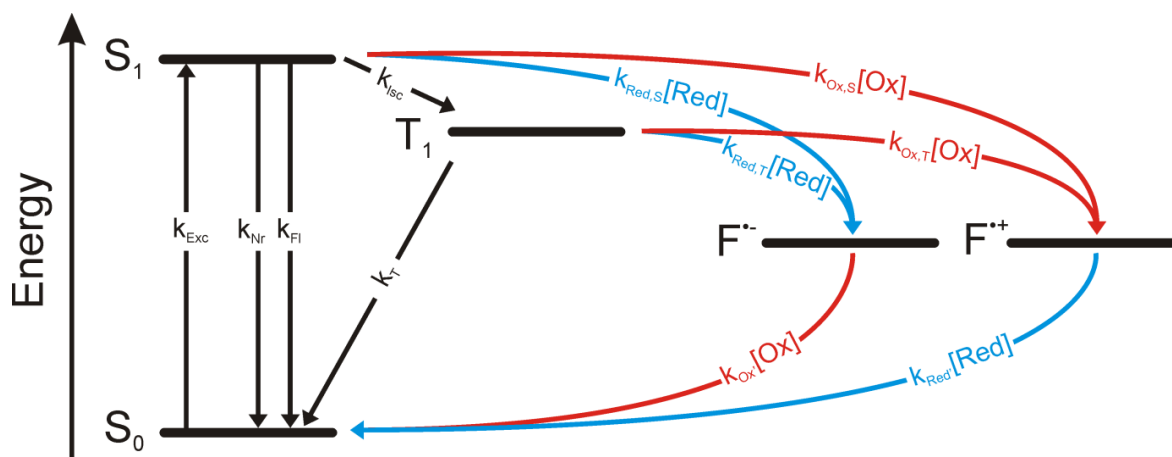


**Figure 2.3.** Schematic drawing of photoinduced processes of common organic fluorophores including radical states. After excitation to the first excited singlet state ( $S_1$ ), fluorescence is emitted at rate  $k_{Fl}$  or the molecule returns to the ground state via non-radiative processes at rate  $k_{Nr}$ . Intersystem crossing competes with fluorescence and non-radiative processes and leads to the infrequent formation of triplet states  $T_1$  with rate constant  $k_{Isc}$ . With ROXS, electron transfer reactions occur; either through reduction (blue arrows starting from the  $S_1$ - and  $T_1$ -State) forming a radical anion  $F^{\bullet-}$  or through oxidation (red arrows starting from the  $S_1$ - and  $T_1$ -State) yielding a radical cation  $F^{\bullet+}$ . The two possible radical ions are recovered to the singlet ground state by the respective oxidation (in case of a radical anion, red arrow starting from  $F^{\bullet-}$ ) or reduction (in case of a radical cation, blue arrow starting from  $F^{\bullet+}$ ).

Experimentally, buffer additives were used, which contain reducing and oxidizing agents concurrently. If the fluorophore is excited and remains in the excited singlet state  $S_1$  or excited triplet state  $T_1$ , there is a certain probability that it will undergo with a charge separation (rate  $k_{cs,Ox}$ ) into the oxidized state  $F^{\bullet+}$  or into the reduced state  $F^{\bullet-}$  (rate  $k_{cs,Red}$ ). Neglecting side reactions, the fluorophore will reside in the radical state until a reaction re-populates the electronic ground state, induced by the respective redox agent: a reductant in the case of a radical cation or an oxidizing agent in the case of a radical anion (denoted with the rates  $k_{cs,Red'}$  and  $k_{cs,Ox'}$ , respectively). The magnitude of these four charge separation rates are mainly dependent on the free energy changes of the electron transfer reaction  $\Delta G^0$  and the concentrations of the reducing and oxidizing agents. This opens the possibility to control the rates by simply alter the concentrations of the reducing and oxidizing agent (see equation (2.3)). Hence, rate constants  $k_{Ox}$ ,  $k_{Red}$ ,  $k_{Ox'}$  and  $k_{Red'}$  can be defined, which are independent of the reductant and oxidant concentrations as follows:  $k_{cs,Ox} = k_{Ox} \cdot [Ox]$ ,  $k_{cs,Red} = k_{Red'} \cdot [Red]$ ,  $k_{cs,Ox'} = k_{Ox'} \cdot [Ox]$  and  $k_{cs,Red'} = k_{Red'} \cdot [Red]$ , where  $[Red]$  and  $[Ox]$  describes the reductant and oxidant concentrations, respectively. Further, it can be distinguished between reduction or oxidation from the excited singlet state  $S_1$  or the excited triplet state  $T_1$  by introducing the rate constants  $k_{Ox,S}$ ,  $k_{Ox,T}$ ,  $k_{Red,S}$  and  $k_{Red,T}$  (see Figure 2.3). These newly defined rate constants are only dependent on the free energy change, which can be estimated using equation (4). So, a comparison can be made with values given in the literature (see ref.<sup>[63]</sup>), evidencing that a broad range is covered (over three orders of magnitude) for the reaction rate constants, starting from  $\sim 0.01 \cdot 10^9 \text{ M}^{-1} \text{ s}^{-1}$  at  $\Delta G^0 = +0.15 \text{ eV}$  going to  $\sim 20 \cdot 10^9 \text{ M}^{-1} \text{ s}^{-1}$  at  $\Delta G^0 = -1 \text{ eV}$ .

### 3. Materials and Methods

In this chapter, an overview of the experimental apparatus, analysis and preparation procedures, which are used for investigating the photophysics of single fluorophores, the applicability of ROXS in single-molecule investigations, and super-resolution techniques will be given.

#### 3.1. Confocal Microscopy

The center of the setup is an inverted microscope (IX70, Olympus), where the fluorophores are excited using a collimated laser beam from a white light laser source (SuperK Extreme, Koheras). The beam is expanded to a diameter of  $\sim 1$  cm by a single-mode fiber and coupled into the objective via an appropriate dichroic mirror through the back aperture of the microscope. This excitation scheme results in a diffraction limited excitation volume. The wavelengths are chosen by an acousto optical tunable filter (AOTF, A.A. Opto-Electronics, France) for excitation of the different fluorophores. A xy-piezotable is used for the surface scan of a probe, which gives the ability to move the probe about  $100 \mu\text{m}$  in x -and y-direction, with sub-nanometer resolution. Hence, the possibility is given to adjust one immobilized single fluorophore inside the excitation focus. The fluorescence is collected by the same objective, spatially filtered by a  $50 \mu\text{m}$  pinhole (defining the observation volume), and spectrally filtered by an appropriate dichroic mirror in combination with emission band pass filters. The resulting fluorescence is imaged onto different avalanche photodiodes (APD) (see Figure 3.1). The control of the AOTF and piezotable, as well as the signal acquisition is realized by an analog I/O card (National Instruments). Data acquisition and analysis is performed with a self-written LabVIEW software package (National Instruments). Details can be found in P1-5. The confocal microscope is used for surface based measurements, as well as for solution based measurements. Whereas on surface based measurements long-term observations of single molecules can be established, a large statistic is gained in solution based measurements, e.g. measuring fluorescence resonance energy transfer (FRET) with alternating laser excitation (ALEX)<sup>[64, 65]</sup> or fluorescence correlation spectroscopy (FCS)<sup>[66-68]</sup>. During the investigation of photophysics different configurations of the microscope are used. Details are found in materials and methods of the respective publication.

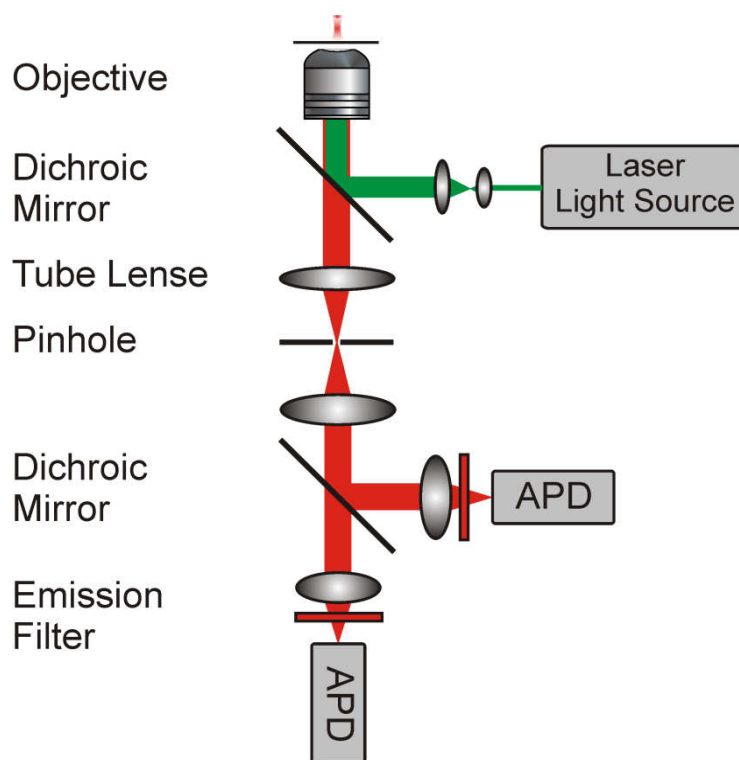


**Figure 3.1.** Schematic drawing of a typical confocal setup. The excitation and emission pathways are represented in green and red, respectively (APD, avalanche photodiode).

### 3.2. Total Internal Reflection Fluorescence Microscopy

The setup for an objective type total internal reflection fluorescence microscope is based on a widefield setup, which is similar to a confocal microscope, but in contrast to the confocal microscope, the whole field of view is illuminated.<sup>[69-71]</sup> This is achieved by focusing the excitation light onto the back focal plane of the objective (see Figure 3.2).

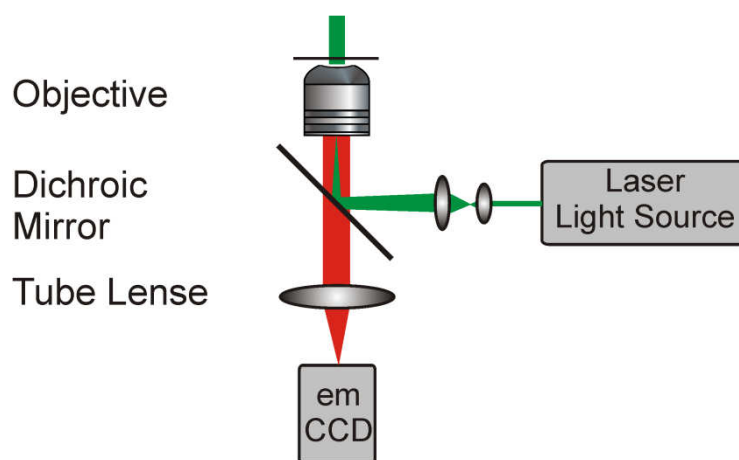


**Figure 3.2.** Schematic drawing of a typical widefield setup. The excitation and emission pathways are represented in green and red, respectively (emCCD, electron-multiplying charged coupled device).

Total internal reflection will take place between the glass of the coverslide and the solution of the probe, if the excitation beam travels at a high incident angle through the solid glass coverslide. Refractive index differences between the glass and water phases regulate how the light is refracted or reflected at the interface as a function of incident angle. At a specific critical angle, the beam of light is totally reflected from the glass/water interface, rather than passing through and refracting in accordance with Snell's Law. The reflection generates a very thin electromagnetic field (spatial width in the range of the excitation wavelength) in the aqueous medium of the probe, which has an identical frequency to that of the incident light. This field, called the evanescent wave or field, undergoes an exponential intensity decay with increasing distance from the surface (see Figure 3.3). This evanescent field is the great advantage in contrast to standard epi-fluorescence microscopy, due to the low background and increased signal. Furthermore, modern objectives exhibit an adequate numerical aperture ( $NA > 1.4$ ) allowing the laser directly coupled into the objective.<sup>[71, 72]</sup> After excitation the fluorescence is again collected by the same objective and detected by a highly sensitive electron-multiplying charged coupled device (emCCD).

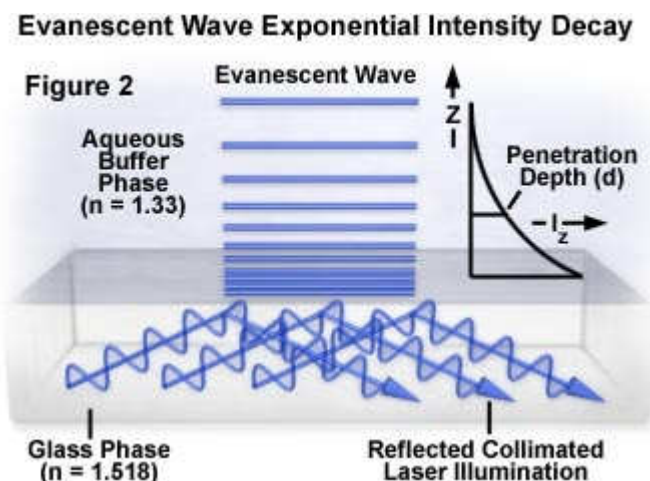


**Figure 3.3.** Schematic drawing of an evanescent wave, due to total internal reflection (Figure taken from: <http://www.olympusmicro.com/primer/techniques/fluorescence/tirf/tirfintro.html>).

### 3.3. Super-Resolution Microscopy

The super-resolution microscopy technique used within this work is based on widefield microscopy in combination with TIRF. Super-resolution microscopy that circumvents the diffraction limit of light by subsequently localizing single photoswitchable molecules has opened up a new field merging single-molecule fluorescence spectroscopy with diffraction-limit breaking microscopy.<sup>[28, 32, 33, 73]</sup> The common principle of subdiffraction resolution microscopy by subsequent single-molecule localizations is that only one fluorophore is active for a diffraction limited area at any given time and this fluorophore is localized by imaging with a sensitive camera (see Figure 3.4).



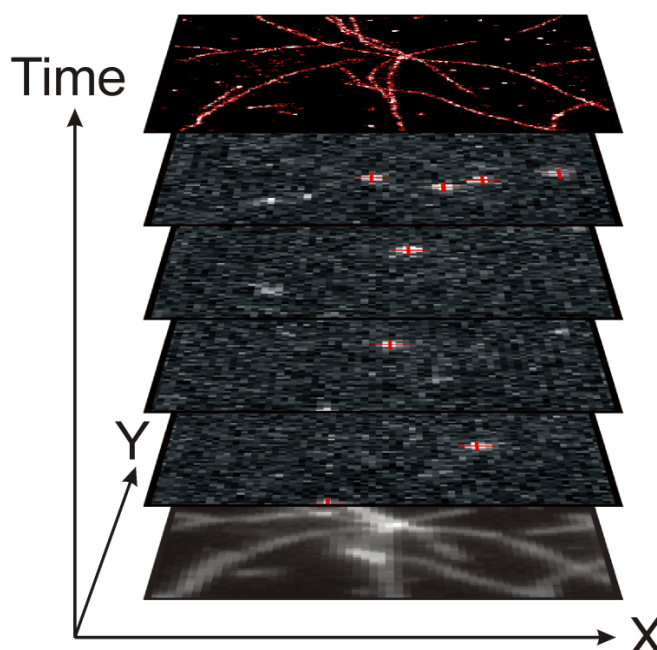


**Figure 3.4.** Super-resolution microscopy based on statistical optical reconstruction microscopy (STORM).<sup>[28]</sup> A sub ensemble of fluorescent molecules is switched into the fluorescent state and subsequently localized with nanometer precision. These localizations are summed up for reconstructing a super-resolution image, where the resolution is given by the localization precision of the fluorophore.

Thus, it is required that at any moment the majority of fluorophores are prepared in a non-fluorescent dark state. Therefore, the fluorescence of the molecules within the area of one point-spread-function is separated in time by switching the largest fraction of molecules into a dark state (Figure 3.4, second frame). This switching is achieved, for example, using photochromic fluorophores (PALM, STORM, FPALM, dSTORM)<sup>[28, 31-33, 36]</sup> or generic metastable dark states of the fluorophores such as radical ion states (Blink-Microscopy, GSDIM).<sup>[34, 35, 74, 75]</sup>

For reconstruction of super-resolution images, movies are recorded of the structure under investigation (lower frame in Figure 3.4), with frame rates up to 1000 frames/s and about 10000 frames overall. Movies are analyzed by custom-made software written in LabView 7.1. Commonly the first 20 frames are discarded since in the beginning all molecules are in the active state and photodynamic equilibrium is achieved after about 20 frames with most molecules being prepared in the off-state. In some cases, if the fluorophore density is too high to resolve single emitters, the first up to 1500 frames will be discarded. The spot finding routine involves a lower and upper threshold as well as a range for the size of the area above the lower threshold. However, in cases of high or inhomogeneous background a flexible threshold is used. In this algorithm the movie is analyzed frame by frame and each peak intensity within a frame is compared to its environment ( $7 \times 7$  pixels). When a certain contrast value is reached, the spot is considered for further analysis. Two-dimensional Gaussian fitting yields the position of the molecules that are histogrammed in 15-nm pixels for image reconstruction (upper frame in Figure 3.4). To further exclude events with two molecules being simultaneously active within one diffraction limited area and to remove cases when the two-dimensional Gaussian fitting does not converge, a circularity criterion of the identified spots has to be met.

### 3.4. Single-Molecule Immobilization

As mentioned in section 3.1, single fluorophores can be investigated in solution and on the surface using a confocal microscope. However, solution based measurements are limited to short acquisition times, due to the short transient time through the diffraction limited observation volume of diffusing molecules. Kinetics are not observable with a typical time constant above 1 ms. Therefore single molecules have to be immobilized on the surface in a way, that the influence of the surface upon the photophysics is minimal.<sup>[76]</sup> During the work presented in this thesis a biotin/streptavidin protocol is used. The following steps are used to prepare the glass surface: (i) The surface is treated with hydrofluoric acid (HF, 100 mM) for cleaning purposes and to favor a negatively charged surface under water, due to negatively charged SiO<sup>-</sup>. (ii) A mixture with a ratio of 5:1 of bovine serum albumin (BSA) and BSA labeled with a biotin in standard phosphate buffered saline (PBS) buffer is incubated on the surface for at least 6 hours. (iii) A streptavidin solution in PBS with a concentration of 0.1 mg/ml is incubated on the surface for about 5 minutes to bind the streptavidin on the biotinylated BSA. (iv) A 10<sup>-9</sup> – 10<sup>-10</sup> M concentrated PBS solution with a 40-60 bp dsDNA labeled with a biotin and the fluorophore (IBA GmbH) under investigation is incubated on the surface, while simultaneously scanning the surface. Finally, the surface will be washed, if the density of the surface is appropriate for single molecule fluorescence spectroscopy (~ 1 molecule/μm<sup>2</sup>). During each preparation step the surface is washed for three times with PBS. This procedure results in an immobilization of a fluorophore-DNA construct as shown in Figure 3.5 and assures that the molecule is immobilized on the surface, that non-specific interaction with the surface will occur and that the molecule is still in the buffer solution of choice.<sup>[77]</sup> Further details on the procedure are provided in the materials and methods sections of the publications.

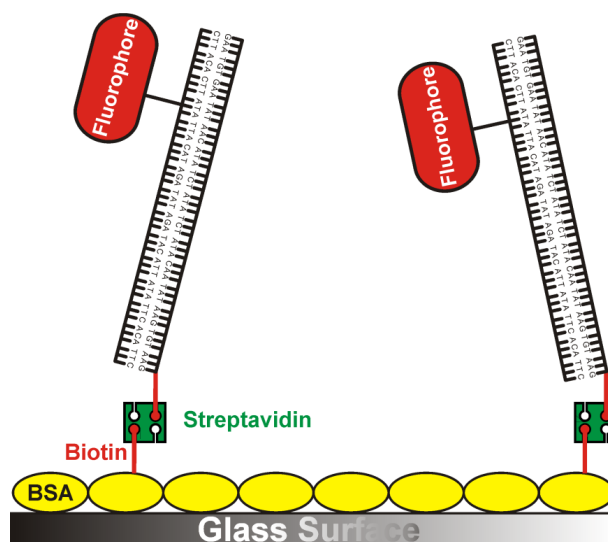


**Figure 3.5.** Schematic drawing of the immobilization technique by using biotin/streptavidin coupling. The density of the surface can be adjusted by varying the ratio of BSA/biotinylated-BSA. a rigid 40-60 bp dsDNA is used to keep a certain distance between the fluorophore and the surface.

### 3.5. Auto-Correlation Analysis

A short introduction is given into auto-correlation analysis (ACA), due to the extensive use of ACA for investigating the photophysics of fluorophores. ACA is an experimental method for

investigating kinetic processes, which analyzes the statistical fluctuations of the fluorescent signal. In ACA the fluorescence signal is analyzed by utilizing an auto-correlation of one fluorescence signal or a cross-correlation of two fluorescence signals. An intensity signal generated by scattered light from a single molecule was the first application of an auto-correlation, followed by investigating the fluorescence signal of freely diffusing fluorophores, also referred to as fluorescence correlation spectroscopy (FCS).<sup>[78, 79]</sup> By the use of the correlation of the intensity signal, information can be acquired on the average transition time of a molecule through the laser focus and typical transition times between fluorescent and non-fluorescent (quenched) conformations of single fluorophores; e.g. triplet-transitions or other photophysical transitions within a fluorophore or interactions of guanosin and tryptophan with oxazine fluorophores.<sup>[80-82]</sup> These fluctuations can be analyzed using the second order auto-correlation function:

$$G(\tau) = \frac{\langle I(t) \cdot I(t + \tau) \rangle}{\langle I(t) \rangle^2} \quad (3.1)$$

Here,  $I$  denotes the intensity given at a certain time  $t$ . In the case of immobilized molecules, the fluctuations in fluorescence intensity can be assigned to conformational changes between a fluorescent state and a non-fluorescent state, with certain rate constants from one state into another (Figure 3.6.). Hence, the second order auto-correlation function can be written as a sum consisting of several exponential functions with corresponding amplitudes  $A_i$  and characteristic time constants  $\tau_{char,i}$ :

$$G(\tau) = 1 + \sum_{i=1}^n A_i \cdot \exp\left(-\frac{\tau}{\tau_{char,i}}\right) \quad (3.2)$$

Based on the amplitudes  $A_i$  and characteristic time constants  $\tau_{char,i}$  the rate constants from the fluorescent to the non-fluorescent state  $k_{OFF,i}$  and from the non-fluorescent state to the fluorescent state  $k_{ON,i}$  can be derived as follows:

$$\frac{1}{\tau_{char,i}} = k_{OFF,i} + k_{ON,i} \quad \text{and} \quad A_i = \frac{k_{ON,i}}{k_{OFF,i}} \quad (3.3, 3.4)$$

By using equations (3.2 – 3.4) rate constants of different photophysical processes are measured (see details in publications). An example is shown in Figure 3.6, where a typical fluorescence transient is shown of an immobilized fluorophore exhibiting frequent blinking together with an autocorrelation analysis of the fluorescent signal (upper right panel in Figure 3.6).

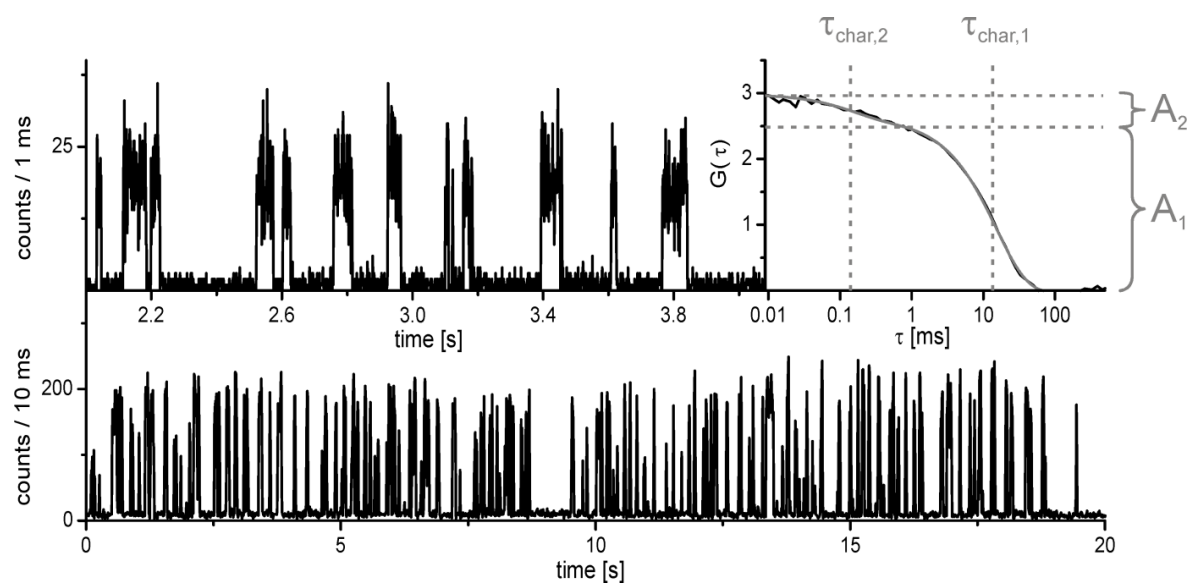


**Figure 3.6.** A typical fluorescent transient is shown of an immobilized fluorophore exhibiting frequent blinking. The fluorescent transient below is binned into 10 ms, the transient in the upper left panel shows a magnified view and is binned into 1 ms. The second order autocorrelation function is shown in the upper right panel (black curve), together with a two-exponential decay (grey curve).

## 4. Results

In this chapter an overview and summary of the experimental results studying single-molecule redox reactions with ROXS and its applicability is given. At first, the influence of ROXS on fluorophores is investigated and allows generating ultrastable fluorophores. The positive interaction of ROXS is demonstrated for a broad range of organic fluorophores (P1). Second, exquisite control is achieved of the fluorescence of ordinary oxazine dyes for single-molecule switching and super-resolution (P2). Additionally, it is shown, that oxazine dyes can be used as single-molecule redox sensors (P3), which is exploited to resolve the antifading mechanism of Trolox (P4). Finally, intrinsic resolution enhancing probes are developed for confocal microscopy, based on an energy transfer blockade probe (ETBP) in combination with ROXS (P5).

### 4.1. Stable Fluorescent Fluorophores (P1)

As will be shown ROXS can be used to substantially increase the photostability of different organic fluorescent dyes in aqueous surrounding. Simultaneously, blinking is dramatically reduced, enabling fluorescence spectroscopy and imaging applications at higher fluorescence count rates over extended periods of time as was ever demonstrated before.

The success of the approach is demonstrated by single-molecule fluorescence spectroscopy of oligonucleotides labeled with different fluorophores types, that is, cyanines, (carbo-)rhodamines, and oxazines, in aqueous solvents; the fluorescence of individual fluorophores can be observed for minutes under moderate excitation conditions with increased fluorescence brightness. Thermodynamic considerations of the underlying redox reactions support the model, yielding a comprehensive picture of blinking and photobleaching of organic fluorophores (see P1).

#### 4.1.1. Depopulation of the Excited States

It is known, that the excited states play a crucial role in photobleaching and blinking. Owing to its longer lifetime, the excited triplet state  $T_1$  is considered to be the photochemically most active state. Quenching of  $T_1$  by molecular oxygen, for example, can generate reactive singlet oxygen, and therefore oxygen is removed in demanding applications, for example, with the aid of an enzymatic oxygen-scavenging system.<sup>[52]</sup> The disadvantage of oxygen removal, however, is the increase of the triplet state lifetime with negative effects for the brightness of the fluorophore and increased probability for subsequent reactions from the triplet state. Alternatively, reducing agents such as ascorbic acid (AA), N-propyl gallate, b-mercaptoethanol, and Trolox (TX) have been used to recover photoionized fluorophores and to remove singlet oxygen. However, the success of this strategy is strongly dependent on the fluorescent dye used, and sometimes photobleaching is even promoted.<sup>[42, 83, 84]</sup>

The key to stable fluorescent fluorophores is given by the usage of photoinduced electron transfer reactions with high rate constants for a quenching of  $T_1$  to a radical state, followed by a fast recovery to the ground state  $S_0$ .

Therefore a first approximation regarding the free energy change for each reaction step is made using the Rehm-Weller equation (see equation (4)). For three dyes from three different chemical classes approximations are made for each charge separation steps. The three chemical classes are: first Cy5 dye from the class of cyanines, second ATTO647N dye from the class of carbo-rhodamines and third MR121 dye from the class of the oxazines (structures given in Figure 4.1).

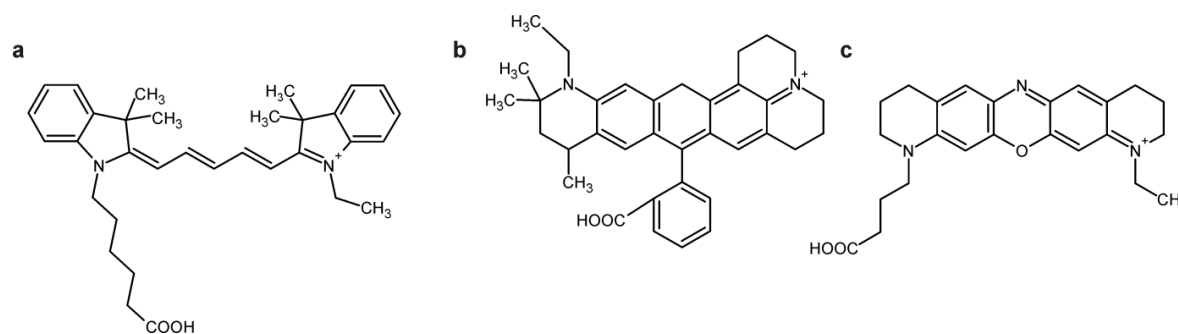


**Figure 4.1.** Chemical structures from three red absorbing typical dyes used in SMFS. (a) Cy5 (cyanine),<sup>[85]</sup> (b) ATTO647N (carbo-rhodamine),<sup>[86]</sup> (c) MR121 (oxazine).<sup>[43]</sup>

The following potentials are given versus saturated calomel electrode (SCE). Ascorbic acid (AA, oxidation potential  $E_{\text{Ox}} \approx 0.06 \text{ V}$ )<sup>[87]</sup> was used as a reducing agent and 1,1'-bipyridinium dichloride hydrate (methylviologen, MV, reduction potential  $E_{\text{Red}} \approx -0.69 \text{ V}$ )<sup>[57]</sup> was used as an oxidizing agent, respectively. The reduction and oxidation potentials of the dyes were measured with cyclic voltammetry.<sup>[88]</sup> All potentials are summarized in Table 4.1, as well as the free energy change  $\Delta G^0$  for each reaction step. The energy for the excited triplet state  $T_1$  is estimated to be  $\sim 0.3 \text{ eV}$  less than  $E_{0,0}$  energy.<sup>[89]</sup>

**Table 4.1.** Reduction, oxidation potentials and free energy changes  $\Delta G^0$  for the three dyes Cy5, ATTO647N and MR121 (for details on calculations see P1 and P2).

Dye	$E_{0,0}$ [eV]	$E_{\text{Red}}$ [V]	$E_{\text{Ox}}$ [V]	$\Delta G^0_{\text{Red,S}}$ [eV]	$\Delta G^0_{\text{Red,T}}$ [eV]	$\Delta G^0_{\text{Ox,S}}$ [eV]	$\Delta G^0_{\text{Ox,T}}$ [eV]	$\Delta G^0_{\text{Red}'}$ [eV]	$\Delta G^0_{\text{Ox}'}$ [eV]
Cy5	1.88	-0.84	0.97	-0.98	-0.68	-0.22	+0.06	-0.91	-0.15
ATTO647N	1.90	-0.64	1.11	-1.20	-0.90	-0.10	+0.20	-1.05	+0.05
MR121	1.86	-0.42	1.31	-1.38	-1.08	+0.14	+0.44	-1.25	+0.27

With the free energy changes, predictions can be made on the efficiency of the according electron transfer reaction rate constants. If the free energy change becomes negative, the reaction will be exergonic, meaning the electron transfer process will become very efficient. For the cyanine dye Cy5 almost every reaction step is exergonic, except the oxidizing step from the  $T_1$ -state, which is slightly endergonic. However, a fast depopulation of the  $T_1$ -state through the radical anion state is still given, as it is the same for the carbo-rhodamine ATTO647N. In contrast, the oxazine dye MR121 exhibits a positive free energy change for the oxidation process into the radical cation state, as well as for the re-oxidizing step from the radical anion state. Therefore, the  $T_1$ -state of the oxazine MR121 cannot be efficiently depopulated by the use of AA and MV as reducing and oxidizing agents, respectively.

#### 4.1.2. Minimizing Photobleaching and Blinking

In the following, single molecule fluorescence transients are shown of ATTO647N recorded in aqueous buffer demonstrating the concept.

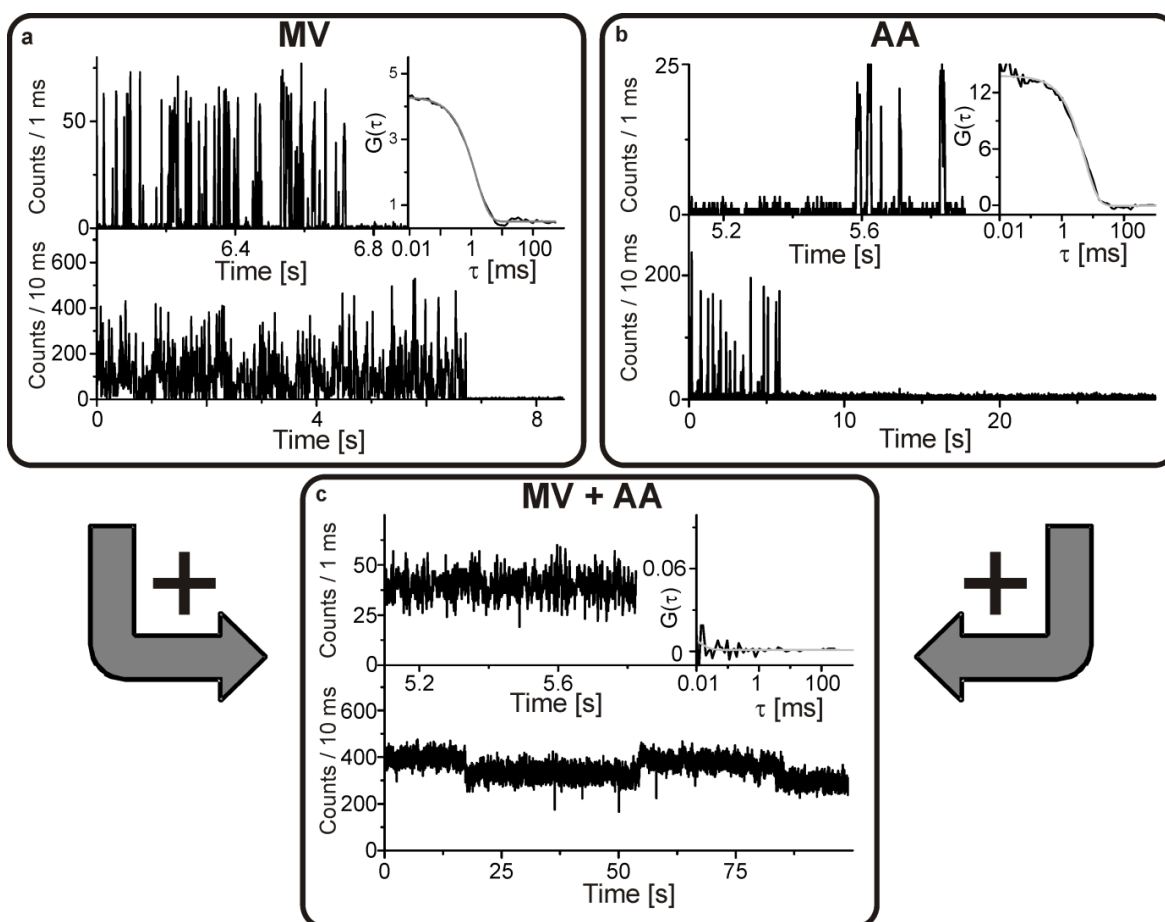


**Figure 4.2.** Fluorescence transients of ATTO647N-labeled DNA immobilized in aqueous environment under the following conditions: a) oxygen removed plus 1 mM MV, b) oxygen removed plus AA (1 mM), and c) oxygen removed plus MV (1 mM) and AA (1 mM). The bottom trace is binned in 10 ms, the left inset provides a magnified view with 1 ms resolution, and the right inset shows the second-order autocorrelation function  $G(\tau)$  with monoexponential fit. Samples were excited at 635 nm with an average excitation intensity of approximately  $2 \text{ kWcm}^{-2}$ .

Figure 4.2a shows a fluorescence transient of ATTO647N after removal of oxygen in buffer containing 1 mM MV as oxidizing agent. Pronounced blinking on the millisecond time scale is visible in the magnified view (left inset of Figure 4.2a). Autocorrelation analysis (right inset) and monoexponential fitting reveals an OFF state with a lifetime  $\tau_{\text{off}} = 8 \pm 1 \text{ ms}$ . This OFF-state is ascribed to photoinduced oxidation and the formation of a radical cation. The formation of radical cations of cyanines and rhodamines with lifetimes in the millisecond range has been known since the 1970s when the dyes were investigated by laser-flash photolysis.<sup>[14, 15]</sup> Their existence has also been suspected on the level of single molecules.<sup>[90-97]</sup> Here, however, blinking due to reversible electron transfer is shown to result in monoexponential kinetics.<sup>[98-100]</sup> In analogy, ATTO647N exhibits similar blinking after removal of oxygen and the addition of the reducing agent AA (1 mM), likely because of the reversible formation of radical anions ( $\tau_{\text{off}} = 28 \pm 7 \text{ ms}$ ). The assignment of the OFF-state to a radical ion is strongly supported by the transient in Figure 4.2c, which depicts a fluorescence transient of ATTO647N after oxygen removal and addition of both AA (1 mM) and MV (1 mM). The molecule emits practically without blinking throughout the 100 s recording time. The same investigation upon the cyanine dye Cy5 results in the same behaviour (see supporting informations of P1). In contrast MR121 shows stable fluorescence under standard PBS-buffer and a pronounced but also long lasting blinking with ROXS buffer conditions (1 mM AA, 1 mM MV and oxygen removal, see Figure 4.3a,b), which can be assigned to an inefficient

depopulation of the  $T_1$ -state. An explanation for the deviating behavior of MR121 is explained in a later caption.

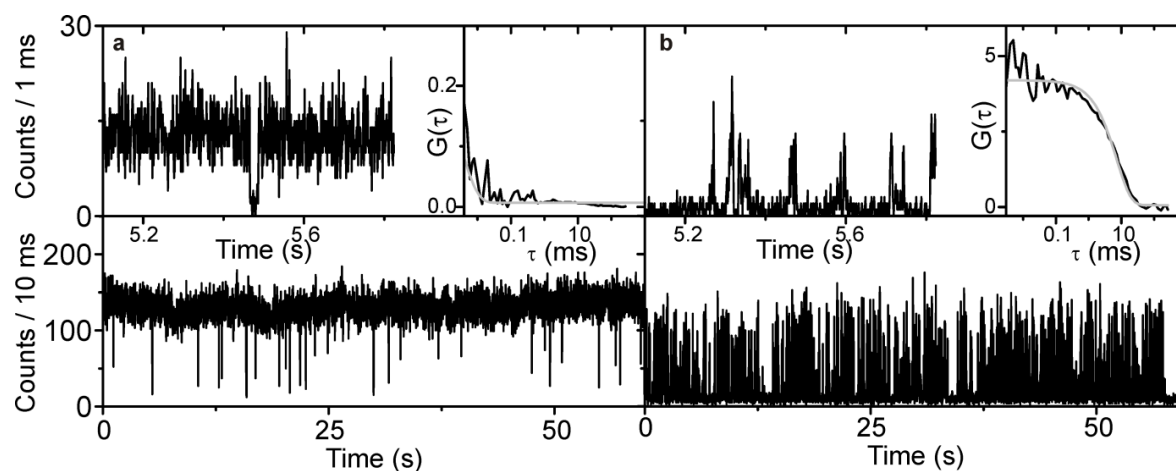


**Figure 4.3.** Fluorescence transients of MR121 labeled DNA in ambient PBS (a) and in the presence of ROXS and oxygen removal (b) obtained with a confocal microscope. The upper left inset shows a magnified view with 1 ms binning. The upper right inset shows the autocorrelation function and a monoexponential fit (gray). The blinking of MR121 is not completely suppressed by ROXS, probably because reduced MR121 is not efficiently recovered by MV due to the very high lying reduction potential of MR121 with  $E_{\text{Red}} = -0.42$  V. Samples were excited at 635 nm with an average excitation intensity of approximately  $2 \text{ kWcm}^{-2}$ .

This investigation was done for several other fluorophores as shown in the supporting information of P1. Additionally, photostabilities for different fluorophores are compared under various conditions, i.e. (i) in PBS buffer, after removal of oxygen and (ii) addition of 1 mM AA, (iii) addition of 1 mM MV, and (iv) after adding ROXS (1 mM AA and 1mM MV). Average overall photon counts from different red and green fluorophores are presented in Figure 4.4a and b, respectively. In case that no bar is visible the detected number of photons is below 1000 (e.g. Cy5 in PBS). For all fluorophores except for the oxazine derivative MR121, we find increased photostability using ROXS compared to PBS buffered solution. Moreover, for all fluorophores the photostability is increased using both reducer (AA) and oxidant (MV) instead of using reducer or oxidant only. Although a similar effect was found regarding blinking reduction for shorter wavelength fluorophores such as Cy3B and ATTO565, the photostabilizing effect was not as pronounced (Figure 4.4b). For details on data acquisition and analysis, see supporting informations of P1.



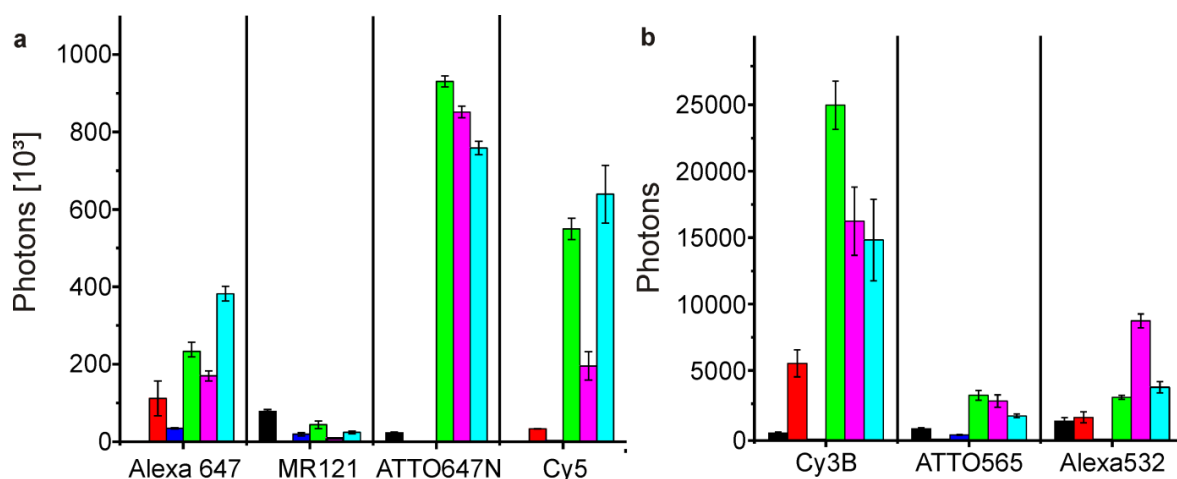


**Figure 4.4.** Average photon counts per molecule (a) for the red fluorophores Alexa647, MR121, ATTO647N, and Cy5, and (b) for the green/yellow fluorophores Cy3B, ATTO565, and Alexa532 were obtained from at least three photobleaching movies using objective-type total internal reflection microscopy. Measurements were carried out in PBS (black bars), oxygen-depleted PBS with 1 mM AA (red), with 1 mM MV (blue), with ROXS (1 mM AA plus 1 mM MV) (green), or 2 mM TX plus 1 mM MV (cyan), or 2 mM TX (magenta).

#### 4.1.3. Applicability in Biological Systems

ROXS has to work under physiologically relevant buffer conditions, without influencing the biological system. Further it is known, that methyl viologen interacts with the DNA. Therefore, investigations on Holliday junctions<sup>1</sup> were performed to demonstrate the applicability of ROXS to biomolecular single-molecule studies. Single Holliday junctions are immobilized and the dynamics are visualized using a Cy3 donor and Cy5 acceptor dye. Fluorescence transients were recorded and the average lifetimes  $\tau$  of the high-FRET and low-FRET states were measured at different MV concentrations (Figure S4, supporting informations of P1). The functioning of the surface immobilization, successful enzymatic oxygen removal, and studies of the dynamics of Holliday junctions, which is independent of MV concentration, however, indicate that many biological functions are not influenced by the presence of ROXS at low millimolar concentrations.

## 4.2. Controlling the Fluorescence (P2)

Within this chapter it is shown that ROXS can be used to control the blinking kinetics of ordinary oxazine dyes. As discussed in chapter 4.1 the oxazine dye MR121 exhibits a pronounced blinking upon addition of ROXS in the millimolar range, due to the particular redox potentials. The very similar oxazine dye ATTO655 and the two red-shifted derivatives ATTO680 and ATTO700 are investigated. First it is demonstrated, that ordinary oxazine dyes can act as efficient single-molecule switches that report sensitively on their local redox condition and a detailed picture of the underlying photo-induced and redox reactions is elaborated. Secondly, it is shown that the kinetically parameters can be adjusted in a “continuous switching mode”, also referred to as “blinking”. This “continuous switching mode” is advantageously used for imaging actin filament and actin filament bundles in fixed cells with sub-diffraction limited resolution.

<sup>1</sup> The Holliday junction consists of four DNA strands that hybridize to a four-way junction. In the presence of metal ions like magnesium the junction forms an x-shaped structure with pair wise antiparallel coaxial stacking of the neighboring helices.<sup>[10]</sup> Dynamic flipping of the helices on the ms-timescale leads to the observation of two conformers.

### 4.2.1. Single-Molecule Switching

In order to switch ordinary dye molecules, the generic radical ion states are used as controllable OFF-states. Therefore, single oxazine dyes were attached to biotinylated double-stranded DNA which itself was immobilized on a glass-surface (see chapter 4.3 for details). Measurements were carried out in aqueous buffers which allowed enzymatic oxygen removal and addition of ROXS (AA as reducing agent and MV as oxidizing agent). While it is comparatively simple to prepare a fluorophore in its radical ion state through photo-induced electron transfer with a reductant or oxidant in solution (see P1 and ref. <sup>[35]</sup>, it is challenging to stabilize the radical anion and prevent thermal return to the ground state. This requires careful removal of all electron acceptors from solution. Using enzymatic oxygen scavenging, the potential oxidant oxygen is only removed to low micro molar concentrations.<sup>[101]</sup> Therefore oxazine derivatives are selected with high reduction potential (see MR121, Table 4.1), i.e. the reduced state has a very low energy so that re-oxidation by oxygen with a reduction potential of  $E_{\text{Red}} = -0.57$  V becomes inefficient.<sup>[102]</sup> To describe the photophysical properties of single fluorophores taking into account the interaction with reducing and oxidizing agents, a five-level scheme was used adapted to the thermodynamic parameters of the oxazine derivative ATTO655 (Figure 4.5).

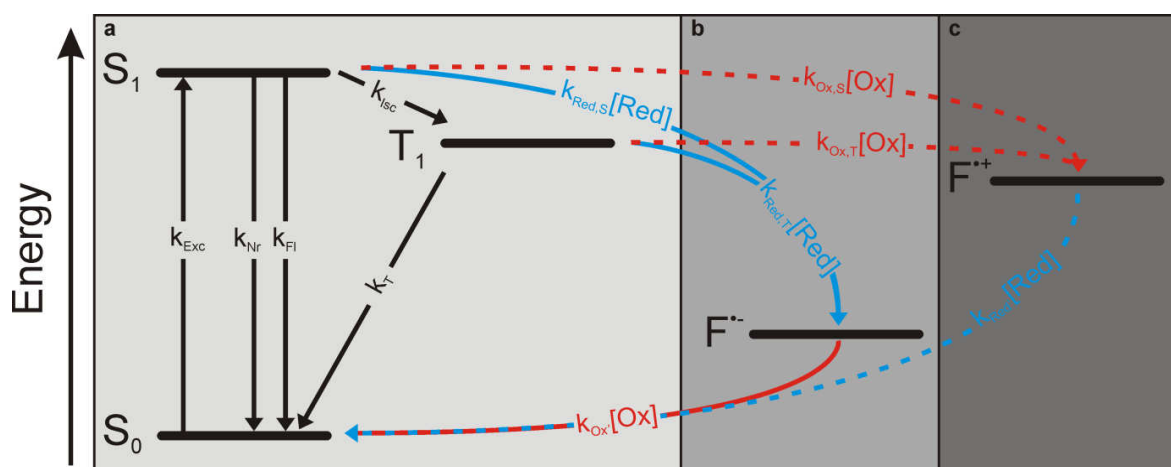


**Figure 4.5.** Scheme of photoinduced processes of the fluorophore ATTO655. After excitation to the first excited singlet state  $S_1$ , fluorescence is emitted at rate  $k_{\text{Fl}}$ . Intersystem crossing competes with fluorescence and leads to the infrequent formation of triplet states  $T_1$  with the rate constant  $k_{\text{Isc}}$  (a). The triplet state is depopulated by intersystem crossing with rate constant  $k_{\text{T}}$  or by electron transfer. This may occur either through reduction by ascorbic acid (AA) forming a radical anion  $F^{\bullet-}$  (b) or through oxidation by methylviologen (MV) yielding a radical cation  $F^{\bullet+}$  (c). The radical ions could be recovered to singlet ground-state fluorophores by the complementary redox reaction. Direct electron transfer from the single manifold ( $k_{\text{Red,s}}$ ,  $k_{\text{Ox,s}}$ ) has to be taken into account at higher redox-agent concentration.

The energy levels were obtained by cyclic voltammetry as well as from steady state absorption and fluorescence spectra and are the same as for the oxazine dye MR121. Hence, the PET through the radical cation state is very inefficient and therefore this path is shaded dark grey (Figure 4.5c). Once the molecule is reduced by AA, it is kept into the radical anion state until it is reoxidized by MV (Figure 4.5b). Due to the low-lying reduced state this reaction step is also inefficient, due to the endergonic free energy change (see Table 4.1). This theory is confirmed by the following measurements. After placing a molecule in the laser focus, addition of AA (100  $\mu\text{M}$ ) as reductant and removing oxygen, single-molecule fluorescence transients such as in Figure 4.6a are obtained. A short fluorescent spike at the beginning is observed terminated by rapid apparent photobleaching.

In the presence of AA and MV (both 100  $\mu\text{M}$ ), however, single ATTO655 molecules show pronounced blinking with typical ON- and OFF-times in the millisecond range (Figure 4.6b).

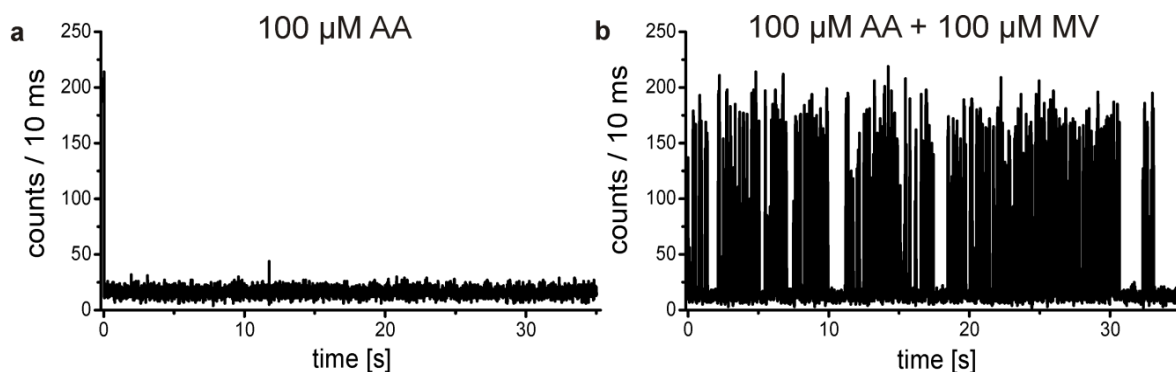


**Figure 4.6.** Fluorescence transients of ATTO655-labeled dsDNA immobilized in aqueous environment after oxygen removal, addition of 100  $\mu\text{M}$  AA (a) and additionally 100  $\mu\text{M}$  MV (b), respectively. The transients are binned in 10 ms. Samples were excited at 640 nm with an average excitation intensity of 1.5  $\text{kW}/\text{cm}^2$ .

To test the hypothesis that ATTO655 in the presence of only AA is not photobleached but indeed switched off to a stable reduced state, surfaces are scanned of immobilized dsDNA doubly labeled with Cy3B and ATTO655 using alternating laser excitation (Figure 4.7).<sup>[103]</sup> Half of the time per pixel, the sample is excited with 533 nm for excitation of the green dye Cy3B, and half of the time the red dye ATTO655 is excited by 640 nm. The first scan (Figure 4.7a) was carried out in PBS containing ambient concentrations of oxygen, in which ATTO655 shows stable emission, to locate the doubly labeled DNAs. Molecules containing only Cy3B (Figure 4.7, green), only ATTO655 (red) or both green and red dyes (yellow) were observed. Before taking the second scan of the same area, oxygen was removed and 100  $\mu\text{M}$  AA was added. Under these conditions, the scanned area shows only green spots because ATTO655 rapidly enters a long-lived dark state (Figure 4.7b). The green spots exhibit some dark pixels due to the transient formation of radical anions (see P1). Since the sample can slightly move upon buffer exchange, the green dye merely served to identify the same molecule positions as in the previous scan. After all red dyes are switched off, the buffer is exchanged again by washing the surface three times with PBS, which contains oxygen. In the subsequent scan (Figure 4.7c), all ATTO655 molecules reappear. This procedure can be repeated several times and three such cycles with perfect switching of ATTO655 (see circled molecules) are shown in Figure 4.7a-g.

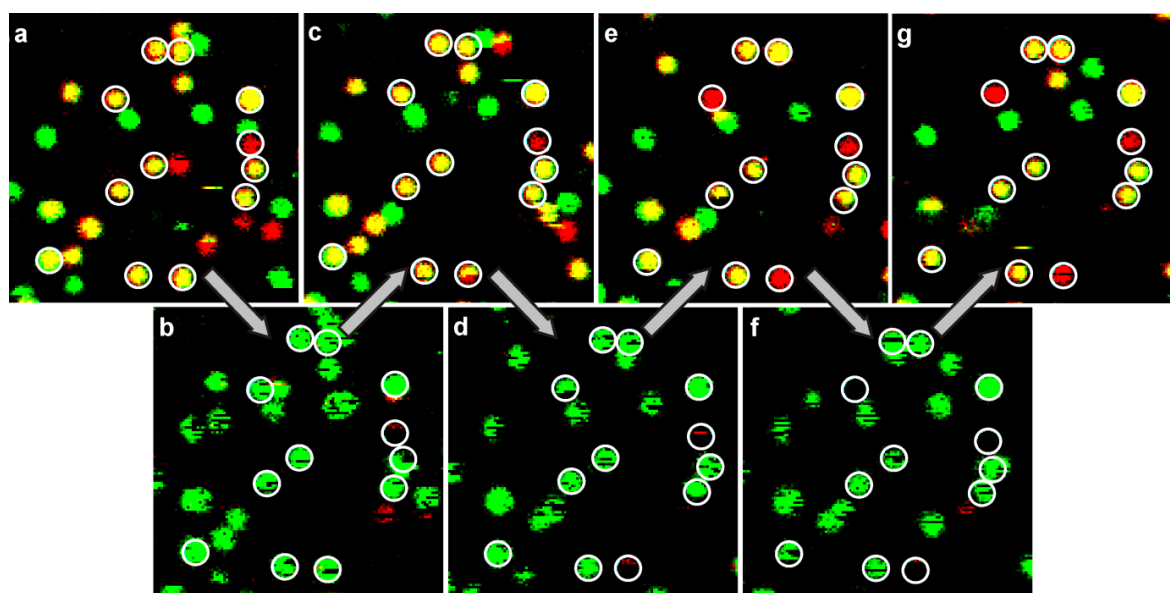


**Figure 4.7.** Confocal fluorescence images ( $6\ \mu\text{m} \times 6\ \mu\text{m}$ ) of ATTO655-Cy3B-labeled dsDNA. The colors green and red encode for the overall fluorescence intensity after green and red excitation, respectively. dsDNA bearing the two dyes are hence visible as yellow spots. (a) The first image was acquired in PBS. (b) The second scan shows the same part of the cover slide after the buffer was deaerated and  $100\ \mu\text{M}$  AA was added. (c) Rinsing of the surface and refilling the chamber with standard PBS switches the molecules back into their fluorescent form. This cycle of reversible redox-switching of single ATTO655-molecules was repeated several times, three cycles are shown in panels (a-g).

The described switching procedure was also conducted with other oxazine-dyes such as described in the supporting information of P2 (see Figure S2 of P2). Furthermore, important properties of the molecular switch are investigated, e.g. (i) their bi-stability, (ii) the reliability and response time of switching and (iii) their fatigue resistance (see P2 for detailed informations).

The presence of reductant and oxidant at the same time offers the possibility of a “continuous switching mode”, whose response time is influenced by the encounter rate with the redox agents (i.e. their concentrations) and the reaction rate constants. In the following, the influence is studied of different concentrations of the redox agents on the switching properties and the details are elaborated of the photophysical scheme shown in Figure 4.5, i.e., the rate constants are determined for photophysical processes (see Table 1 of supporting informations of P2). First, we determined the intersystem crossing rate  $k_{\text{isc}}$  and the reverse intersystem crossing rate  $k_{\text{T}}$  for ATTO655 in the presence of oxygen using FCS to  $k_{\text{isc}} = (1.2 \pm 0.2) \times 10^5\ \text{s}^{-1}$  and  $k_{\text{T}} = (6.6 \pm 2.2) \times 10^4\ \text{s}^{-1}$  (experimental results from FCS and further details are found in supporting information of P2, see Figure S4 of P2).<sup>[66]</sup> As can be seen from the inverse intersystem rate constant  $k_{\text{T}}$ , the lifetime of the  $\text{T}_1$ -state is in the order of several  $\mu\text{s}$  for ATTO655. Hence, the  $\text{T}_1$ -state is not visible in single molecule transients of ATTO655 under ROXS conditions (Figure 4.8a) with an observation time (binning) of several ms, resulting in an ON-state consisting of the states  $\text{S}_0$ ,  $\text{S}_1$  and  $\text{T}_1$  (see Figure 4.8b). The lifetime (number of cycles before a reduction occurs into the radical anion state) of this ON-state can be adjusted by the reductant concentration (see Figure 4.8d). On the other hand, the lifetime of the radical anion state, also referred to as OFF-state (Figure 4.8c), is given by the rate  $k_{\text{ox}}[\text{MV}]$  and is controlled by the oxidant concentration (see Figure 4.8e). The independence of the action of AA and MV is a remarkable result since it implies that two variables are available to independently manipulate ON- and OFF-state lifetimes over a broad range. AA controls the duration of the ON-states whereas MV influences the OFF-states. When both redox reagents are

used simultaneously at equal concentrations the effects of them are additive further proving their independent applicability (Figure 4.8f).

The single-molecule sensing capability can be also used for localized redox sensing and has also been exploited to resolve the antiblinking mechanism of the vitamin E analogue Trolox as shown in chapter 4.4 and P4. For further details on data acquisition, analysis and follow-up experiments see P2.

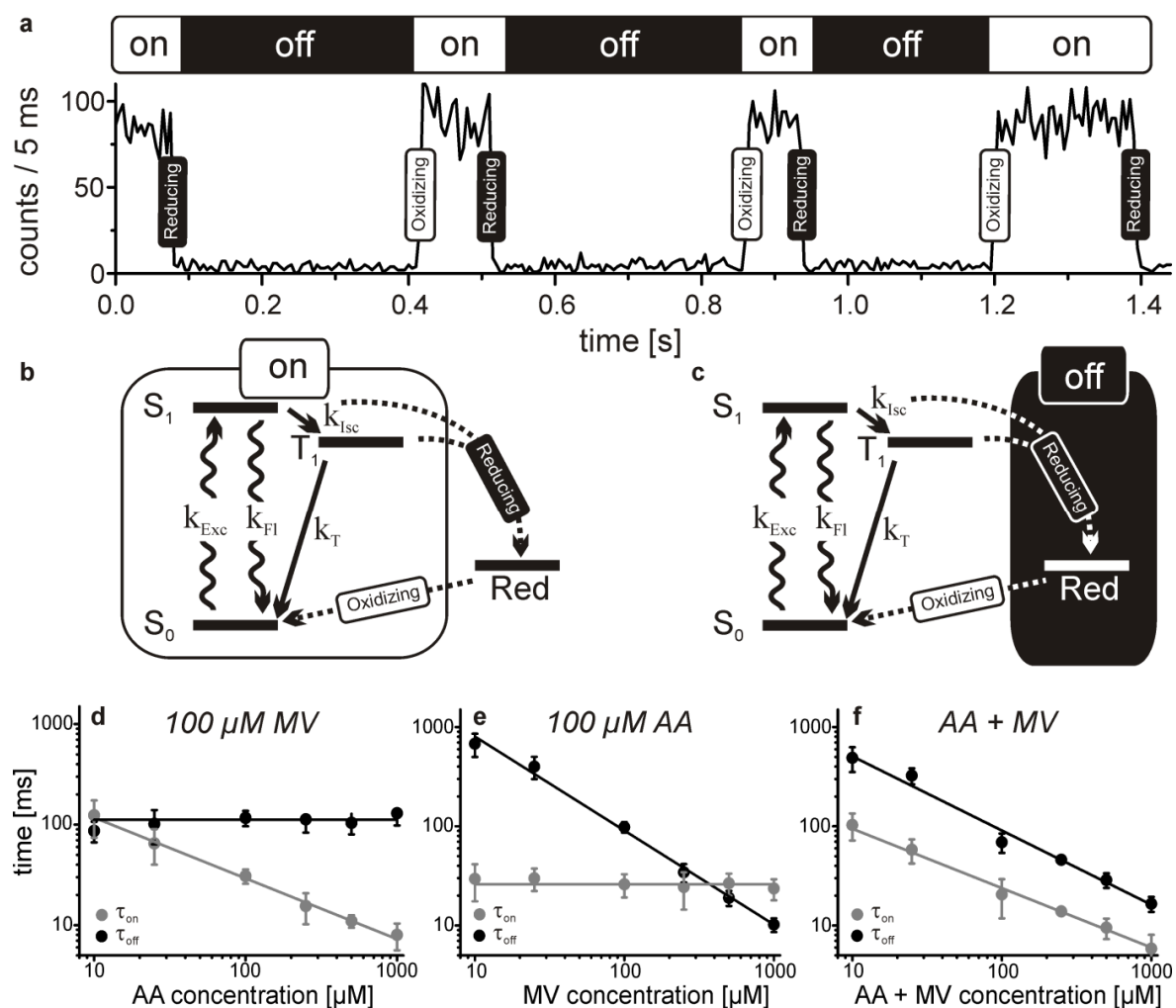


**Figure 4.8.** Schematics of the photophysical pathways of the oxazine dye ATTO655: a representative part of a fluorescence transient immobilized in phosphate buffered saline (PBS) with 25  $\mu\text{M}$  AA, MV and enzymatic oxygen removal is shown in the upper panel. The oxazine-dye is frequently switched between a fluorescent ON-state (b) and a dark-state (c). Switching is manifested as stochastic blinking with time-constants  $\tau_{on}$  and  $\tau_{off}$  that are specific for the environment (marked in the fluorescent time trace in a). The fluorophore cycles between the electronic ground-state and the first excited singlet state emitting a specific number of photons per ON-time. This number depends on several thermodynamic and kinetic parameters of the electron transfer reaction and is influenced by the reductant concentration in the sample. The lifetime of the off-state is analogously influenced by the amount of oxidant. Under the applied conditions triplet states are rapidly depopulated and so short-lived that they are not observed in the transient as dark states. Therefore, they are integrated into the fluorescent ON-cycle thus accounting for cases that triplet depopulation occurs directly with rate constant  $k_T$ . Oxidized states of the fluorophore are not populated due to the very high-lying oxidation potential of these oxazines (see P2). (d) AA dependence of switching at constant 100  $\mu\text{M}$  MV concentration. (e) MV dependence of switching at constant 100  $\mu\text{M}$  AA concentration. The panel (f) shows the ON- and OFF-times with simultaneous change of MV and AA.

#### 4.2.2. Super-Resolution Microscopy

To demonstrate the potential of the presented molecular switch for super-resolution microscopy, sub-diffraction resolution ‘blink microscopy’ images are recorded of ATTO655-phalloidin stained actin filaments immobilized on cover slides (Figure 4.9a,b) and actin bundles in fixed cells (Figure 4.9d,e).<sup>[35]</sup>

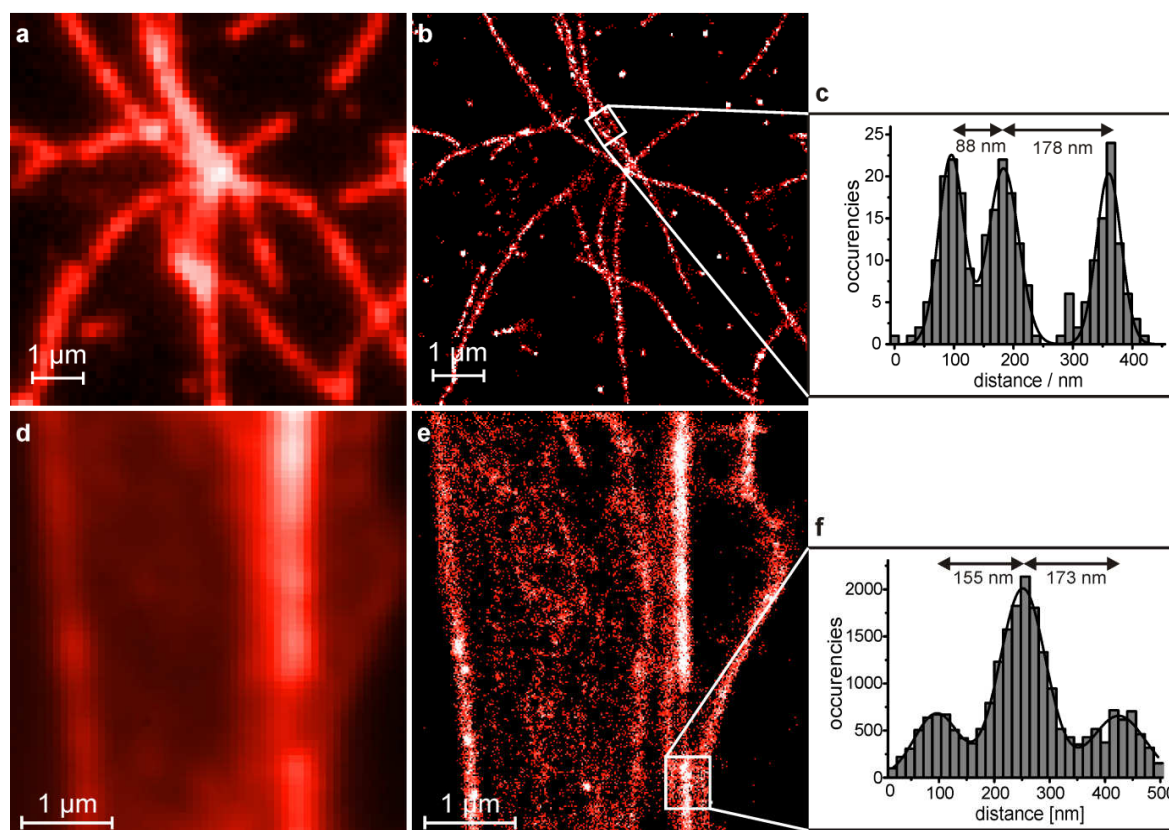


**Figure 4.9.** Total internal reflection fluorescence microscopy of ATTO655-phalloidin labeled single actin filaments (a, b) and bundled actin filaments in fixed NIH/3T3 cells (d, e). (a, d) TIRF microscopy images and (b, e) *Blink microscopy* images with sub-diffraction resolution. (c, f) Histograms over the regions marked with a white rectangle in (b) and (e) and the corresponding peak to peak distances derived from Gaussian fits. The images were recorded with reductant and oxidant concentrations optimized for imaging speed, fluorophore density and excitation intensity (see supporting information of P2 for details).

For data acquisition, 8000-16000 frames were recorded with total internal reflection fluorescence (TIRF) microscopy using appropriate concentrations of redox-active agents (see supporting information of P2 for details on super-resolution imaging and analysis).<sup>[28, 32]</sup> Figure 4.9a shows a TIRF microscopy image of actin filaments immobilized on glass coverslips obtained from the first image frames when most molecules are still in their ON-state. The reconstructed super-resolution image in Figure 4.9b clearly resolves structures that are not discernable in the standard TIRF image, as, for example, three actin fibers whose cross section profile is displayed in Figure 4.9c. Using Gaussian fits we determined the distance between two adjacent fibers to 88 nm (Figure 4.9c). In cells, actin filaments form bundles that are observed in the TIRF image of NIH/3T3 fibroblasts labeled with ATTO655-phalloidin. These bundles are broader than the individual filaments shown in Figure 4.9a,b, but the ‘‘blink microscopy’’ image in Figure 4.9e still resolves, for example, three actin bundles that are not resolved in the TIRF image (see Figure 4.9e,f).

The resolution of a ‘blink microscopy’ image is mainly determined by the localization precision and the number of molecules that can be localized in a diffraction limited spot.<sup>[35]</sup> The on-counts  $N_{\text{on}}$  mainly determine the localization precision.<sup>[1]</sup> Since reductants are used to control  $N_{\text{on}}$ , the localization precision is controlled simultaneously. This influence is exemplarily shown for the localization of single ATTO655 labeled dsDNA at 100  $\mu\text{M}$  AA and 25  $\mu\text{M}$  AA, yielding standard deviations of 26.8 nm and 18.7 nm, respectively (see Figure 4.10).

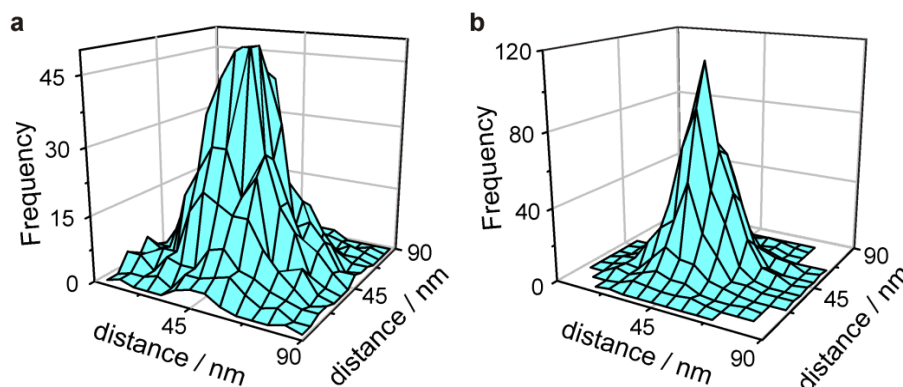


**Figure 4.10.** Histograms of localizations of single immobilized ATTO655 molecules obtained from successive localizations of the same blinking molecules. (a) Histogram obtained at 100  $\mu\text{M}$  AA and 500  $\mu\text{M}$  MV corresponding to  $\sim 190$  on-counts per frame (recorded at 10 ms/frame). (b) Histogram obtained at 25  $\mu\text{M}$  AA and 500  $\mu\text{M}$  MV corresponding to  $\sim 376$  on-counts per frame (recorded at 20 ms/frame). The standard deviation is 26.8 nm in A and 18.7 nm in B in agreement with theoretical values of 26.1 nm and 18.5 nm obtained by  $\text{FWHM}/(n/2)^{1/2}$  <sup>[104]</sup>. These data exemplify the possibility to choose between spatial and temporal resolution by fine tuning on-counts and the ratio of on- to off-times.<sup>[35, 105]</sup>

To increase the number of molecules localizable within a diffraction limited area, the ratio of  $\tau_{\text{off}}/(\tau_{\text{off}} + \tau_{\text{on}})$  should be as high as possible. Therefore, the ON-times are reduced by using higher excitation intensities for imaging (16 – 50  $\text{kW}/\text{cm}^2$ ) compared to confocal measurements and kept the OFF-times long by using low concentrations of oxidant. Thus, the adjustability of the ON-counts and OFF-times allows choosing between spatial and temporal resolution.

### 4.3. Single-molecule Redox Sensor (SMRS) (P3)

In order to demonstrate a second application of oxazine dyes – next to super-resolution microscopy – their controlled blinking kinetics and fluorescence properties are further elaborated. In particular, it is shown that oxazines interact strongly with DNA, especially when internally labeled, by ensemble and single-molecule spectroscopy. Besides redox active agents, the pH also influences the blinking kinetics and in particular the OFF-time duration. Moreover, the extension of ATTO655 as a single-molecule redox sensor to a ratiometric fluorescence-resonance-energy-transfer (FRET) based sensor is presented. Therefore, FRET probes are designed that showed the highest possible contrast of FRET changes and demonstrate reversible FRET-switching of Cy3B-ATTO655 DNA constructs.

#### 4.3.1. Influence of Accessibility on Redox-Blinking

The tight interaction of the oxazine ATTO655 with the DNA also shielded it from redox active agents in solution strongly altering redox blinking kinetics depending on the labeling position (see

Figure 4.11). The blinking kinetics, expressed by the on-counts  $N_{\text{ON}}$  and the OFF-time  $\tau_{\text{OFF}}$ , are compared between terminal labeled ATTO655 and internal labeled ATTO655. The ON-counts decrease by a factor of  $\sim 7$  as can be seen from Figure 4.10a, whereas the OFF-time decrease by a factor of  $\sim 3.5$  for terminal labeled ATTO655. The difference of the on-counts and off-times might be related to the different properties of AA and MV. MV carries two positive charges and likely interacts with the negatively charged backbone of the DNA promoting interaction with the dye also in case of internal labeling. At the pH of the buffer, AA is almost completely deprotonated ( $pK_a = 4.2$ ) and is therefore repelled from the negatively charged DNA especially when trying to approach the internally attached fluorophore. The data indicate that the accessibility of the dye for redox-active agents is decreased several fold for the internally labeled DNA compared to the end-labeled construct. This assumption is further justified by control measurements regarding the fluorescence lifetime and the anisotropy (see P3 for detailed informations). This has implications for the right adjustment of redox active agents when blinking is used for super-resolution ‘Blink microscopy’. Further, the single-molecule data to investigate the accessibility of the dye to quenchers indicate a very unique sensitivity. Analyzing blinking allowed the determination of rates as low as a  $3 \text{ s}^{-1}$  (see Fig. 4.11a), a value not accessible by most techniques. Therefore, the SMRS has some unique abilities to locally detect very small reaction rates as for example in the case of endergonic photoinduced electron transfer reactions.

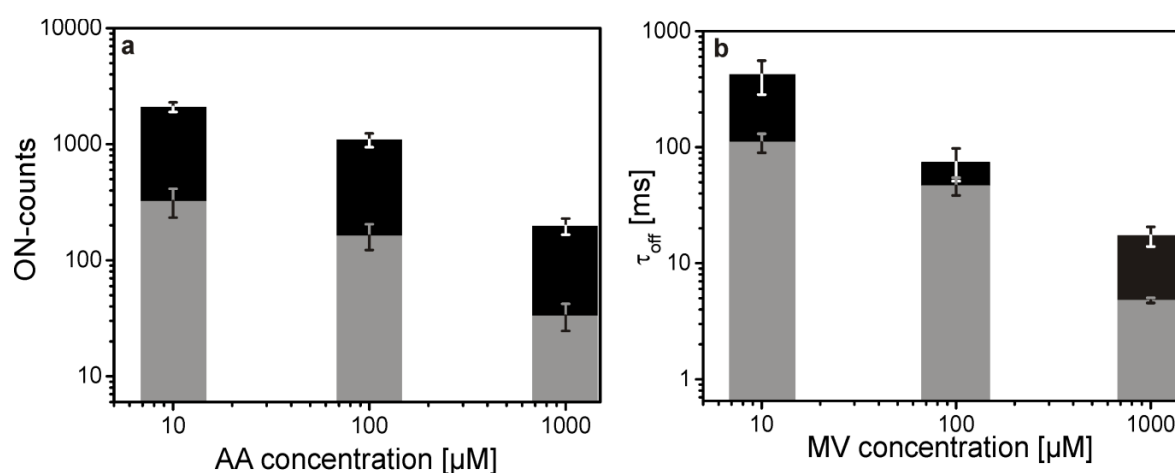


**Figure 4.11.** SMRS-measurements: ON-counts  $N_{\text{on}}$  and  $\tau_{\text{off}}$ -times of ATTO655-labeled DNA immobilized in aqueous environment under different MV and AA concentrations. (a)  $N_{\text{on}}$  at three different AA concentrations with a constant MV concentration of  $100 \mu\text{M}$ . (b)  $\tau_{\text{off}}$  at three different MV concentrations with a constant AA concentration of  $100 \mu\text{M}$ . The black bars correspond to internally labeled SMRS-probe with ATTO655, whereas the grey bars correspond to terminally labeled SMRS.

#### 4.3.2. Influence of the DNA Sequence on Redox-Blinking

The strong interaction of the oxazine with the DNA has further implication for studying electron transfer through DNA. Due to its electron donating properties guanosine is the nucleobase that influences the fluorescence of many fluorophores most significant. Commonly, interactions of fluorophores and guanosine residues in DNA have been detected by changes in fluorescence lifetime or through intensity fluctuations using fluorescence correlation spectroscopy.<sup>[56, 106-108]</sup> Therefore, DNA without guanosine in the vicinity of the attachment point of the ATTO 655 fluorophore is used, i.e. the next guanosine is the forth base from the attachment point in the DNA strands used. At this distance direct interaction between the fluorophore and the guanosine appears



very unlikely. For verification, we compared single-molecule transients of ATTO655 labeled DNA with a guanosine four base pairs away to a DNA where the first guanosine was replaced by an adenosine creating a single-pair mismatch. Representative transients of the DNA without guanosine and with guanosine at four base-pairs separation are shown in Figure 4.12a and b together with the corresponding autocorrelation functions. A pronounced difference is observed for all transients with blinking of ATTO655 when a guanosine is at a separation of four base-pairs (Figure 4.12b). In contrast almost no blinking is observed when two guanosines are removed (Figure 4.12a). Guanosine residues at a distance of four base-pairs still lead to pronounced blinking of ATTO655, which can hardly be explained by direct interaction of guanosine and the fluorophore (see Figure 4.12). This blinking of ATTO655 can be explained by electron transfer from guanosine to the fluorophore. Here, the on-times (on-counts) are a measure of the rate of electron transfer and the off-times represent the time until ATTO655 is re-oxidized either through reversible electron transfer or by another electron acceptor. This adds a new time window to previous fluorophore-guanosine interaction studies that accessed the picoseconds to microsecond range using fluorescence lifetime and correlation spectroscopy. Very low reaction rates become accessible with the fluorescence blinking of single immobilized ATTO655-DNA constructs as parameter (see P2). Possibly ATTO655 constitutes a probe to study charge transfer through DNA on the level of single molecules.

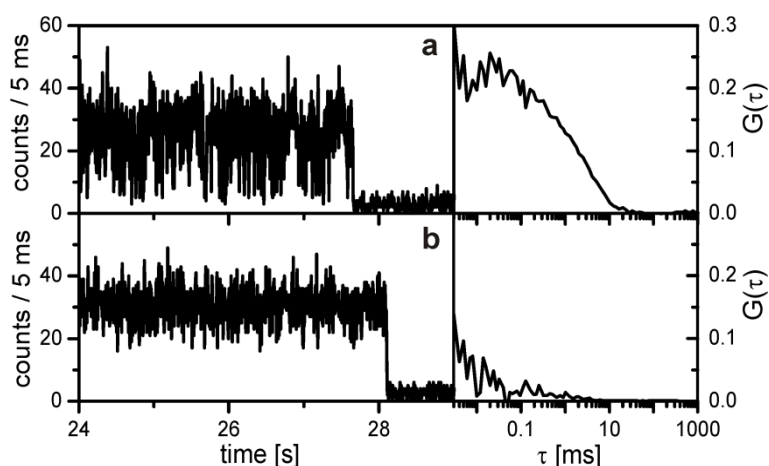


**Figure 4.12.** Fluorescent transients (left) and results from an autocorrelation analysis (black curve, right) of ATTO655-labeled DNA immobilized in aqueous environment (PBS-buffer). The gray curve in the right panel represents a stretched exponential fit. (a) Internally labeled dsDNA-probe with two guanosine exchanged by adenosine. (b) The same probe with the guanosine bases at 4 and 5 base-pairs distance of the ATTO655 fluorophore.

### 4.3.3. pH-Dependency

Besides the concentration of reductant and oxidant it is found, that the pH-value is another important parameter that can influence blinking. Interestingly, slight changes of the pH-value significantly alter the OFF-times while the ON-counts remain nearly unchanged within experimental error (see Figure 4.13). Figure 4.13 shows different fluorescent time-traces for internally labeled ATTO655 using a mixture of 10  $\mu$ M AA and 100  $\mu$ M MV in deaerated PBS-buffer. The pH is varied from pH = 8.0 to pH 6.7. Under these conditions, a frequent blinking is observed, and an autocorrelation analysis reveals the involvement of two different OFF-states (Figure 4.13). As shown in P1 and P2, the short component can likely be assigned to the triplet-

state with a lifetime of  $\sim 0.1$  ms. Blinking due to transitions into the radical-anion are found on longer timescales with an OFF-time of  $(130 \pm 31)$  ms and on-counts of  $(2600 \pm 630)$  at pH 7.2 (Figure 4.13c). Next, the pH-value is varied by adding small amounts of a 1 M  $\text{NaH}_2\text{PO}_4$  solution (weak acid) or a 1 M  $\text{Na}_2\text{HPO}_4$  solution (weak base). From Figure 4.13a-e it is apparent that pH changes cause significant alterations of the SMRS blinking kinetics: while the on-counts remain nearly constant with an average  $N_{\text{ON}} = (2640 \pm 680)$ , the lifetime of the radical anion is significantly increased to  $(464 \pm 161)$  ms. The data shows that the SMRS is sensitive for pH changes in the investigated range: the OFF-times vary from  $(43 \pm 17)$  ms for pH = 8.0 over  $(129 \pm 31)$  ms at pH = 7.2 to  $(464 \pm 162)$  ms at a pH of 6.7 (Figure 4.13). Considering the SMRS-values ( $\tau_{\text{OFF}}$ ) and errors corresponding to a certain pH-change, allows determining the sensitivity of our method to pH changes as small as  $\pm 0.2$ . It is noteworthy that the same qualitative behavior, i.e. increasing OFF-times for a decreasing pH value, is also found when oxygen is present (pH = 7.4:  $\tau_{\text{OFF}} = 107 \pm 50$  ms; pH = 6.7:  $\tau_{\text{OFF}} = 480 \pm 90$  ms).

A changing rate constant from the radical anion back to the electronic ground-state can either be caused by the properties of the SMRS (ATTO655) or by the oxidizing agent MV. As known from the literature, the oxidation potential of MV is not strongly affected by the pH-value.<sup>[109]</sup> Hence, it seems more likely that the energetic position of the dye radical-anion itself is altered. Protonation of the reduced form could be an explanation for the stabilization as is known for related thiazine dyes.<sup>[110]</sup> These insights are important for applications of oxazines as redox sensor or as pH indicator.

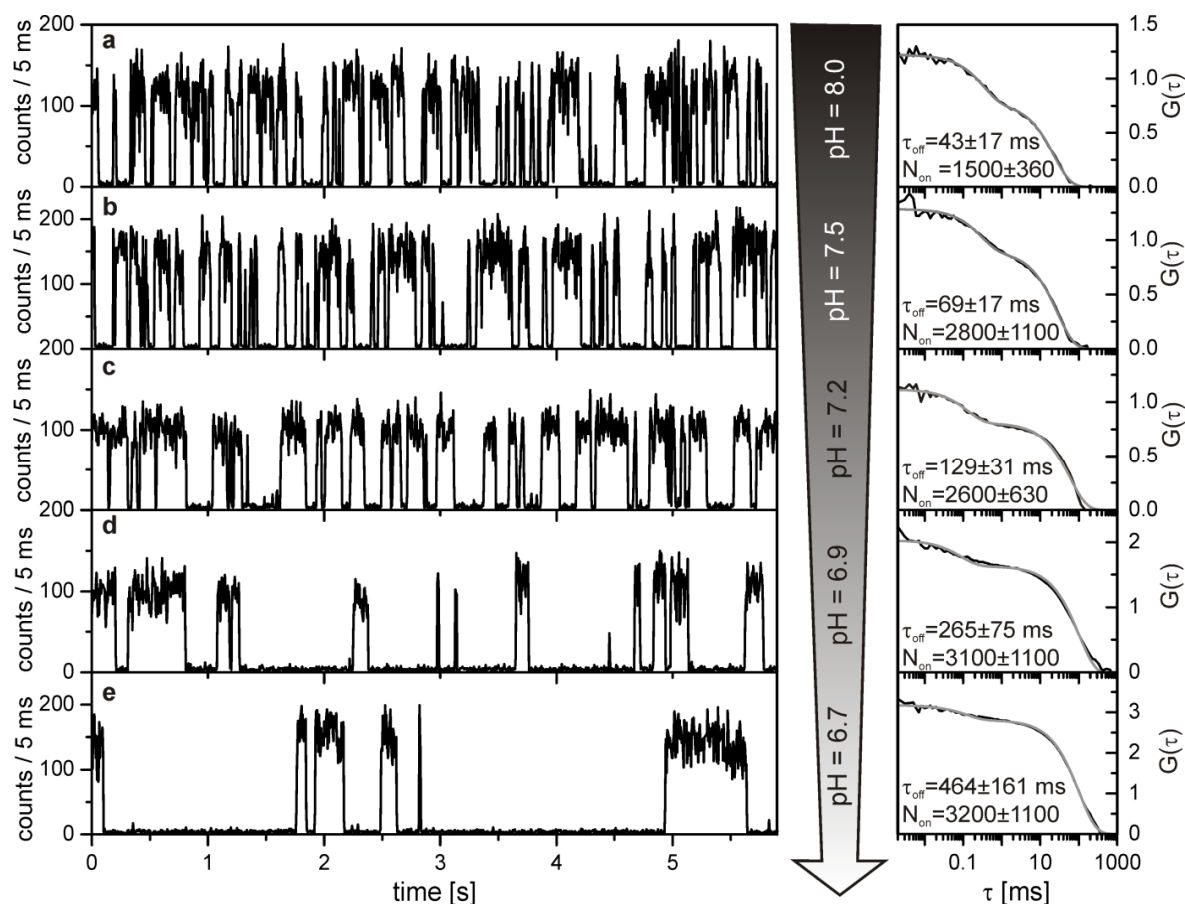


**Figure 4.13.** pH dependency of ATTO655 in deaerated PBS-buffer containing 10  $\mu\text{M}$  AA, 100  $\mu\text{M}$  MV. The intensity of the 640 nm excitation was 1.5  $\text{kW}/\text{cm}^2$ . The left panel shows fluorescent transients of immobilized ATTO655-labeled DNA at different pH-values: pH = 8.0 (a), pH = 7.5 (b), pH = 7.2 (c), pH = 6.9 (d) and pH = 6.7 (e). The right panel shows the corresponding autocorrelation (black) together with a bi-exponential fit (grey). The resulting average kinetic parameters for the long component (this OFF-state is assigned to the radical-anion) are displayed in the figure. The short component in the time-range below 0.1 ms is likely due to the triplet-state.

#### 4.3.4. Ratiometric SMRS

The idea of a ratiometric SMRS is to observe e.g. red emission in an oxidizing environment that is switched to green emission in a reducing environment. Accordingly, such a FRET switch also represents a ratiometric sensor of redox conditions. Ratiometric sensors generally provide an advantageous, self-calibrating signal, which is independent of instrumental and environmental conditions and especially is independent of the sensor concentration (see e.g. <sup>[111]</sup>). Probes are designed that sense their redox environment in terms of FRET-efficiencies rather than just intensities. The idea is to use a FRET-pair in which the oxazine acceptor (ATTO655) is the redox sensor and a donor (Cy3B) is insensitive to the redox species detected (see P1). In such a FRET-pair the oxazine FRET-acceptor is selectively switched off by a reductant thus prohibiting energy transfer. When the acceptor is switched off, the fluorescence of the donor appears thus reporting on the redox state of the acceptor.

For FRET switching Cy3B-ATTO655 FRET-pairs are immobilized on a cover slide and the surface is scanned with a confocal microscope (see chapter 4.1 and 4.4). In PBS buffer, stable emission of ATTO655 is observed (see P2). Accordingly, efficient FRET between the donor Cy3B and

ATTO655 occurs. The FRET efficiency is represented as proximity ratios (PR) in the gray-scale images of Figure 4.14. Bright spots correspond to spots with high PR (see most of the circled spots in Figure 4.14). Dark gray spots represent donor only molecules that exhibited no energy transfer due to lacking acceptor (see upper and upper left circled spots in Figure 4.14a-e). Upon removing oxygen and adding 100  $\mu\text{M}$  AA, ATTO655 is prepared in its dark radical ion state through photoinduced electron transfer. This state is stable in the absence of oxidizing agents. Accordingly, all spots in Figure 4.14b resemble the donor-only spots of Figure 4.14a and b. These spots also appear patchier since Cy3B exhibits blinking in the presence of reductant only (see P1). Upon exchanging buffer to aerated PBS the dissolved oxygen restores ATTO655 in its fluorescent state by serving as electron acceptor so that high energy transfer is observed again for the same circled spots as in Figure 4.14a (see Figure 4.14c). This process of switching on and off FRET is repeated several times and is mainly limited by the photostability of the donor, here Cy3B. Three switching cycles are shown in Figure 4.14.

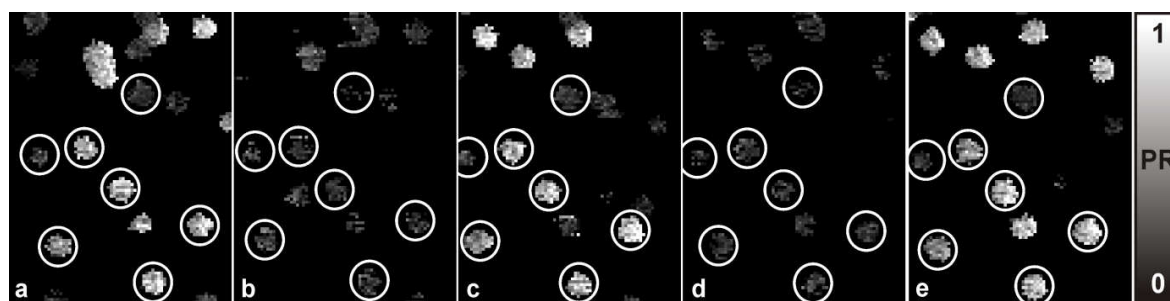


**Figure 4.14.** Confocal fluorescence images ( $3.75 \mu\text{m} \times 5 \mu\text{m}$ ) of Cy3B-ATTO655-labeled dsDNA converted into proximity ratio (PR) images. For each pixel the PR-value is calculated using  $\text{PR} = F_D^A / (F_D^A + F_D^D)$  (with  $F_D^A$  as fluorescence intensity in the acceptor channel upon donor excitation and  $F_D^D$  fluorescence intensity in the donor channel upon donor excitation) and is encoded in a gray scale between zero and one. The first image was acquired in PBS (a). (b) The second scan shows the same part of the cover slide after the buffer was deaerated and 100  $\mu\text{M}$  AA was added. (c) Rinsing of the surface and refilling the chamber with standard PBS switches the PR-value of the molecules back to their on-state. This cycle of reversible redox-switching of the PR-value for single Cy3B-ATTO655-FRET pairs was repeated several times, two cycles are shown in panels (a-e).

#### 4.4. Trolox as Antiblinking and Antibleaching Reagent (P4)

In chapter 4.1 and in P1 is shown that a reducing and oxidizing system is used to stabilize the fluorescence of common organic fluorophores. Interestingly, it was shown by Rasnik et al. that removal of oxygen together with millimolar concentrations of the vitamin E analogue Trolox (TX) could drastically reduce photobleaching, as well.<sup>[84]</sup> This observation comes also apparent during the investigations with ROXS (see Figure 4.4 magenta bars). In this chapter the fluorescence protecting mechanism of TX is investigated and it is concluded that its antiblinking effect is due to quinoid derivatives of TX that form in buffer through (photo-) reactions with molecular oxygen. The combination of TX and its oxidized form (TX-quinone, TQ) then acts according to the ROXS scheme. Ensemble and single-molecule fluorescence spectroscopy in combination with the established single-molecule redox sensor (SMRS) are used to find experimental evidence for the hypotheses above.

#### 4.4.1. SMRS and Trolox

As shown in chapter 4.2 and 4.3, the oxazine SMRS reports sensitively and independently on the local environment, i.e., presence and concentration of reducing and oxidizing agents, through a change of the blinking kinetics. The number of photons emitted per on-time,  $N_{\text{ON}}$ , and the OFF-state lifetime,  $\tau_{\text{OFF}}$ , are the parameters that quantitatively report on the presence of reductants and oxidants (see Figure 4.8 and 4.11).

First, it is investigated whether an oxidizing effect of TX can be detected by measuring  $N_{\text{ON}}$  and  $\tau_{\text{OFF}}$  at different TX concentrations. As expected, the on-counts are reduced with increasing TX concentration (Figure 4.15a, black data points) representing the reducing properties of TX. The OFF-times are interestingly reduced as well, indicating that this TX sample has considerable oxidizing properties. Replacing TX by ascorbic acid, for example, yields a constant  $\tau_{\text{OFF}}$  independent of concentration (Figure 4.8). Two different grades of TX are dissolved (sample II: 97% purity as received from Sigma Aldrich; sample I: >98% purity with HPLC purification) in PBS (1 mM) to check, whether oxidizing impurities in the TX batch are the origin of its antiblinking capability. Since TX is not very soluble in PBS, dissolving was carried out over  $\sim 18$  h. The black data points in Figure 4.15 were obtained from sample I, and the blue data points, from sample II, yielding the same results within experimental error. If an impurity in the TX batch is the origin of the oxidizing properties, a systematic difference in the OFF-time dependency will be expected since it is unlikely that the oxidizing impurity has the same concentration in two different purity grades.

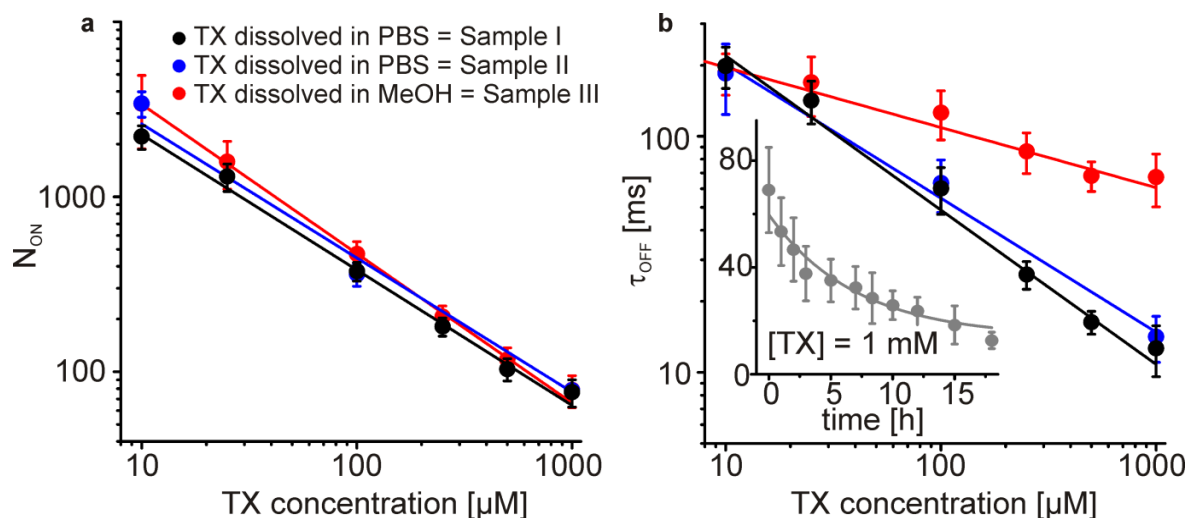


**Figure 4.15.** Dependency of the on-counts  $N_{\text{ON}}$  (a) and OFF-state lifetime  $\tau_{\text{OFF}}$  (b) on the concentration of different TX samples. The data were fitted using an allometric function of the form  $f(x) = a \cdot x^b$  to guide the eye. The inset in panel (b) shows the temporal evolution of the OFF-times of sample III after dissolved in PBS (1 mM TX concentration) (Details on data acquisition and analysis are found in P4).

To distinguish between intrinsic yet unknown oxidizing capabilities of TX and impurities the properties of TX sample I to a TX sample that was prepared very freshly as a 100 mM solution in methanol (sample III) are compared. Methanol was used to circumvent the slow dissolving process in PBS. Control measurements were carried out to exclude the effect of methanol. Small amounts of this stock solution were added to PBS, and the concentration dependent on-counts and OFF-times were examined. For the very fresh TX sample, the on-counts show the same dependency on the concentration as observed for the TX dissolved in PBS over 18 h (Figure 4.15a, sample III, red

data points). This proves that indeed the same TX concentrations are present and TX does not precipitate during the dilution of the methanol solution in PBS. The OFF-times, however, show that the oxidizing ability is drastically decreased for the fresh TX solution (Figure 4.15b) and only a weak reduction of OFF-times at higher TX concentration is observed. We conclude that a fraction of TX in sample I is oxidized during the slow 18 h dissolving process in PBS most likely due to reaction with oxygen. This idea is further elaborated by recording fluorescence transients at a concentration of 1 mM TX (sample III) as a function of time after dissolving: the OFF-times gradually decrease as depicted in the inset of Figure 4.15b indicating the increasing oxidizing potential.

These results are explained by the fact that, upon (photo-) oxidation, TX tends to form quinoid structures such as TX-quinone (TQ), as shown by absorption spectroscopy in the following chapter.

#### 4.4.2. (Photo-) Oxidation of Trolox

It is known that TX can form stable quinone-derivatives after enzymatic oxidation or photoinduced oxidation.<sup>[112-114]</sup> During these processes, the absorption properties of the sample change considerably: the TX-absorption band of lowest energy is found at ~290 nm in aqueous buffer or water/ethanol mixtures (ref. <sup>[112-114]</sup>). When oxidized to the quinoid form (TX-quinone, TQ) - either by enzymatic reactions or light - a new band appears at ~270 nm. This absorption is clearly associated to the TX-quinone as shown in refs <sup>[112-114]</sup> and references cited therein. Hence, these spectroscopic marker bands are used to probe the composition of the samples and to verify the presence and influence of TQ in the experiments. We detected the photoinduced formation of TQ (Figure 4.16) using a standard absorption spectrometer. Therefore the UV/VIS spectra of TX and TQ were recorded in the region from 225 – 500 nm with a Specord S100 from Analytik Jena. In order to induce the photochemical oxidation of TX, a Hg/Xe lamp ( $\lambda_{\text{exc}} < 300$  nm, ~450 mW, Hamamatsu) is used in combination with suitable filtering (BG20, 1 mm, Schott) to minimize secondary photochemistry. As seen in Figure 4.16a the same absorbance changes, as reported in refs <sup>[112-114]</sup>, are found when freshly dissolved TX (Figure 4.16, black,  $\lambda_{\text{max}} \sim 290$  nm) is illuminated with UV-light. Already after few minutes a distinct absorption band of TQ is clearly observed at ~270 nm (Figure 4.16, blue). The isosbestic point ( $\lambda_{\text{iso}} \sim 280$  nm) found for illumination times < 10 minutes indicates a one-step transformation from TX into its quinone derivative. Side reactions, most likely due to photoreactions of the quinone, cause absorbance changes in the range > 300 nm for long illumination periods. The formation of TQ is observed in a less pronounced way for solutions that underwent aging without specific UV-illumination. Here, the exact same absorbance changes as observed for UV-illumination (Figure 4.16a) can be detected and account for the temporal evolution of the SMRS-values (see Figure 4.15).

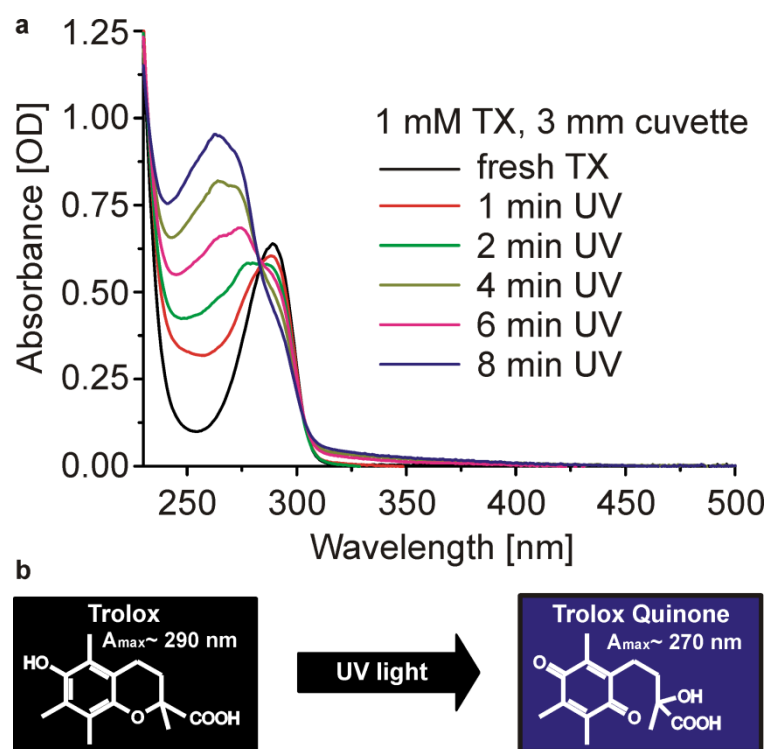


**Figure 4.16.** Scheme of TX undergoing light-induced oxidation to its quinone derivative. (a) Spectroscopic investigation of TX under UV-exposure: 100  $\mu$ l of a 1 mM TX-solution are illuminated with UV-light around 300 nm for periods described in the figure. Thereby the absorption peak of TX at  $\sim$ 290 nm decreased with increasing illumination time, while a new peak corresponding to the TX-quinone appears at  $\sim$ 270 nm. An isosbestic point is observed around  $\sim$ 280 nm, which is partially lost for long illumination times  $>$  8 min. (b) Chemical structures from the reducing agent Trolox (black) and the oxidizing agent Trolox Quinone (blue).

The data demonstrate that the antiblinking and antibleaching effect of TX is due to a combination of its reducing properties and a TX quinone formed during the dissolving process in aerated PBS. In agreement with the ROXS scheme (see Figure 3.3), this oxidizing fraction depopulates reduced states and thereby minimizes blinking (further experiments are found in the supporting information of P4, e.g. photostabilizing effect of TX and TQ upon ATTO647N). The obtained unifying picture substantiates the potential of quenching triplet states via electron transfer reactions and recovering the singlet manifold via the complementary redox reaction. Very importantly, this work sheds light on many of the reports in the field that presented contradicting results concerning the efficiency and recommended concentrations of antifading agents (see ref. <sup>[83]</sup> and references therein). Finally, a recipe for the reliable application of TX is provided that shows how to circumvent problems with fresh TX by determining the actual TX and TQ concentrations (see Supporting Information of P4). For dye stabilization based on ROXS, this combination might be advantageous due to its lower toxicity.

#### 4.5. Resolution Enhancing Probes (P5)

Generally, super-resolution methods either require elaborate modification of the excitation scheme (as in case of e.g. STED, SIM, SPEM, GSD)<sup>[20, 22, 23, 25]</sup> and/or computational post processing to reconstruct images (PALM, STORM, FPALM, dSTORM, GSDIM, Blink-Microscopy).<sup>[28, 31-35, 74]</sup> It is also noteworthy that increasing resolution is commonly accompanied by increasing demands on

the fluorescent probes, which have to be improved with respect to functionality (e.g. switchability, labeling procedures, physical size...) and photostability (see P1 and ref. <sup>[115]</sup>).

First a short introduction is given into resolution enhancement in a confocal scanning microscope. Second, fluorescent probes are presented that are comparably photostable and intrinsically exhibit a superlinear fluorescence response that directly translates into resolution enhancement in confocal microscopy. These probes are called “energy transfer blockade probes (ETBPs)”. A theoretical description highlights the parameters that have to be optimized to fully exploit the potential of the approach. Finally, single ETBPs are used to demonstrate resolution enhancement in a confocal microscope.

#### 4.5.1. Resolution Enhancement in Confocal Microscopy

The image of confocal scanning microscope is given by the convolution of the structure under investigation and the point spread function from a point source (PSF) of the microscope. Furthermore, the PSF is a multiplication of the excitation volume and the detection volume, whereas the observation volume is defined by the used pinhole and magnification used. The size of the detection volume is chosen to be five to six times larger compared to the excitation volume for best signal to noise ratio.<sup>[116]</sup> Therefore the PSF from a point source is predominantly given by the excitation volume, which can be calculated by:

$$PSF_{Exc}(\nu) = |2 \cdot J_1(\nu) / \nu|^2 \quad \text{with} \quad \nu = \frac{2 \cdot \pi \cdot r \cdot NA}{\lambda_{Exc}} \quad (4.1, 4.2)$$

Here,  $J_1$  denotes the first-order Bessel function,  $r$  the coordinate with respect to the point source,  $NA$  is the numerical aperture of the objective and  $\lambda_{Exc}$  the wavelength used for excitation. Based on this description the minimal distance to resolve two point sources is given by the Rayleigh criterion:

$$d_{min} = 0.61 \cdot \frac{\lambda_{Exc}}{NA} \quad (4.3)$$

However, the signal obtained by a confocal microscope is the fluorescence response upon the excitation intensity of the probe used. This leads to the conclusion that a non-linear fluorescence response alters the shape of the PSF. A negatively bend non-linear fluorescence response, e.g. saturation, would broaden the PSF, whereas a positively bend non-linear (superlinear) response would sharpen the PSF as illustrated in Figure 4.17. In Figure 4.17a an intensity distribution of a focus in a confocal microscope is shown based on equations (4.1 and 4.2). A numerical aperture of  $NA = 1.35$  and an excitation wavelength  $\lambda_{Exc} = 640$  nm was used for calculation. A new PSF of the excitation volume is given after each intensity value is translated into a fluorescence value through the superlinear fluorescence response function (SFRF) (Figure 4.17b), resulting in a smaller width of the PSF (Figure 4.17c). Hence, superlinear fluorescent probes are needed to circumvent the diffraction limited resolution in a confocal scanning microscope.<sup>[117, 118]</sup>



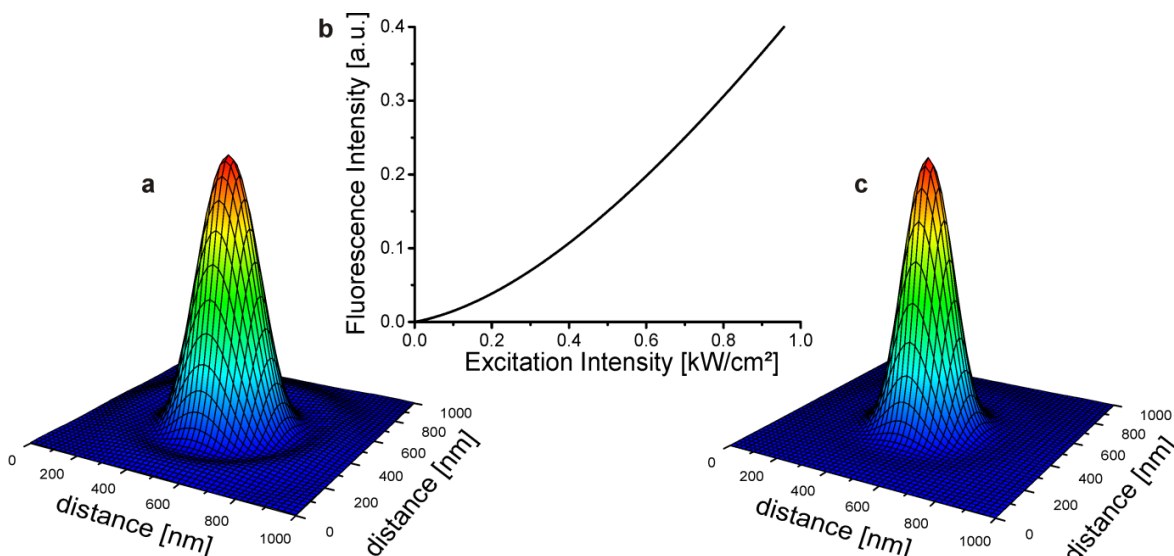


**Figure 4.17.** Influence of a superlinear fluorescence response upon the point spread function (PSF). (a) PSF calculated with equations (4.1 and 4.2) using  $NA = 1.35$  and  $\lambda_{Exc} = 640$  nm. (b) Arbitrary superlinear fluorescence response function (SFRF). (c) PSF after translation with the SFRF.

#### 4.5.2. Energy Transfer Blockade Probe

The ETBPs consist of a donor fluorophore surrounded by one to  $n$  acceptors (with  $n = 0, 1, 2, \dots$ ), which are not necessarily fluorophores. Upon excitation, the donor efficiently transfers its excited state energy to the acceptors via fluorescence resonance energy transfer (FRET). To achieve a superlinear fluorescence response of the donor, the acceptor has to show a photoinduced transition to a state that does not act as an acceptor for FRET. The resulting superlinearity is related to the fact that the observed donor emission depends on two different processes that add up: the donor fluorescence linearly increases with higher excitation intensity. Additionally, the probability that the donor is not quenched by the acceptor(s) also increases due to decreasing ON-times of the acceptor(s) at higher excitation intensity. In other words, saturation of the acceptor(s) is converted into superlinear fluorescence of the donor.

The radical anion state of the acceptor fluorophore is used as a non-absorbing state, since radical anion states of many fluorophores such as rhodamines, oxazines and cyanines do not exhibit extinction above  $\sim 500$  nm (see e.g. <sup>[13-15]</sup>). Therefore, an ETBP is constructed from dsDNA as rigid scaffold labeled with ATTO647N as donor and zero, one or two ATTO680 as acceptor(s) at a distance of 12 base pairs for a 0-, 1- or 2-acceptor ETBP, respectively (see Figure 4.18). The 12 base pair distance was used to prevent non-FRET interchromophore interactions.

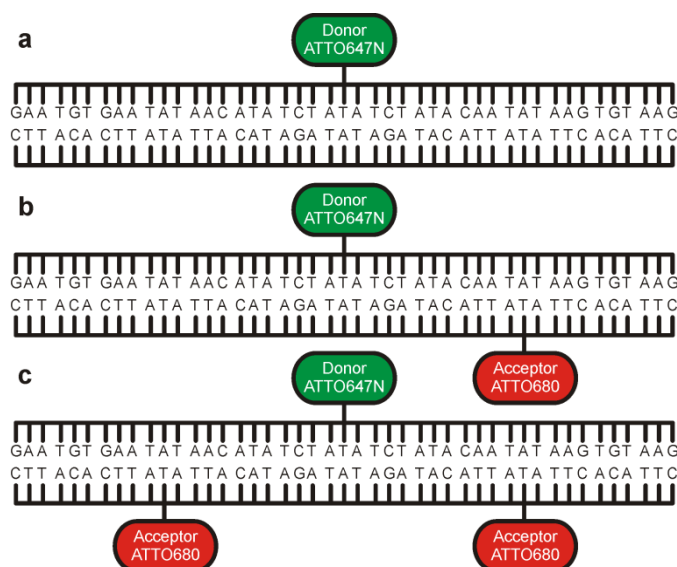


**Figure 4.18.** Scheme of the energy transfer blockade probes (ETBPs) used: 0-acceptor ETBP (a), 1-acceptor ETBP (b), and 2-acceptor ETBP (c).

Potentially long-lived intermediate states such as triplet and radical ion states of the carborhodamine ATTO647N are rapidly depopulated via electron transfer reactions yielding very stable emission without observable blinking (see Figure 4.19a, chapter 4.1. and P1). In contrast, the radical anion state of the oxazine ATTO680 is so stable that it is not efficiently depopulated by the oxidant methyl viologen or oxygen. Consequently, transitions to the radical anion state yield an oxidant-concentration dependent OFF-time of  $1 - 10^6$  ms (see P2). This OFF-state is directly visualized in single-molecule transients of oxazines such as ATTO680 in the presence of ascorbic acid (AA) and methyl viologen (MV) (Figure 4.19b).

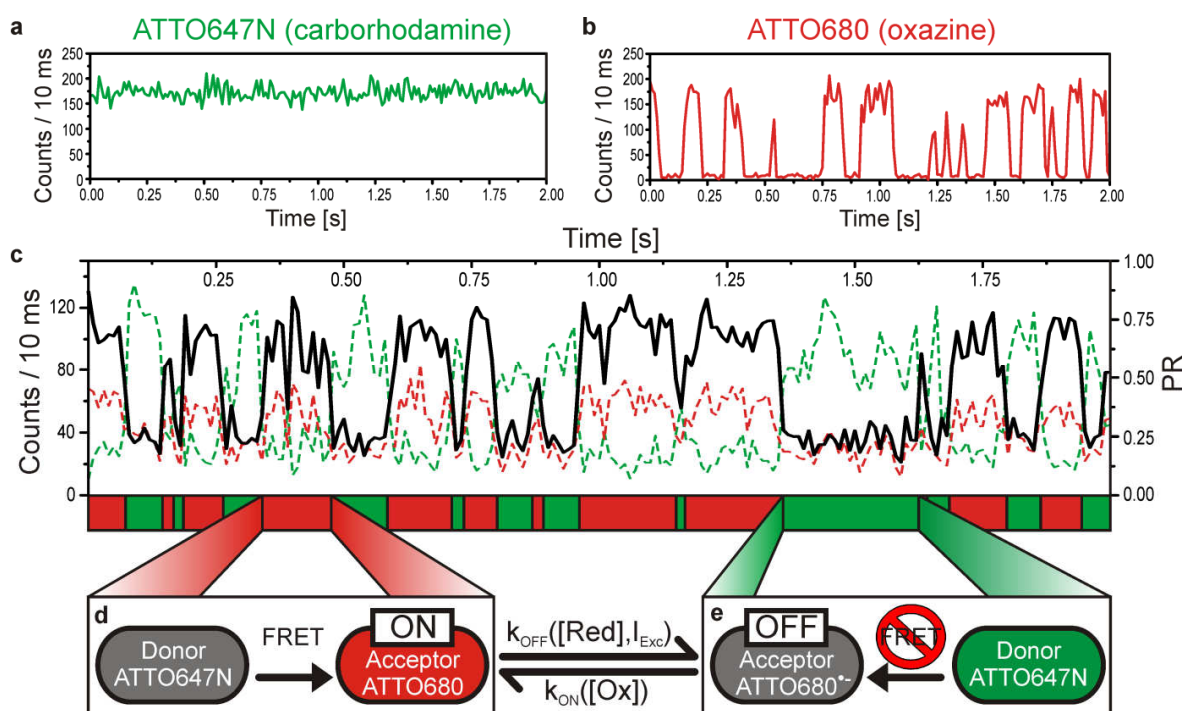


**Figure 4.19.** Scheme of the photophysics in a 1-acceptor ETBP. (a, b) Typical fluorescence transients of immobilized dsDNA labeled with ATTO647N (a) or ATTO680 (b) using AA (250  $\mu$ M) and MV (100  $\mu$ M) at an excitation intensity of 1.7 kW/cm<sup>2</sup> for ATTO647N and 3.5 kW/cm<sup>2</sup> for ATTO680 at  $\lambda_{\text{Exc}} = 640$  nm. (c) Representative fluorescence transient of an immobilized 1-acceptor ETBP bearing ATTO647N and ATTO680 using the same buffer and excitation conditions as described for ATTO647N (a). The fluorescence was split by a dichroic beamsplitter (BS685) so that the green transient primarily represents ATTO647N emission and the red transient ATTO680 emission. The black transient in (c) corresponds to the proximity ratio (PR =  $F_D^A / (F_D^D + F_D^A)$ ) demonstrating the fluctuating FRET. The red/green bar indicates switching between the two states of the acceptor. In the ON-state the acceptor can accept the energy from the donor (d), while in the OFF-state, FRET is blocked and the donor fluoresces (e). The lifetime of the acceptor ON-state is controlled by the reductant concentration and excitation intensity while its OFF-state is controlled by the oxidant concentration (d,e).

To check whether the acceptor in the OFF-state still acts as FRET acceptor or whether the FRET is blocked we used the 1-acceptor ETBP (see Figure 1b). DNAs were immobilized according to chapter 4.4 (see materials and methods of P5 for details on sample preparation and experimental setup). Donor and acceptor emission were separated using an appropriate beamsplitter and the fluorescence was detected by two avalanche photodiodes in a confocal single-molecule setup. Fluorescence transients of single FRET pairs were recorded exciting at 640 nm in the presence of AA (250  $\mu$ M) and MV (100  $\mu$ M). Oxygen was removed enzymatically. When excited via FRET, the acceptor shows similar blinking as with direct excitation (compare Figure 4.19b, red transient, and Figure 4.19c, red transient). When the acceptor is ON, FRET occurs and the donor is efficiently quenched (Figure 4.19d). Every time the acceptor enters an OFF-state the fluorescence of the donor recovers indicating that in contrast to other approaches and especially in contrast to blinking due to triplet states,<sup>[119]</sup> the donor emission is not in resonance with the acceptor in the OFF-state (Figure 4.19e). The anticorrelation of the green and red transient is also evident from the transient of the proximity ratio (PR) (Figure 4.19c, black transient), which is the ratio of acceptor fluorescence to the sum of donor and acceptor fluorescence. For the quality of an ETBP, it is important that quenching by the acceptor radical anion is absolutely negligible. Therefore transients are inspected, in which the acceptor bleached before the donor and the intensity is compared of the donor after acceptor photobleaching with the intensity of the donor when the acceptor is in its

radical anion state. As shown in Figure 4.20 these intensities are essentially identical evidencing 100% donor dequenching when the acceptor is OFF.

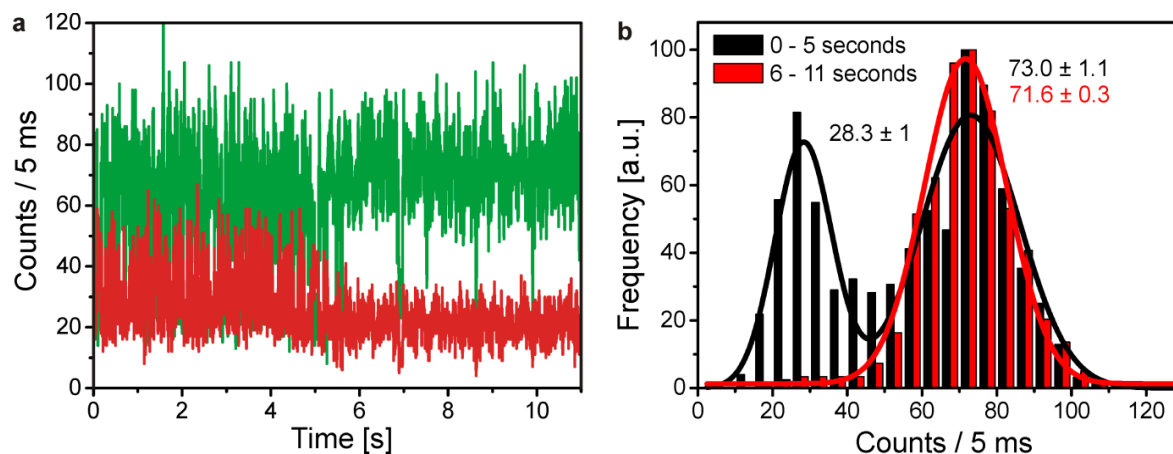


**Figure 4.20.** Fluorescence transient of an immobilized 1-acceptor ETBP using the ROXS buffer conditions (250  $\mu$ M AA, 1mM MV) at an excitation intensity of 1.7 kW/cm<sup>2</sup> at  $\lambda_{\text{Exc}} = 640$  nm. The green and red curves correspond to donor and acceptor emission, respectively. Bleaching of the acceptor occurs after  $\sim 5$  s (a). Histograms of donor emission intensities are shown in (b) before acceptor bleaching (black bars) and after acceptor bleaching (red bars). A two-peak Gaussian fit (black) to the intensity distribution before acceptor bleaching and a Gaussian fit to the intensity distribution after acceptor bleaching reveal the same fluorescence intensity of the donor, evidencing that no FRET occurs during the time the acceptor spends in the radical anion (OFF-) state.

The next step towards resolution enhancement with an ETBP is to prove the superlinear fluorescence response of the donor. Therefore, the process leading to the acceptor radical anion has to be photoinduced resulting in a superlinear fluorescence dependence of the donor with increasing excitation intensity. Single-molecule PR transients are recorded and the excitation intensity is increased every 10 s during the acquisition (from 0.34 kW/cm<sup>2</sup> to 1.9 kW/cm<sup>2</sup>). Subsequently, 10 s periods are analyzed with respect to their PR. A fraction of a transient recorded at an average excitation intensity of 1.7 kW/cm<sup>2</sup> is shown in Figure 4.21a together with the corresponding PR histogram. The ratio of the number of ON- and OFF-state bins in the transient,  $\#_{\text{on}}$  to  $\#_{\text{off}}$ , obtained from fitting the histogram by a two-peak Gaussian function, directly reports on the excitation dependence of the ON-time since  $\tau_{\text{OFF}}$  is known to be intensity independent (see P2 and ref. [35]). The procedure was repeated for different excitation intensities yielding the excitation power dependence depicted in Figure 4.21b (black dots). Averaging over twenty molecules and fitting by an allometric function  $f(x) = a \cdot x^b$  (Figure 4.21b, black curve), yielded a value of  $b = -0.99 \pm 0.38$  and proved the anti proportional dependence of ON-time on excitation intensity. This decrease of the acceptor ON-times goes along with a superlinear dependence of the donor fluorescence on excitation intensity plotted in Figure 4.21b (grey dots) that is fitted using equation (4.4) ( see below).

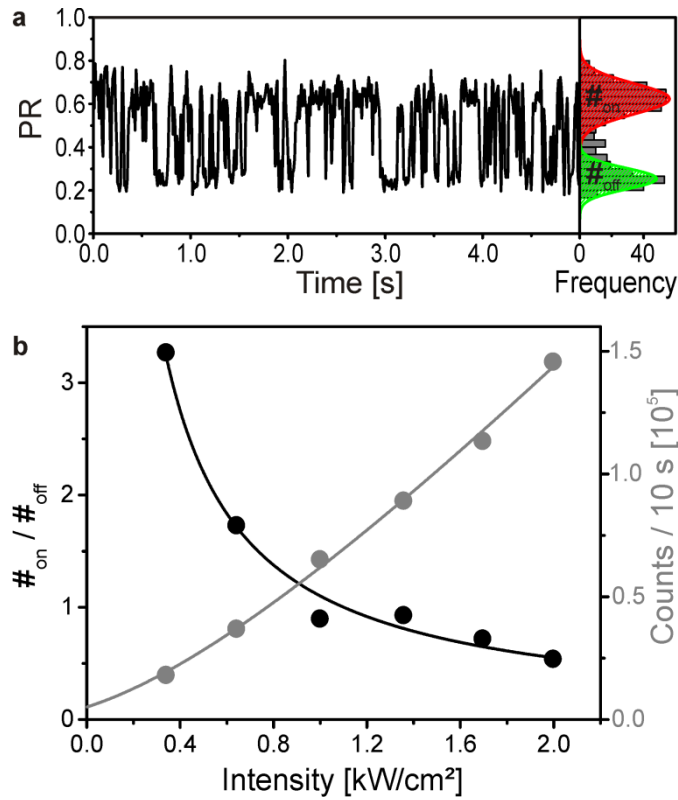


**Figure 4.21.** Demonstration of the superlinear fluorescence behavior of a 1-acceptor ETBP: (a) Proximity ratio transient of an ETBP (250  $\mu\text{M}$  AA, 1 mM MV and oxygen removal) with 10 ms binning excited at  $\lambda_{\text{Exc}} = 640$  nm with 1.7  $\text{kW}/\text{cm}^2$ . The right panel shows a histogram of the PR-values. The histogram is additionally fitted with a two peak Gaussian function (green, red). (b) Plot of the ratio  $\#_{\text{on}}/\#_{\text{off}}$  versus excitation intensity (black dots) of one ETBP fitted with an allometric function  $f(x)=a \cdot x^b$  (black curve) and plot of the superlinear donor fluorescence versus excitation intensity (grey dots) of the same molecule fitted using equation (5.4) (see below). The fit is based on a 1-acceptor ETBP plus an offset with the experimentally obtained values  $C_1 = 0.71$  and  $\alpha_1 = 1.8$   $\text{kW}/\text{cm}^2$  (grey, see below for definitions of  $C_1$  and  $\alpha_1$ ). For each data point the average intensity over 10 s was plotted against the excitation intensity.

#### 4.5.3. Theoretical Description of the ETBP

In the following the superlinear fluorescence dependence of the donor on excitation intensity is quantified and the consequences for the optical resolution are discussed. With the assumption, that the energy transfer rate is the same to all acceptors within an  $n$ -acceptor ETBP, the donor fluorescence  $F_D$  is given by (see supporting information of P5 for a detailed derivation):

$$F_D(I) \propto I \cdot \sum_{i=0}^n (1 - C_i) \cdot \binom{n}{i} \cdot \left(1 + \frac{I}{\alpha_i}\right)^{-i} \cdot \left(1 + \frac{\alpha_{i+1}}{I}\right)^{i-n} \quad (4.4)$$

This proportionality neglects parameters such as detection efficiency, quantum yield and absorption cross section that are not necessary for the quantification of resolution. Here,  $C_i$  corresponds to the contrast of the donor fluorescence. The contrast describes the ratio of each intensity level  $F_{D,i}$  of the donor with  $i$  acceptors being ON with respect to the intensity level  $F_{D,0}$  of the donor with 0 acceptors being ON ( $C_i = (F_{D,0} - F_{D,i})/F_{D,0}$ ). The contrast is influenced by the FRET efficiency, the background intensity in the donor channel and possible crosstalk from acceptor fluorescence into the donor channel. The value  $\alpha_i$  describes the ratio of ON- to OFF- times at a certain excitation intensity and is defined as:

$$\alpha_i = \frac{I_0 \cdot \tau_{on,i}(I_0)}{\tau_{off}} \quad (4.5)$$

In this equation  $\tau_{on,i}(I_0)$  corresponds to the average ON-time the acceptors spend in the ON-state at a certain excitation intensity  $I_0$  with  $i$  acceptors actually being in the ON-state.  $\tau_{off}$  denotes the average OFF-time of the acceptors.  $C_i$  and  $\alpha_i$  can be written in terms of a 1-acceptor ETBP, i.e.  $C_1$  and  $\alpha_1$  as follows:

$$C_i = 1 - \left( 1 + i \cdot \frac{C_1}{1 - C_1} \right)^{-1} \quad (4.6)$$

and

$$\alpha_i = \frac{C_1 + dx_D^A}{\left( \frac{1 - C_1}{C_1} + i \right)^{-1} + dx_D^A} \cdot \alpha_1 \quad (4.7)$$

where  $dx_D^A$  denotes the direct excitation of the acceptor at the donor excitation wavelength, which has to be taken into account since it alters the blinking kinetics of the acceptors. For the FRET-pair ATTO647N and ATTO680 excited at 640 nm direct excitation was determined to  $dx_D^A = 0.44$ .

$C_1$  and  $\alpha_1$  are determined from transients such as in Figure 4.20a and Figure 4.21a. A histogram of the donor intensity exhibits two populations resulting from the blinking of the acceptor (Figure 4.21b, black bars). Fitting the histogram with a two-peak Gaussian function yields the mean values for  $F_{D,0}$  and  $F_{D,1}$  that allow straightforward calculation of  $C_1$  (see equation S2 of P5). From 40 ETBP molecules  $C_1$  is found to be  $C_1 = 0.71 \pm 0.05$ .

Since the ratio  $\#_{on}/\#_{off}$  is equal to the ratio  $\tau_{on,1}(I_0)/\tau_{off}$ , equation (4.5) can be rewritten to:

$$\frac{\#_{on}}{\#_{off}} = \frac{\tau_{on,1}(I_0)}{\tau_{off}} = \frac{\alpha_1}{I_0} \quad (4.8)$$

To determine  $\alpha_1$ , the ratio  $\#_{on}/\#_{off}$  was analyzed for a 1-acceptor ETBP at different excitation intensities  $I_0$ . Fitting the plot of  $\#_{on}/\#_{off}$  versus  $I_0$  with equation 5 yields  $\alpha_1$  (see Figure 4.21b, black dots). Since  $\alpha_1$  is controllable by the concentrations of reductant and oxidant, we chose 250  $\mu$ M AA and 1 mM MV for comparable fast blinking kinetics ( $\tau_{on,1}(I_0 = 1.5 \text{ kW/cm}^2) = 16 \pm 5 \text{ ms}$ ,  $\tau_{off} = 10 \pm 2 \text{ ms}$ ) and high photostability (see P2). Under these conditions we determined  $\alpha_1$  averaged over 20 molecules to  $\alpha_1 = 1.8 \pm 0.8 \text{ kW/cm}^2$ .

As already pointed out, the PSF is mainly given by the excitation volume and the width of the excitation volume  $W_{Exc}$  can be estimated using equation (4.1 and 4.2). Approximating the excitation intensity profile with a Gaussian function allows estimating the width of the excitation volume to  $W_{Exc} \sim 230 \text{ nm}$  at  $\lambda_{Exc} = 640 \text{ nm}$ , a numerical aperture of the objective of  $NA = 1.40$  and a perfect illumination of the back aperture. Due to the superlinear fluorescence of the ETBP, the detected PSF is altered with respect to the excitation volume. To calculate the effective width of the excitation volume  $W_{Exc,Eff}$  the Gaussian intensity profile with a width of 230 nm is inserted into equation (4.4) and the resulting fluorescence profile is fitted by a Gaussian function. This procedure allows estimating  $W_{Exc,Eff}$  of the ETBP as well as the influence of the excitation intensity. Figure 4.22a shows the dependence of  $W_{Exc,Eff}$  for a 1-acceptor ETBP on the excitation intensity and varying values of  $\alpha_1$  and  $C_1$ . The calculations are performed for different (realistic)

values of  $\alpha_1$  and  $C_1$ , recalling that  $\alpha_1$  is determined by the ROXS controlled blinking kinetics and  $C_1$  is strongly related to the FRET efficiency. Interestingly, a minimum of the PSF exists for each condition at a specific excitation intensity. For a constant value of  $\alpha_1$ , for example, the minimum  $W_{\text{Exc, Eff}}$  is strongly decreasing with increasing  $C_1$  (Figure 4.22a, blue) indicating that the FRET efficiency is a crucial value for resolution enhancement with ETBPs. In contrast,  $\alpha_1$  has no influence on the obtainable resolution but determines the optimal excitation intensity (Figure 4.22a, red). This shows that the ETBP can be adjusted to reasonable values of excitation intensity and also of acquisition time by adapting ROXS (or by using a different acceptor with different redox potential) (see P1, P2 and P4).

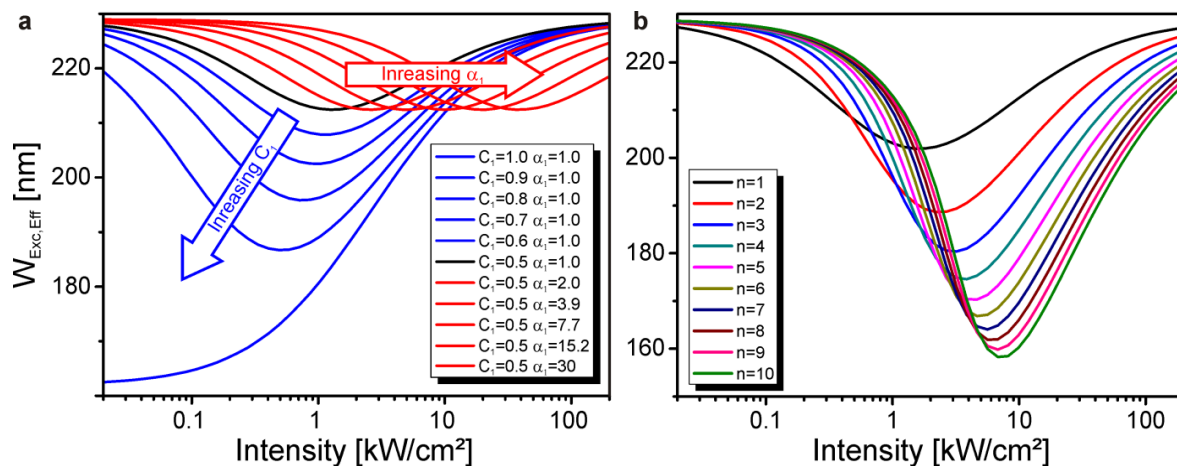


**Figure 4.22.** Effective width of the excitation volume  $W_{\text{Exc, Eff}}$  dependence with respect to the excitation intensity is shown. (a)  $W_{\text{Exc, Eff}}$  shown for a 1-acceptor ETBP at different values for  $C_1$  and  $\alpha_1$  and direct excitation  $dx_D^A = 0.44$ . (b)  $W_{\text{Exc, Eff}}$  shown for different number of acceptor fluorophores in an ETBP at constant – experimentally obtained – values for  $C_1$  and  $\alpha_1$  ( $C_1 = 0.71$ ;  $\alpha_1 = 1.8$  kW/cm<sup>2</sup>).

Another important factor for the resolution is the number of acceptors whose influence on  $W_{\text{Exc, Eff}}$  is plotted in Figure 4.23 for the  $C_1$  and  $\alpha_1$  value of the ETBP used ( $C_1 = 0.71$  and  $\alpha_1 = 1.8$  kW/cm<sup>2</sup>). More acceptors increase the superlinearity of the donor fluorescence and thus increase the achievable resolution to below 180 nm for  $n > 3$ . Figure 4.23 also demonstrates that the minimum  $W_{\text{Exc, eff}}$  is achieved at higher excitation intensity for increasing  $n$ . Since the FRET efficiency strongly influences the achievable resolution and because FRET efficiencies close to unity have already been demonstrated on the level of single molecules (see e.g. ref.<sup>[120]</sup>), the realistic potential of ETBPs is evaluated by plotting the best achievable  $W_{\text{Exc, Eff}}$  versus the number of acceptors for the contrast of  $C_1=0.71$  used in this work (grey dots in Figure 4.23) and a maximum  $C_1$  of  $C_1 = 0.999$  (black dots in Figure 4.23). Accordingly, a  $W_{\text{Exc, eff}}$  below 100 nm can be achieved with probes bearing 10 acceptors.

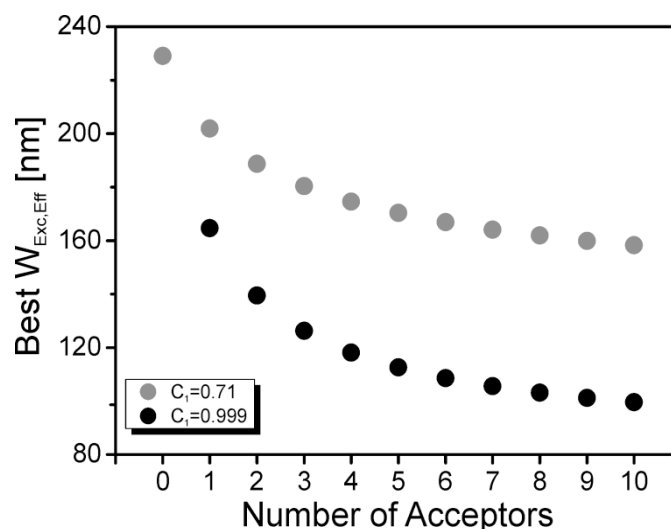


**Figure 4.23.** Best obtainable  $W_{Exc, Eff}$  with respect to the number of acceptors at two different values for  $C_1$  (grey dots,  $C_1 = 0.71$ ; black dots  $C_1 = 0.999$ ).

#### 4.5.4. Demonstration of Intrinsic Sub-Diffraction Resolution

For an experimental verification of the intrinsic resolution enhancement by ETBPs constructs with zero, one, and two acceptor(s) are used (Figure 4.18). Based on the theoretical treatment (see Figure 4.22a), we adapted  $\alpha_1$  to an optimal excitation intensity of  $\sim 1.7$  kW/cm<sup>2</sup> for a 1-acceptor ETBP and  $\sim 2.4$  kW/cm<sup>2</sup> for a 2-acceptor ETBP using ROXS (250  $\mu$ M AA, 1 mM MV). Confocal scans of the surface revealed the positions of individual ETBPs such as the one in the inset of Figure 4.24a. The false color image indicates the higher FRET value at the rim and the lower FRET value in the center that is due to the described saturation of the acceptor and superlinearity of the donor. the centers of each spot is scanned several times over a range of 1.5  $\mu$ m with a step size of 50 nm, and a time resolution of 1 s per step (as indicated in the spot of Figure 4.24a) to obtain statistics on PSFs.



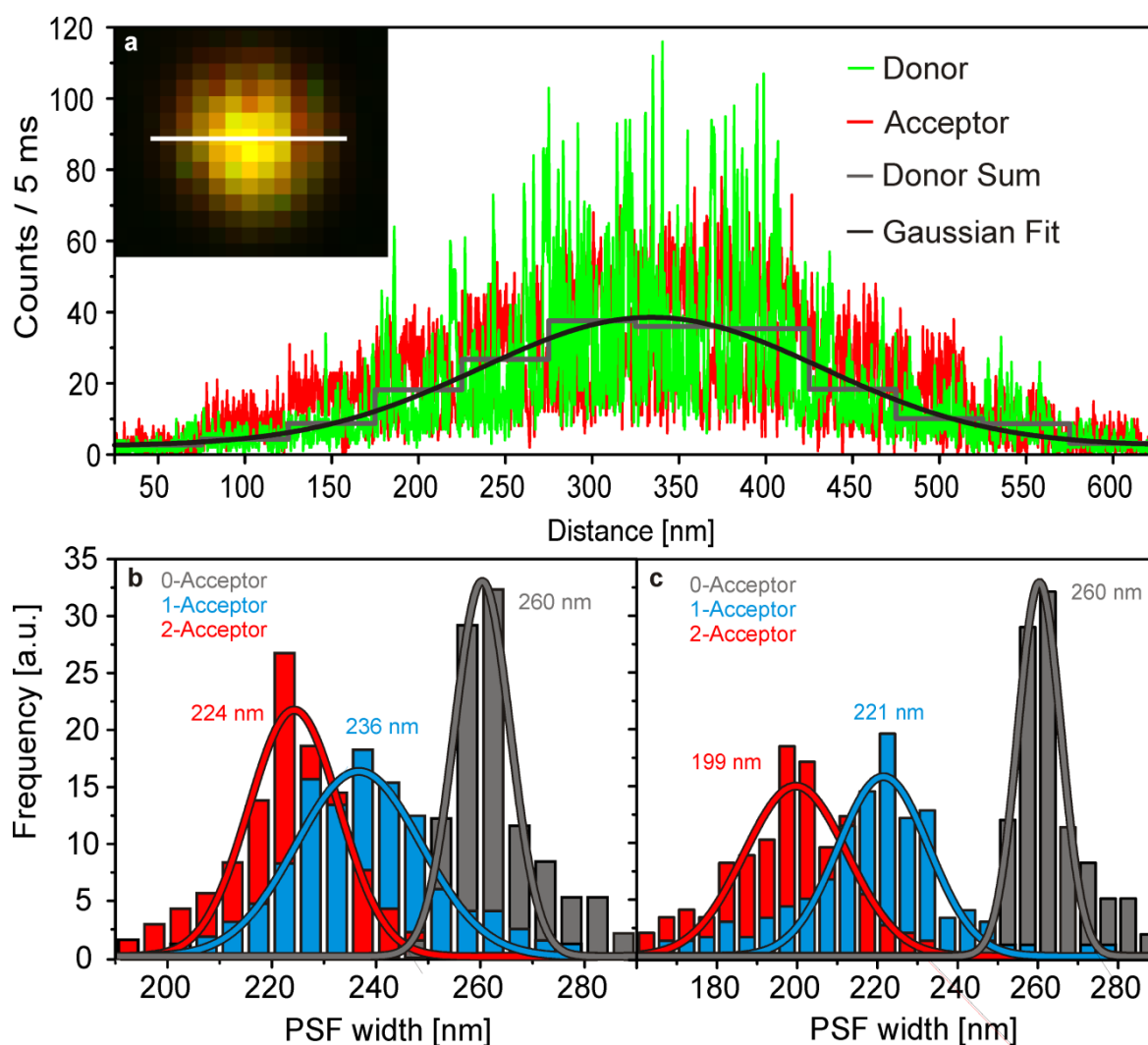


**Figure 4.24.** Determination of the PSF-width for different ETBPs in a confocal microscope. (a) One-dimensional scan of a single immobilized 1-acceptor ETBP. The fluorescence of the donor (green) and acceptor (red) channel was recorded for 1 s per 50 nm step and displayed at 5 ms time binning. The black graph corresponds to a Gaussian fit over the sum donor fluorescence intensity for each step. The upper left inset shows a complete two-dimensional scan of a 1-acceptor ETBP (50 nm / pixel). The white line illustrates the one dimensional scan. (b) Normalized PSF-histograms obtained from Gaussian fits of the donor fluorescence for a 0- (grey), 1- (blue) and 2- (red) acceptor ETBP. (c) Corresponding normalized PSF-Histograms for an idealized  $C_1$ -value of 1 for a 0- (grey), 1- (blue) and 2- (red) acceptor ETBP. The values were obtained by omitting donor photons emitted when one of the acceptors was ON.

This yields transients such as the one shown in Figure 4.24a (red = acceptor emission, green = donor emission). To determine the PSF-width of each scan, the overall donor-fluorescence for each scanning step is plotted against the position (Figure 4.24a, donor sum, grey) and fitted with a Gaussian function (Figure 4.24a, Gaussian fit, black). Repeating the procedure for >200 single ETBPs yields histograms of PSF-widths displayed in Figure 4.24b. Gaussian fits to the PSF distributions show that experimentally ~260 nm wide PSFs are obtained for the donor only molecules (Figure 4.24b, grey), ~236 nm for the 1-acceptor ETBP (Figure 4.24b, blue), and ~224 nm for the 2-acceptor ETBP (Figure 4.24b, red). Based on the 260 nm measured for the donor-only sample, the expected resolution is calculated with the ETBPs using equation 4.4 – 4.7 (see supporting informations of P5 for details). The calculated values of 232 nm for the 1-acceptor ETBP and 219 nm for the 2-acceptor ETBP deviate from the experimental values only slightly, which is assigned to minor inhomogeneities of photophysical parameters from ETBP to ETBP (the

excitation intensity was optimized for the average molecule and slightly varies from molecule to molecule) and the not fully achieved photodynamic equilibrium in the outer parts of the spots.

As pointed out, a key parameter for the achievable resolution is the contrast value  $C_1$  (see Figure 4.22a). To show the potential of ETBPs for resolution enhancement in confocal microscopes 100% FRET efficiency is emulated, i.e. a  $C_1$ -value of 1. This is possible because single ETBPs are studied whose blinking was adapted to the millisecond range. By omitting the donor photons emitted when the acceptor was ON,  $C_1 = 1$  is emulated. Therefore, the fluorescence transients measured to determine the PSFs are binned in 5 ms steps and analyzed with respect to the PR. For bins with  $PR > 0.6$ , the photons of the donor are omitted yielding new PSF-widths histogrammed in Figure 4.24c with a mean of  $\sim 221$  nm for the 1-acceptor ETBP and  $\sim 199$  nm for the 2-acceptor ETBP (see Figure 4.24c). These values deviate slightly more from the theoretical values of 210 nm and 185 nm because the binning and thresholding are not perfectly separating the states. The almost doubling of the resolution improvement emulating  $C_1 = 1$ , however, indicates the importance of a high FRET efficiency for the further development of intrinsic resolution enhancing probes for confocal microscopy.

## 5. Conclusion and Outlook

In this work, it was demonstrated that photo-induced electron transfer reactions and charge separated states play an important role in SMFS and super-resolution microscopy. At first, a unifying concept was introduced, which includes charge separated states into the description of the photophysics of organic fluorophores. By thermodynamic considerations different applications of the concept were proposed to exploit the charge separated states: (i) The charge separated states can be used as transition states for a fast depopulation of the triplet state to reduce blinking and to prevent photobleaching. (ii) Provided that one of the radical states is sufficiently stable, this state can be used as a long-lived dark state, which results in long lasting blinking of the fluorophores with controllable on- and off-state lifetimes.

These theoretical considerations were followed by the introduction of a buffer system containing reducing as well as oxidizing agents (ROXS), for exploiting charge separated states to generate stable and non-blinking fluorophores. The success of this approach was demonstrated by single-molecule fluorescence spectroscopy of oligonucleotides labeled with different fluorophores, that is, cyanines, (carbo-)rhodamines, and oxazines, in aqueous solvents; individual fluorophores could be observed for minutes under moderate excitation conditions with increased fluorophore brightness. In particular, it was shown that the photostability of the fluorophores can be strongly extended using the combination of reductant and oxidant, for example, by a factor of > 800 for ATTO647N. Although a similar effect was found regarding the reduction of blinking for shorter wavelength fluorophores such as Cy3B and ATTO565, the photostabilizing effect was not as pronounced.

The underlying unifying concept represents a paradigm change in photobleaching prevention and a step away from the purely empirical search for anti-fading formulas. Further, the increased photostability can be used to investigate conformational changes in biological systems with a significant improvement of the statistics, as was evidenced by the investigation of the influence of methylviologen on the dynamics of Holliday junctions.

As detailed in the introduction section, the resolution in STED microscopy is dependent on the number of switching cycles between a fluorescent and a dark state, i.e., the ground state  $S_0$  and the excited state  $S_1$ .<sup>[115]</sup> ROXS increases the number of cycles between these two states substantially, increasing the achievable resolution by using organic fluorophores in STED microscopy.

Regarding the second application, fluorophores were investigated with a very low lying reduction potential. It could be shown via cyclic voltammetry that the fluorophores belonging to the class of oxazines exhibit a low reduction potential compared to other classes, e.g., cyanines and (carbo-)rhodamines. Further, it was demonstrated by SMFS that the radical anion states of oxazines are stable within the range of minutes, if no oxidizing agent is present. This was exploited to switch oxazines between a stable fluorescent state and a stable dark state, resulting in a very high number of switching cycles between these two states. Cycle numbers up to 3000 could be demonstrated. The generic nature of the dark state, i.e., the anionic state, indicates the universal character of the switching mechanism and suggests that for the development of switchable molecules the interaction with the environment might be as important as the design of the molecular switch itself. By using oxidizing and reducing agents simultaneously, continuous switching was demonstrated and exploited for the elaboration of a detailed kinetic scheme. Importantly, the oxidant and the reductant represent two independent variables to control on- and off-times, respectively. This control of fluorescence could even be carried out in the presence of oxygen and furthermore enabled super-resolution 'Blink microscopy' of oxazine labeled actin filaments immobilized on glass slides and actin bundles in fixed cells.

Since the reduced state is sensitive to oxidizing species, this combination of dye properties and buffer ingredients could be regarded as a single molecules redox sensor (SMRS). By applying this SMRS the anti-fading mechanism of the vitamin E analog Trolox could be resolved. It was proven by the use of the SMRS and ensemble measurements that Trolox works according to the ROXS concept. Trolox generates a Trolox -quinone upon UV irradiation, which can then act as an oxidizing agent.

The high number of switching cycles makes oxazines, in combination with the ROXS buffer, an excellent candidate for GSD microscopy.<sup>[21]</sup> Here, the ground state depletion can be achieved by shelving the molecules into the stable reduced state. In addition, the long lifetime of the reduced state can be used to saturate the fluorophore at very low excitation intensities. Moreover it is even possible to adjust the saturation since the on and off-times are controllable by the amount of reductant and oxidant. In the future this saturation can be used for SPEM or SSIM with organic fluorophores.

Finally, it was demonstrated that this saturation at low excitation intensities can increase the resolution in a standard confocal microscope. Therefore a fluorescent probe was developed which converts the saturation of the oxazine fluorophore into a superlinear fluorescent dependency, by using FRET. Under ROXS buffer conditions these probes are called energy transfer blockade probes (ETBP). In this context, the whole chain of development was shown: First, the principles of how to engineer ETBPs were explained. Second, a theoretical model was developed that quantitatively describes the fluorescence of the ETBP. Third, the feasibility of resolution enhancement was demonstrated by measuring single ETBPs.

In summary, the introduction of charge separated states into the photophysics of organic fluorophores opens the door to exciting new techniques in SMFS and super-resolution microscopy. The exquisite control over the fluorescence allows the development of novel applications, ranging from advanced single molecule experiments over mechanistic studies of photophysics to sophisticated new super-resolution techniques.

## 6. References

1. Thompson, R.E., Larson, D.R. & Webb, W.W. Precise nanometer localization analysis for individual fluorescent probes. *Biophys. J.* **82**, 2775-2783 (2002).
2. Yildiz, A. et al. Myosin V walks hand-over-hand: Single fluorophore imaging with 1.5-nm localization. *Science* **300**, 2061-2065 (2003).
3. Yildiz, A. & Selvin, P.R. Fluorescence imaging with one nanometer accuracy: Application to molecular motors. *Accounts Chem. Res.* **38**, 574-582 (2005).
4. Tardin, C., Cognet, L., Bats, C., Lounis, B. & Choquet, D. Direct imaging of lateral movements of AMPA receptors inside synapses. *Embo J.* **22**, 4656-4665 (2003).
5. Schutz, G.J., Schindler, H. & Schmidt, T. Single-molecule microscopy on model membranes reveals anomalous diffusion. *Biophys. J.* **73**, 1073-1080 (1997).
6. Xu, X.H. & Yeung, E.S. Direct measurement of single-molecule diffusion and photodecomposition in free solution. *Science* **275**, 1106-1109 (1997).
7. Ha, T. et al. Probing the interaction between two single molecules: Fluorescence resonance energy transfer between a single donor and a single acceptor. *Proc. Natl. Acad. Sci. U. S. A.* **93**, 6264-6268 (1996).
8. Kapanidis, A.N. et al. Fluorescence-aided molecule sorting: Analysis of structure and interactions by alternating-laser excitation of single molecules. *Proc. Natl. Acad. Sci. U. S. A.* **101**, 8936-8941 (2004).
9. Ha, T. et al. Initiation and re-initiation of DNA unwinding by the Escherichia coli Rep helicase. *Nature* **419**, 638-641 (2002).
10. McKinney, S.A., Declais, A.-C., Lilley, D.M.J. & Ha, T. Structural dynamics of individual Holliday junctions. *Nat. Struct. Biol.* **10**, 93-97 (2003).
11. Tomschik, M., Zheng, H.C., van Holde, K., Zlatanova, J. & Leuba, S.H. Fast, long-range, reversible conformational fluctuations in nucleosomes revealed by single-pair fluorescence resonance energy transfer. *Proc. Natl. Acad. Sci. U. S. A.* **102**, 3278-3283 (2005).
12. Tomschik, M., van Holde, K. & Zlatanova, J. Nucleosome Dynamics as Studied by Single-pair Fluorescence Resonance Energy Transfer: A Reevaluation. *J. Fluoresc.* **19**, 53-62 (2009).
13. Kandori, H., Kemnitz, K. & Yoshihara, K. Subpicosecond Transient Absorption Study of Intermolecular Electron-Transfer between Solute and Electron-Donating Solvents. *J. Phys. Chem.* **96**, 8042-8048 (1992).
14. Chibisov, A.K. Triplet-States of Cyanine Dyes and Reactions of Electron-Transfer with Their Participation. *J Photochem* **6**, 199-214 (1977).
15. Korobov, V.E. & Chibisov, A.K. Primary Processes in Photochemistry of Rhodamine Dyes. *J Photochem* **9**, 411-424 (1978).
16. Verdet, É. Leçons d'optique physique. (Victor Masson et fils, Paris; 1869).
17. Abbe, E. Beiträge zur Theorie des Mikroskops und der mikroskopischen Wahrnehmung. *Arch. Mikr. Anat.* **9**, 413-468 (1873).
18. Rayleigh, L. On the theory of optical images, with special reference to the microscope. *Philos. Mag.* **XLII**, 167-195 (1896).

19. Hell, S.W. & Wichmann, J. Breaking the Diffraction Resolution Limit by Stimulated-Emission - Stimulated-Emission-Depletion Fluorescence Microscopy. *Opt. Lett.* **19**, 780-782 (1994).
20. Klar, T.A., Jakobs, S., Dyba, M., Egner, A. & Hell, S.W. Fluorescence microscopy with diffraction resolution barrier broken by stimulated emission. *Proc. Natl. Acad. Sci. U. S. A.* **97**, 8206-8210 (2000).
21. Hell, S.W. & Kroug, M. Ground-State-Depletion Fluorescence Microscopy - a Concept for Breaking the Diffraction Resolution Limit. *Appl. Phys. B-Lasers Opt.* **60**, 495-497 (1995).
22. Bretschneider, S., Eggeling, C. & Hell, S.W. Breaking the diffraction barrier in fluorescence microscopy by optical shelving. *Phys. Rev. Lett.* **98**, - (2007).
23. Heintzmann, R., Jovin, T.M. & Cremer, C. Saturated patterned excitation microscopy - a concept for optical resolution improvement. *J. Opt. Soc. Am. A-Opt. Image Sci. Vis.* **19**, 1599-1609 (2002).
24. Gustafsson, M.G.L. Nonlinear structured-illumination microscopy: Wide-field fluorescence imaging with theoretically unlimited resolution. *Proc. Natl. Acad. Sci. U. S. A.* **102**, 13081-13086 (2005).
25. Gustafsson, M.G.L. Surpassing the lateral resolution limit by a factor of two using structured illumination microscopy. *J. Microsc.-Oxf.* **198**, 82-87 (2000).
26. Heintzmann, R. & Benedetti, P.A. High-resolution image reconstruction in fluorescence microscopy with patterned excitation. *Appl Opt* **45**, 5037-5045 (2006).
27. Shannon, C.E. Communication in the Presence of Noise. *Proceedings of the Institute of Radio Engineers* **37**, 10-21 (1949).
28. Rust, M.J., Bates, M. & Zhuang, X. Sub-diffraction-limit imaging by stochastic optical reconstruction microscopy (STORM). *Nat Methods* **3**, 793-795 (2006).
29. Bates, M., Huang, B., Dempsey, G.T. & Zhuang, X. Multicolor super-resolution imaging with photo-switchable fluorescent probes. *Science* **317**, 1749-1753 (2007).
30. Huang, B., Wang, W., Bates, M. & Zhuang, X. Three-dimensional super-resolution imaging by stochastic optical reconstruction microscopy. *Science* **319**, 810-813 (2008).
31. Heilemann, M. et al. Subdiffraction-Resolution Fluorescence Imaging with Conventional Fluorescent Probes. *Angew Chem Int Ed Engl* **47**, 6172-6176 (2008).
32. Betzig, E. et al. Imaging intracellular fluorescent proteins at nanometer resolution. *Science* **313**, 1642-1645 (2006).
33. Hess, S.T., Girirajan, T.P. & Mason, M.D. Ultra-high resolution imaging by fluorescence photoactivation localization microscopy. *Biophys. J.* **91**, 4258-4272 (2006).
34. Folling, J. et al. Fluorescence nanoscopy by ground-state depletion and single-molecule return. *Nat Methods* **5**, 943-945 (2008).
35. Steinhauer, C., Forthmann, C., Vogelsang, J. & Tinnefeld, P. Superresolution microscopy on the basis of engineered dark states. *J. Am. Chem. Soc.* **130**, 16840-16841 (2008).
36. Sharonov, A. & Hochstrasser, R.M. Wide-field subdiffraction imaging by accumulated binding of diffusing probes. *Proc. Natl. Acad. Sci. U. S. A.* **103**, 18911-18916 (2006).
37. Michalet, X. et al. Properties of fluorescent semiconductor nanocrystals and their application to biological labeling. *Single Mol.* **2**, 261-276 (2001).
38. Gruber, A. et al. Scanning confocal optical microscopy and magnetic resonance on single defect centers. *Science* **276**, 2012-2014 (1997).

39. VandenBout, D.A. et al. Discrete intensity jumps and intramolecular electronic energy transfer in the spectroscopy of single conjugated polymer molecules. *Science* **277**, 1074-1077 (1997).
40. Harms, G.S., Cognet, L., Lommerse, P.H.M., Blab, G.A. & Schmidt, T. Autofluorescent proteins in single-molecule research: Applications to live cell imaging microscopy. *Biophys. J.* **80**, 2396-2408 (2001).
41. Weiss, S. Fluorescence spectroscopy of single biomolecules. *Science* **283**, 1676-1683 (1999).
42. Ha, T. Single-molecule fluorescence resonance energy transfer. *Methods* **25**, 78-86 (2001).
43. Doose, S., Neuweiler, H. & Sauer, M. Fluorescence Quenching by Photoinduced Electron Transfer: A Reporter for Conformational Dynamics of Macromolecules. *ChemPhysChem* **10**, 1389-1398 (2009).
44. Liphardt, B., Liphardt, B. & Luttko, W. Laser-Dyes .3. Concepts to Increase the Photostability of Laser-Dyes. *Opt. Commun.* **48**, 129-133 (1983).
45. Liphardt, B., Liphardt, B. & Luttko, W. Laser-Dyes with Intramolecular Triplet Quenching. *Opt. Commun.* **38**, 207-210 (1981).
46. Condon, E.U. Nuclear motions associated with electron transitions in diatomic molecules. *Phys. Rev.* **32**, 0858-0872 (1928).
47. Wolf, H.C. & Haken, H. *Molekülphysik und Quantenchemie*. (Springer Verlag, 1997).
48. Atkins, P.W., Trapp, C.A. & Paula, J.D. *Physikalische Chemie*. (Wiley-VCH: Weinheim [u.a.]).
49. Ambrose, W.P. et al. Fluorescence photon antibunching from single molecules on a surface. *Chem. Phys. Lett.* **269**, 365-370 (1997).
50. Basche, T., Moerner, W.E., Orrit, M. & Talon, H. Photon antibunching in the fluorescence of a single dye molecule trapped in a solid. *Phys. Rev. Lett.* **69**, 1516-1519 (1992).
51. Mets, U., Widengren, J. & Rigler, R. Application of the antibunching in dye fluorescence: Measuring the excitation rates in solution. *Chem. Phys.* **218**, 191-198 (1997).
52. Harada, Y., Sakurada, K., Aoki, T., Thomas, D.D. & Yanagida, T. Mechanochemical Coupling in Actomyosin Energy Transduction Studied By Invitro Movement Assay. *J. Mol. Biol.* **216**, 49-68 (1990).
53. Wang, H.L., MacDiarmid, A.G., Wang, Y.Z., Gebler, D.D. & Epstein, A.J. Application of polyaniline (emeraldine base, EB) in polymer light-emitting devices. *Synth. Met.* **78**, 33-37 (1996).
54. Hide, F., DiazGarcia, M.A., Schwartz, B.J. & Heeger, A.J. New developments in the photonic applications of conjugated polymers. *Accounts Chem. Res.* **30**, 430-436 (1997).
55. Deisenhofer, J., Epp, O., Miki, K. & Michel, H. X-ray structure analysis of a membrane protein complex. *J. Mol. Biol.* **180**, 385-398 (1984).
56. Knemeyer, J.P., Marme, N. & Sauer, M. Probes for detection of specific DNA sequences at the single- molecule level. *Anal. Chem.* **72**, 3717-3724 (2000).
57. Kavarnos, G.J. *Fundamentals of Photoinduced Electron Transfer*. (John Wiley & Sons, 1993).
58. Gilch, P., PollingerDammer, F., Steiner, U.E. & MichelBeyerle, M.E. Ultrafast electron transfer, recombination and spin dynamics. *Chem. Phys. Lett.* **275**, 339-348 (1997).
59. Marcus, R.A. On the theory of oxidation-reduction reactions involving electron transfer. *J. Chem. Phys.* **24**, 966-978 (1956).

60. Rehm, D. & Weller, A. Kinetics of fluorescence quenching by electron and hydrogen-atom transfer. *Isr. J. Chem.* **8**, 259-271 (1970).
61. Grabowski, Z.R. & Grabowska, A. The Förster cycle reconsidered. *Z. Phys. Chem. Neue Folge* **101**, 197-208 (1976).
62. Nicholson, R.S. Theory and Application of Cyclic Voltammetry for Measurement of Electrode Reaction Kinetics. *Anal. Chem.* **37**, 1351-& (1965).
63. Rosspeintner, A., Kattinig, D.R., Angulo, G., Landgraf, S. & Grampp, G. The Rehm-Weller experiment in view of distant electron transfer. *Chem.-Eur. J.* **14**, 6213-6221 (2008).
64. Vogelsang, J., Doose, S., Sauer, M. & Tinnefeld, P. Single-molecule fluorescence resonance energy transfer in nanopipets: Improving distance resolution and concentration range. *Anal. Chem.* **79**, 7367-7375 (2007).
65. Person, B., Stein, I.H., Steinhauer, C., Vogelsang, J. & Tinnefeld, P. Correlated Movement and Bending of Nucleic Acid Structures Visualized by Multicolor Single-Molecule Spectroscopy. *ChemPhysChem* **10**, 1455-1460 (2009).
66. Widengren, J. & Rigler, R. Mechanisms of photobleaching investigated by fluorescence correlation spectroscopy. *Bioimaging* **4**, 149-157 (1996).
67. Widengren, J. & Rigler, R. Review - Fluorescence correlation spectroscopy as a tool to investigate chemical reactions in solutions and on cell surfaces. *Cell. Mol. Biol.* **44**, 857-879 (1998).
68. Sterrer, S. & Henco, K. Fluorescence correlation spectroscopy (FCS) - A highly sensitive method to analyze drug/target interactions. *J. Recept. Signal Transduct. Res.* **17**, 511-520 (1997).
69. Axelrod, D. Total internal reflection fluorescence microscopy in cell biology. *Traffic* **2**, 764-774 (2001).
70. Funatsu, T., Harada, Y., Tokunaga, M., Saito, K. & Yanagida, T. Imaging of Single Fluorescent Molecules and Individual Atp Turnovers By Single Myosin Molecules in Aqueous-Solution. *Nature* **374**, 555-559 (1995).
71. Tokunaga, M., Kitamura, K., Saito, K., Iwane, A.H. & Yanagida, T. Single molecule imaging of fluorophores and enzymatic reactions achieved by objective-type total internal reflection fluorescence microscopy. *Biochem. Biophys. Res. Commun.* **235**, 47-53 (1997).
72. Axelrod, D. Selective imaging of surface fluorescence with very high aperture microscope objectives. *J. Biomed. Opt.* **6**, 6-13 (2001).
73. Hell, S.W. Far-field optical nanoscopy. *Science* **316**, 1153-1158 (2007).
74. van de Linde, S., Kapsner, R., Heilemann, M. & Sauer, M. Photoswitching microscopy with standard fluorophores. *Applied Physics B* (2008).
75. Vogelsang, J., Cordes, T., Forthmann, C., Steinhauer, C. & Tinnefeld, P. Controlling the fluorescence of ordinary oxazine dyes for single-molecule switching and superresolution microscopy. *Proc. Natl. Acad. Sci. U. S. A.* **106**, 8107 - 8112 (2009).
76. Dontha, N., Nowall, W.B. & Kuhr, W.G. Generation of biotin/avidin/enzyme nanostructures with maskless photolithography. *Anal. Chem.* **69**, 2619-2625 (1997).
77. Piestert, O. et al. A single-molecule sensitive DNA hairpin system based on intramolecular electron transfer. *Nano Lett.* **3**, 979-982 (2003).
78. Elson, E.L. & Magde, D. Fluorescence Correlation Spectroscopy .1. Conceptual Basis and Theory. *Biopolymers* **13**, 1-27 (1974).
79. Magde, D., Elson, E.L. & Webb, W.W. Fluorescence Correlation Spectroscopy .2. Experimental Realization. *Biopolymers* **13**, 29-61 (1974).



80. Widengren, J. & Schwille, P. Characterization of photoinduced isomerization and back-isomerization of the cyanine dye Cy5 by fluorescence correlation spectroscopy. *J. Phys. Chem. A* **104**, 6416-6428 (2000).
81. Neuweiler, H. & Sauer, M. Using photoinduced charge transfer reactions to study conformational dynamics of biopolymers at the single-molecule level. *Curr. Pharm. Biotech.* **5**, 285-298 (2004).
82. Neuweiler, H., Schulz, A., Boehmer, M., Enderlein, J. & Sauer, M. Measurement of submicrosecond intramolecular contact formation in peptides at the single-molecule level. *J. Am. Chem. Soc.* **125**, 5324-5330 (2003).
83. Widengren, J., Chmyrov, A., Eggeling, C., Lofdahl, P.A. & Seidel, C.A.M. Strategies to improve photostabilities in ultrasensitive fluorescence spectroscopy. *J. Phys. Chem. A* **111**, 429-440 (2007).
84. Rasnik, I., McKinney, S.A. & Ha, T. Nonblinking and long-lasting single-molecule fluorescence imaging. *Nat Methods* **3**, 891-893 (2006).
85. Heilemann, M., Margeat, E., Kasper, R., Sauer, M. & Tinnefeld, P. Carbocyanine dyes as efficient reversible single-molecule optical switch. *J. Am. Chem. Soc.* **127**, 3801-3806 (2005).
86. Eggeling, C. et al. Direct observation of the nanoscale dynamics of membrane lipids in a living cell. *Nature* **457**, 1159-U1121 (2009).
87. Lambert, C.R. & Kochevar, I.E. Electron transfer quenching of the rose Bengal triplet state. *Photochem. Photobiol.* **66**, 15-25 (1997).
88. Kasper, R., Heilemann, M., Tinnefeld, P. & Sauer, M. Towards Ultra-Stable Fluorescent Dyes for Single-Molecule Spectroscopy. *Proc. SPIE* **6633**, 66331Z66331-66331Z66312 (2007).
89. Huang, Z. et al. Direct Observation of Delayed Fluorescence from a Remarkable Back-Isomerization in Cy5. *J. Am. Chem. Soc.* **127**, 8064-8066 (2005).
90. Kiel, A., Kovacs, J., Mokhir, A., Kramer, R. & Hertel, D.P. Direct monitoring of formation and dissociation of individual metal complexes by single-molecule fluorescence spectroscopy. *Angew. Chem. Int. Ed.* **46**, 5049-5049 (2007).
91. Vosch, T. et al. Probing Foerster Type Energy Pathways in a First Generation Rigid Dendrimer Bearing Two Perylene Imide Chromophores. *J. Phys. Chem. A* **107**, 6920-6931 (2003).
92. Lu, H.P. & Xie, X.S. Single-molecule kinetics of interfacial electron transfer. *J. Phys. Chem. B* **101**, 2753-2757 (1997).
93. Holman, M.W., Liu, R. & Adams, D.M. Single-molecule spectroscopy of interfacial electron transfer. *J. Am. Chem. Soc.* **125**, 12649-12654 (2003).
94. Liu, R., Holman, M.W., Zang, L. & Adams, D.M. Single-Molecule Spectroscopy of Intramolecular Electron Transfer in Donor-Bridge-Acceptor Systems. *J. Phys. Chem. A* **107**, 6522-6526 (2003).
95. Cotlet, M. et al. Probing intramolecular Forster resonance energy transfer in a naphthaleneimide-peryleneimide-terrylenediimide-based dendrimer by ensemble and single-molecule fluorescence spectroscopy. *J. Am. Chem. Soc.* **127**, 9760-9768 (2005).
96. Cotlet, M. et al. Probing conformational dynamics in single donor-acceptor synthetic molecules by means of photoinduced reversible electron transfer. *Proc. Natl. Acad. Sci. U. S. A.* **101**, 14343-14348 (2004).
97. Zondervan, R., Kulzer, F., Orlinskii, S.B. & Orrit, M. Photoblinking of Rhodamine 6G in Poly(vinyl alcohol): Radical Dark State Formed through the Triplet. *J. Phys. Chem. A* **107**, 6770-6776 (2003).

98. Hoogenboom, J.P., van Dijk, E.M.H.P., Hernando, J., van Hulst, N.F. & Garcia-Parajo, M.F. Power-Law-Distributed Dark States are the Main Pathway for Photobleaching of Single Organic Molecules. *Phys. Rev. Lett.* **95**, 097401/097401-097401/097404 (2005).
99. Yeow, E.K.L., Melnikov, S.M., Bell, T.D.M., De Schryver, F.C. & Hofkens, J. Characterizing the Fluorescence Intermittency and Photobleaching Kinetics of Dye Molecules Immobilized on a Glass Surface. *J. Phys. Chem. A* **110**, 1726-1734 (2006).
100. Schuster, J., Cichos, F. & von Borczyskowski, C. Blinking of Single Molecules in Various Environments. *Opt. Spectrosc.* **98**, 712-717 (2005).
101. Aitken, C.E., Marshall, R.A. & Puglisi, J.D. An oxygen scavenging system for improvement of dye stability in single-molecule fluorescence experiments. *Biophys. J.* **94**, 1826-1835 (2008).
102. Holleman, A.F. & Wiberg, E. *Lehrbuch der Anorganischen Chemie.* (de Gruyter, New York, 1995).
103. Kapanidis, A.N. et al. Alternating-laser excitation of single molecules. *Accounts Chem. Res.* **38**, 523-533 (2005).
104. Bossi, M. et al. Multicolor Far-Field Fluorescence Nanoscopy through Isolated Detection of Distinct Molecular Species. *Nano Lett* (2008).
105. Shroff, H., Galbraith, C.G., Galbraith, J.A. & Betzig, E. Live-cell photoactivated localization microscopy of nanoscale adhesion dynamics. *Nat Methods* **5**, 417-423 (2008).
106. Neubauer, H. et al. Orientational and dynamical heterogeneity of rhodamine 6G terminally attached to a DNA helix revealed by NMR and single-molecule fluorescence spectroscopy. *J. Am. Chem. Soc.* **129**, 12746-12755 (2007).
107. Eggeling, C., Fries, J.R., Brand, L., Gunther, R. & Seidel, C.A.M. Monitoring conformational dynamics of a single molecule by selective fluorescence spectroscopy. *Proc. Natl. Acad. Sci. U. S. A.* **95**, 1556-1561 (1998).
108. Kim, J., Doose, S., Neuweiler, H. & Sauer, M. The initial step of DNA hairpin folding: a kinetic analysis using fluorescence correlation spectroscopy. *Nucleic Acids Res* **34**, 2516-2527 (2006).
109. Lacey, A.L.d. & Fernández, V.M. pH-Dependent redox behaviour of asymmetric viologens. *J. Electroanal. Chem.* **399**, 163-167 (1995).
110. Heineken, F.W., Bruin, F. & Bruin, M. ESR Investigation of Some Thiazine and Oxazine Dye Radicals. *J. Chem. Phys.* **37**, 1479-& (1962).
111. Zhang, R., Wang, Z., Wu, Y., Fu, H. & Yao, J. A novel redox-fluorescence switch based on a triad containing ferrocene and perylene diimide units. *Org Lett* **10**, 3065-3068 (2008).
112. Kim, H.J., Lee, H.O. & Min, D.B. Effects and prooxidant mechanisms of oxidized alpha-tocopherol on the oxidative stability of soybean oil. *Journal of food science* **72**, C223-C230 (2007).
113. Carlotti, M.E., Sapino, S., Vione, D., Pelizzetti, E. & Trota, M. Photostability of trolox in water/ethanol, water, and oramix CG 110 in the absence and in the presence of TiO<sub>2</sub>. *Journal of Dispersion Science and Technology* **25**, 193-207 (2004).
114. Delicado, E.N., Ferrer, A.S. & Carmona, F.G. A kinetic study of the one-electron oxidation of Trolox C by the hydroperoxidase activity of lipoxygenase. *Biochim. Biophys. Acta-Gen. Subj.* **1335**, 127-134 (1997).
115. Hell, S.W. Microscopy and its focal switch. *Nature Methods* **6**, 24-32 (2009).
116. Pawley, J.B. *Handbook of Biological Confocal Microscopy*, Edn. 2nd ed. (Plenum., New York; 1995).

117. Schönle, A., Hanninen, P.E. & Hell, S.W. Nonlinear fluorescence through intermolecular energy transfer and resolution increase in fluorescence microscopy. *Ann. Phys.-Berlin* **8**, 115-133 (1999).
118. Schönle, A. & Hell, S.W. Far-field fluorescence microscopy with repetitive excitation. *Eur. Phys. J. D* **6**, 283-290 (1999).
119. Tinnefeld, P., Buschmann, V., Weston, K.D. & Sauer, M. Direct observation of collective blinking and energy transfer in a bichromophoric system. *J. Phys. Chem. A* **107**, 323-327 (2003).
120. Remi, M., Fabian, N., Klaus, M. & Thomas, B. Electronic Excitation Energy Transfer between Two Single Molecules Embedded in a Polymer Host. *Phys. Rev. Lett.* **98**, 47802 (2007).

## 7. Acknowledgements

At this point I thank everyone, who made this work possible and accompanied me during my PhD time. Until now it was the best time in my life and I still enjoy every second, which I can spend in the university.

At first, for this great experience I want to thank Prof. Philip Tinnefeld, who has the main contribution to this. He gave me the opportunity to get out of Bielefeld and to broaden my mind, by getting into a new environment and establishing a lab out of scratch in Munich. Further, he was always available for great scientific and non-scientific discussions and came up with a lot of enlightened ideas. Sometimes it was a little stressful to fulfill all the great ideas, but it was always definitely worth the time.

Prof. Markus Sauer, for bringing me into the exciting field of single molecule fluorescence spectroscopy at the University of Bielefeld and for accompanying me during my first steps in the scientific world.

Prof. Wolfgang Zinth for the acceptance of the second expertise and the work involved.

Thorben for the great assistance in the last year regarding lab work, writing, helpful discussions and not to forget the exciting rubber boat tours on the Isar.

Britta for all the help and support in the lab especially for the preparation of the probes.

Daniel, Zazralt and Tino for the great assistance in building the setup during the first six months. It was a lot of fun and I didn't want to have to do this on my own.

At this point, thanks to the Machine Shop for all the small and big things.

Christian and Carsten for acquiring the super-resolution images and for the ongoing LabVIEW support and programming.

Robert for the collaboration in Bielefeld, regarding the reducing and oxidizing system.

All people in the group of Philip for the great working atmosphere.

For proofreading the manuscript I am grateful to Thorben, Kristin, Ingo, Matthias and Dominik.

Thanks to Prof. Hermann Gaub and the whole Gambi' Crew for feeling to be a part of this great chair in physics. The christmas parties and the food are the best, of course the scientific work, too.

Special thanks to the Stempler Crew (Dominik, Philip S., Katja and Uta) for giving me a place to be, when the room wasn't there and the great evening discussions.

For stimulating and helpful discussions I also want to thank Dominik, Philip S., Matthias, Elias and everyone else who wasn't fast enough.

Ralf, Thorben, Carolin, Stefan S. for being a part of the best Doppelkopf community I have ever met.

In the end I want to thank my parents, who always supported me in every possible way. Thank you for giving me the opportunity to do the things I want to do.

## 8. Appendix:

### 8.1. Associated Publications

In the following the publications are presented, on which this work is based on (labeled P1-P5).

- P1 Vogelsang J., Kasper R., Steinhauer C., Person B., Heilemann M., Sauer M. and Tinnefeld P., (2008) A reducing and oxidizing system minimizes photobleaching and blinking of fluorescent dyes. **Angew. Chem. Int. Ed.**, 47(29):5465-5469 (including cover picture).
- P2 Vogelsang J., Cordes T., Forthmann C., Steinhauer C. and Tinnefeld P., (2009) Controlling the fluorescence of ordinary oxazine dyes for single-molecule switching and super-resolution microscopy. **Proc. Natl. Acad. Sci. USA**, 106(20):8107-8112.
- P3 Vogelsang J., Cordes T. and Tinnefeld P., (2009) Single-molecule photophysics of oxazines on DNA and its application in a FRET switch. **Photochem. Photobiol. Sci.**, 8:486-496.
- P4 Cordes T., Vogelsang J. and Tinnefeld P., (2009) On the mechanism of Trolox as antiblinking and antibleaching reagent. **J. Am. Chem. Soc.**, 131(14):5018-5019.
- P5 Vogelsang J., Cordes T., Forthmann C., Steinhauer C. and Tinnefeld P., (2009) Intrinsically Resolution Enhancing Probes for Confocal Microscopy. **Nature Chemistry**, submitted.



P1

**A reducing and oxidizing system minimizes photobleaching and  
blinking of fluorescent dyes**

By

Vogelsang J., Kasper R., Steinhauer C., Person B., Heilemann M., Sauer M.  
and Tinnefeld P.

Published in

Angewandte Chemie International Edition, (2008) 47(29):5465-5469





P2

**Controlling the fluorescence of ordinary oxazine dyes for single-molecule switching and super-resolution microscopy**

By

Vogelsang J., Cordes T., Forthmann C. Steinhauer C. and Tinnefeld P.

Published in

Proceedings of the National Academy of Sciences of the United States of America, (2009) 106(20):8107-8112



P3

**Single-molecule photophysics of oxazines on DNA and its  
application in a FRET switch**

By

Vogelsang J., Cordes T. and Tinnefeld P.

Published in

Photochemical & Photobiological Sciences, (2009) 8:486-496.



P4

**On the mechanism of Trolox as antiblinking and antibleaching  
reagent**

By

Cordes T., Vogelsang J. and Tinnefeld P.

Published in

Journal of the American Chemical Society, (2009) 131(14):5018-5019.



P5

**Intrinsically Resolution Enhancing Probes for Confocal  
Microscopy**

By

Vogelsang J., Cordes T., Forthmann C., Steinhauer C. and Tinnefeld P.

Submitted to

Nature Chemistry





## 8.2. Further Publications

Further publication, which evolved during the PhD time are summarized here.

Vogelsang J., Doose S., Sauer M. and Tinnefeld P., (2007) Single-molecule fluorescence resonance energy transfer in nanopipets: improving distance resolution and concentration range. **Anal. Chem.**, 79(19):7367-7375.

Steinhauer C., Forthmann C., Vogelsang J. and Tinnefeld P., (2008) Super-resolution Microscopy Based on Engineered Dark States. **J. Am. Chem. Soc.**, 130(50):16840–16841.

Person B., Stein I. H., Steinhauer C., Vogelsang J. and Tinnefeld P., (2009) Correlated movement and bending of nucleotide acid structures visualized by multicolor single-molecule spectroscopy. **ChemPhysChem**, 10(9-10):1455-1460.



**Single-molecule fluorescence resonance energy transfer in  
nanopipets: improving distance resolution and concentration  
range**

By

Vogelsang J., Doose S., Sauer M. and Tinnefeld P.

Published in

*Analytical Chemistry*, (2007) 79(19):7367-7375.



## **Super-resolution Microscopy Based on Engineered Dark States**

By

Steinhauer C., Forthmann C., Vogelsang J. and Tinnefeld P.

Published in

Journal of the American Chemical Society, (2008) 130(50):16840–16841.



**Correlated movement and bending of nucleotide acid structures  
visualized by multicolor single-molecule spectroscopy**

By

Person B., Stein I. H., Steinhauer C., Vogelsang J. and Tinnefeld P.

Published in

ChemPhysChem, (2009) 13010(9-10):1455-1460.





## 9. Curriculum Vitae

Name	Vogelsang Jan
Date of birth	12 /16 / 1978
Place of birth	Herford, Germany
Nationality	German
Marital status	Unmarried



### Education

1985 - 1998	<b>Elementary School and High School in Bielefeld</b> Abitur (German school-leaving examination): Good (2.1) Advanced courses: Physics and mathematics
1998 – 1999	<b>Civil service</b> Retirement home v. Plettenberg-Stift Bethel, Bielefeld
10 / 1999 – 04 / 2006	<b>University of Bielefeld</b> <u>Studies of Physics</u> (Diploma)
04 / 2002	<u>Vordiplom (pre-degree examination)</u> : Good (2.00)
04 / 2005 – 04 / 2006	Diploma thesis in physics in the group of Prof. Dr. M. Sauer “Development of a Single Molecule Fluorescence Setup for Investigating of Switching Mechanisms of Doubly Labeled DNA in Micro Capillaries”: Very good (1.0)
04 / 2006	<u>Diploma in Physics</u> : Very good (1.0)
04 / 2006 – 06 / 2007	<b>University of Bielefeld</b> <u>PhD program in physics</u> , Single molecule fluorescence spectroscopy in the group of Prof. Dr. M Sauer (Applied laserphysics and laserspectroscopy)
06 / 2007 - today	<b>Ludwig-Maximilians University of Munich</b> PhD program in physics, Single molecule fluorescence spectroscopy in the group of Prof. Dr. P. Tinnefeld (Applied physics – Biophysics; Chair of Prof. Hermann Gaub)

## Awards

---

- 06 / 1998                      **High School in Bielefeld**  
Book Prize for the best school-leaving examinations in physics  
in the year 1998 at the Brackweder Gymnasium in Bielefeld
- 09 / 2008                      **Ludwig-Maximilians University of Munich**  
Students Award for best talk at the single molecule workshop at  
Picoquant (Berlin)

## Research Interests & Areas of Expertise

---

- Photochemistry and photophysics
- Molecular switches, photochromic compounds, photoswitchable fluorophores
- Single-molecule spectroscopy/microscopy (confocal microscopy, total-internal-reflection microscopy, alternating laser excitation, fluorescence correlation spectroscopy)
- Current projects: (i) ultra stable fluorophores in single molecule fluorescence spectroscopy; (ii) methods for resolution enhancement beyond the diffraction limit; (iii) single-molecule photophysics; (iv) charge-transfer processes in DNA

## References

---

- Prof. Dr. Markus Sauer, University of Bielefeld, sauer@physik.uni-bielefeld.de
- Prof. Dr. Philip Tinnefeld, LMU München, philip.tinnefeld@physik.uni-muenchen.de

## Peer-Reviewed Publications

---

- J. Vogelsang, S. Doose, M. Sauer, P. Tinnefeld “Single-Molecule FRET Measurements by Confining Molecules in Nanopipettes“, Proc. SPIE, 6633 (2007) 66331L.
- J. Vogelsang, S. Doose, M. Sauer, P. Tinnefeld “Single-Molecule FRET in Nanopipettes: Improving Distance Resolution and Concentration Range“, Anal. Chem., 79 (2007) 7367 – 7375.
- J. Vogelsang, R. Kasper, C. Steinhauer, B. Person, M. Heilemann, M. Sauer, P. Tinnefeld “A Reducing and Oxidizing System Minimizes Photobleaching and Blinking of Fluorescent Dyes“, Angew. Chem. Int. Ed., 47(29) (2008) 5465-5469 (including cover picture).
- C. Steinhauer, C. Forthmann, J. Vogelsang, P. Tinnefeld “Superresolution Microscopy on the Basis of Engineered Dark States“, J. Am. Chem. Soc., 130(50) (2008) 16840-16841.

- T. Cordes, J. Vogelsang, P. Tinnefeld "On the Mechanism of Trolox as Antiblinking and Antibleaching Reagent", J. Am. Chem. Soc., 131(14) (**2009**) 5018-5019.
- J. Vogelsang, T. Cordes, P. Tinnefeld "Single-molecule photophysics of oxazines on DNA and its application in a FRET switch", Photochem. Photobiol. Sci., 8 (**2009**) 486.
- B. Person, I. H. Stein, C. Steinhauer, J. Vogelsang, P. Tinnefeld "Correlated Movement and Bending of Nucleic Acid Structures Visualized by Multicolor Single-Molecule Spectroscopy", Chem. Phys. Chem., 13010 (9-10) (**2009**) 1455-1460.
- J. Vogelsang, T. Cordes, C. Forthmann, C. Steinhauer, P. Tinnefeld "Controlling the fluorescence of ordinary oxazine dyes for single-molecule switching and superresolution microscopy", Proc. Natl. Acad. Sci. USA, 106(20) (**2009**) 8107-8112.

### Manuscripts submitted

---

- J. Vogelsang, T. Cordes, C. Forthmann, C. Steinhauer, P. Tinnefeld "Intrinsically Resolution Enhancing Probes for Confocal Microscopy" submitted to Nature Chemistry

### Conferences & Presentations

---

- 06 / 2007      Poster presentation at the SPIE Photonics in Munich: "Improving Single-Molecule FRET Measurements by Confining Molecules in Nanopipettes".
- 09 / 2007      Oral presentation at the Picoquant single molecule workshop, Berlin: "smFRET in Nanopipettes: Improving Distance Resolution and Concentration Range".
- 09 / 2008      Oral presentation at the Picoquant single molecule workshop, Berlin: "Control of Fluorescence Characteristics by Photoinduced Redox Reactions".
- 01 / 2009      Poster presentation at the Single Molecule Biophysics in Aspen: "Single-Molecule Photophysics of Oxazines and its Applications".
- 08 / 2009      Oral presentation at the BioImaging in Bielefeld: "Make them blink: Photophysics for super-resolution microscopy".